

Deglaciation history of Frøyabanken and Halsafjorden, Norway

Waqas Hussain



Master thesis in Geology
Department of Earth Science
University of Bergen
February 2023

Abstract

This thesis aims to reconstruct post-glacial ice sheet dynamics on the Norwegian coast and adjacent continental shelf area, a region for which there is significant uncertainty regarding ice sheet movement due to a lack of reliable and accurate chronological data. To address this gap, new data from Halsafjorden Frøyabanken and previously published dates were analyzed using various geological and geophysical methods, including analyzing a 4.27 m gravity core from Frøyabanken. They were compared with geological and geophysical data provided by Fugro in Halsafjorden. The chronology of the events was compared with previously published data to retrace the ice sheet movement from Frøyabanken to Halsafjorden. All data were recalibrated using the Normarine18 curve to correct for potential dating errors.

Based on the combined analysis of seismic stratigraphy, lithostratigraphy, and chronology, it is concluded that the deglaciation of Frøyabanken began around 17.7-17.1 ka cal. yrs BP was followed by a readvance, the Frøyabanken readvance, approximately 15.1 ka cal. yrs BP. The Halsafjorden region is believed to have become ice-free around 16-18 ka cal. yrs BP, with the overall retreat of the regional ice sheet across the mid-Norwegian continental shelf beginning around 18 ka cal. yrs BP. This retreat was followed by a Late Karmøy/Bremanger readvance of around 16-15 ka cal. yrs BP, possibly correlated with the Heinrich Event 1. The ice sheet then retreated from the shelf at around 15-14 ka cal. yrs BP, with the following possible local readvance occurring in the Haltenbanken region.

The findings of this master thesis provide essential insights into the ice sheet dynamics of the Norwegian coast and continental shelf area following the last glacial maximum. These findings significantly impact our understanding of the glacial history of this region and have potential impacts on future research in this field.

Acknowledgments

First, I would like to express my deepest gratitude to my main supervisor, researcher Jo Brendryen at the Department of Earth Science, for excellent guidance and follow-up with my master's thesis. Thank you very much for answering my every question through email and at the door of your office. Thank you for teaching me everything from lab work to different software. Without your help and guidance, this master's thesis would not have been possible. I would also like to thank my co-supervisor, Professor Haflidi Haflidason, at the Department of Earth Science. Thank you very much for the excellent guidance, reading through all my drafts, and raising questions that made me think in a new way. You and Jo were my best supervisors; they taught me so many things. I would also like to thank Anna Svendal Aase for helping me with Petrel and CorelDraw.

I would also like to thank my parents, who have supported me and encouraged me to go to Norway for higher education. I wouldn't be here without their support.

Finally, I would like to thank the University of Bergen for allowing me to get higher education for free. I also want to thank my fellow students who shared good memories with me and encouraged me in every possible way to achieve my dreams.

Bergen, February 2023.

Waqas Hussain

Contents

1.	Introduction	1
1.1	Scientific Objectives	3
2	Geological Framework.....	5
2.1	Study Area	5
2.2	Glacial History	8
2.3	Postglacial mass movements.....	11
3	Materials and Methods	15
3.1	Core material.....	15
3.2	Research Vessel	15
3.3	Seismic data acquisition.....	16
3.4	Laboratory methods	16
3.4.1	ITRAX XRF core scanner.....	16
3.4.2	Mastersizer	17
3.4.5	Radiocarbon samples.....	19
3.4.6	Radiocarbon Dating.....	19
3.4.7	Calibration.....	20
3.5	Seismic Interpretation	21
4	Results	25
4.1	Seismic interpretation of the Frøyabanken.....	25
4.1.1	Seismic stratigraphy	26
4.1.2	Core GS20-229-28GC (Frøyabanken).....	32
4.1.3	Correlation between the seismostratigraphy and core stratigraphy on Frøyabanken 37	
4.1.4	Chronology of Frøyabanken	38
4.2	Halsafjorden	41
4.2.1	Seismic Interpretation of Halsafjorden	41
4.2.2	Lithostratigraphy of Halsafjorden.....	47
4.2.3	Shear strength analysis.....	48
4.2.4	Chronology recalibration of Halsafjorden	48
4.3	Recalibration of previously published ¹⁴ C dates	51
5	Discussion.....	55
5.1	Glacial Dynamics and chronology of Frøyabanken and Halsafjorden	55
5.1.1	Frøyabanken	55

5.1.2	Halsafjorden	60
5.1.3	Correlation between Halsafjorden and Frøyabanken:	62
5.2	Regional Ice Movement	66
5.3	Postglacial mass movements in mid-Norwegian continental shelf	70
5.3.1	Frøyabanken	70
5.4	Implications of results of Halsafjorden for E39 project.....	72
6.	Conclusion.....	73
7.	Future work	74
	References	75

1. Introduction

This master project contributes to the ferry-free highway E39 project, where the Norwegian Public Road Authorities plans to build fjord crossings that require seabed installations. One of these fjord crossings is planned in Halsafjorden, Nordmøre. To ensure the safety of this infrastructure, a thorough understanding of the regional geological history and processes is needed.

Halsafjorden, the Møre-Trondelag coast, and the near shore continental shelf area during the Last Glacial Maximum (LGM) and deglaciation were heavily impacted by the waxing and waning of the Fennoscandian Ice sheet (FIS) that repeatedly reached the edge of the Norwegian Continental shelf (Bøe et al., 2004; Haflidason et al., 2013; King et al., 1998; Nygård et al., 2004; Sejrup et al., 2001; Sejrup et al., 1994; Sejrup et al., 2022).

The processes related to ice sheet actions are responsible for most of the sedimentary deposits seen in the fjords and the coastal areas; hence, to address sedimentary processes and potential hazards relevant to sea-bed infrastructure such as bridges or offshore wind turbines, it is essential to also understand the processes related to the glacial dynamics of the fjords and continental shelf. This thesis seeks to enhance the understanding of the regional geological history by describing the sedimentary deposits and reconstructing the deglacial regional ice sheet movement of the Mid-Norwegian coastal areas with a focus on Frøyabanken and Halsafjorden.

Compared to other coastal areas, detailed evidence of deglaciation and ice movement across Frøyabanken, Haltenbanken, and Halsafjorden is limited (Bøyum, 2011; Bugge, 1980; Haflidason et al., 2013; Nygård et al., 2004; Rokoengen et al., 1977). The ice readvanced to the shelf around 15-13.5 ¹⁴C ka BP on the Norwegian continental shelf around Haltenbanken and Måloy Platform (Bøyum, 2011; Bugge, 1980; Haflidason et al., 2013; Nygård et al., 2004; Rokoengen et al., 1977; Rokoengen and Frengstad, 1999). Following this readvance of the ice sheet, the FIS retreated to the coast, which has been well documented (Mangerud, 1980, 2004; Nygård et al., 2004; Svendsen and Mangerud, 1987). After a short while, the ice quickly began to retreat inland from the coastal continental edge, causing an isostatic rebound that produced numerous mass movements in the western Norwegian fjords following the Younger Dryas ice sheet readvance (Bellwald et al., 2019; Bøe et al., 2004; Haflidason et al., 2005; Hjelstuen et al., 2009). One example of a regional submarine mass movement after deglaciation is the

submarine landslide, i.e., Storegga Slide on the continental slope off Møre, Norway, which occurred around 8100 cal. yr BP. This submarine slide triggered a tsunami wave that affected the area around Norway, Iceland, Scotland, and Greenland (Bondevik et al., 2012; Dawson et al., 1988; Haflidason et al., 2005; Wagner et al., 2007). To better understand the impact and mechanism behind these mass movements, sediment cores retrieved from fjords were studied to examine environmental records because fjord basins and glacial troughs have acted as sediment traps to catch sediment deposits ranging up to 100s meters in thickness (Aarseth, 1997; Bellwald et al., 2019). Sedimentary deposits in fjords are potential sites for investigating environmental records to elucidate past environmental changes in the coastal areas of Norway (Aarseth, 1997).

The ice sheet's movement over the continental shelf should be carefully dated better to understand the Mid-Norwegian continental shelf's deglaciation history. If these dates are corrected for the ice sheet movement, it could have significant implications for understanding the regional ice sheet movement and events in the deglaciation period. Because the calibration of the pre-Bølling era was not firmly established until recently, there were issues with dating glacial moments (Olsen et al., 2013). Lack of data has hampered the determination of late glacial age. Furthermore, converting conventional ^{14}C ages to calibrated ages does not follow a simple linear function to eliminate dating technique errors (Olsen et al., 2013). Another issue associated with dating is the reservoir age effect, which occurs because most ^{14}C dating is based on marine mollusks. Uncertainties in these dates were rectified by assigning a corrected age of 440 years, particularly for dates in the pre-Bølling era (Brendryen et al., 2020; Mangerud, 2004; Nygård et al., 2004; Olsen et al., 2013). However, as the ^{14}C reservoir age in the Norwegian sea was highly variable during the late glacial these dates must be revised to precisely date the ice sheet movement across the Norwegian continental shelf (Brendryen et al., 2020). Brendryen et al. (2020) constructed a new ^{14}C calibration curve, known as the Normarine18 curve, providing an account of the temporal variation of the late glacial reservoir effect in the Norwegian sea.

The new data from Frøyabanken and Halsafjorden, such as sediment cores and geophysical data, will fill the gaps in the ice sheet movement reconstruction. The chronological order of events in Frøyabanken and Halsafjorden will be then correlated with the previously published older dates to provide the entire perspective of events that occurred on a regional basis, followed by the Last Glacial Maximum. In addition, sediment sequences in seismic lines and sediment

cores will be studied to understand the glacial ice sheet movement and postglacial mass movements from Frøyabanken to Halsafjorden.

To reconstruct the ice sheet's movement along the mid-Norwegian continental margin and correlate it with other recalibrated data using the Normarine18 curve, a gravity core of 427 cm was studied from Frøyabanken (Fig. 1) along with TOPAS seismic survey lines from the field. To accurately retrace the passage of the ice sheet along the coastal area and its postglacial mass movements, followed by ice sheet deglaciation, the findings from Frøyabanken were subsequently compared with the data supplied by Fugro (2019) for Halsafjorden.

1.1 Scientific Objectives

This research's overall objective is to reconstruct the regional ice movement during and after deglaciation from the Frøyabanken area and its movement into Halsafjorden. This study also addresses the associated postglacial mass movements.

The sub-objectives of this thesis are based on the following points:

- 1) Describe, date, and correlate the deglacial sedimentary deposits both within and between Frøyabanken and Halsafjorden.
- 2) Reconstruct the regional glacial ice sheet movement based on the data from Frøyabanken and Halsafjorden, along with previously published dates and interpretations from the Mid-Norwegian continental shelf and coast.
- 3) Describing and dating the postglacial mass movements identified on Frøyabanken and in Halsafjorden.

2 Geological Framework

2.1 Study Area

The study area is Frøyabanken and Halsafjorden, which are situated approximately 50 km apart on the Mid-Norwegian shelf and coast (Fig. 1). The area around Frøyabanken has water depths between 150-400 m deep. In addition, Halsafjorden is up to 500 m deep (Fig. 1). The thickness of Quaternary sediments in the Frøyabanken area varies from place to place (Holtedahl and Bjerkli, 1982). Close to Frøyabanken, it can reach 20m or more, depending on the locality (Bugge et al., 1975; Rokoengen et al., 1977). Holtedahl and Bjerkli (1982) described the stratigraphy of the continental shelf relative to the late Quaternary period. The area around Frøyabanken has been the subject of previous investigations. Horberg (1947) and Holtedahl et al. (1956) described the bathymetry and glacial history of mid-Norwegian continental and concluded that during the last glaciation, the ice sheet could have extended 40 km from the west coast. It was also found that the quaternary sediments in the offshore coastal area were very thin. Mesozoic materials have also been observed in some sediment samples from this area (Holtedahl et al., 1971). Holtedahl and Bjerkli (1982) studied the surface area near the Frøyabanken offshore area to define the stratigraphy of the Late Quaternary sediments. Nygård et al. (2004) studied the Bremanger ice sheet readvance on the central Møre shelf in the mid-Norwegian continental margin (Fig. 2). The mid-Norwegian continental shelf has also been studied for its glacial landforms and variations along with ice sheet movement following the LGM (Ottesen et al., 2022; Rise et al., 2006; Sejrup et al., 2022).

The second part of the study area is Halsafjorden, located on Nordmøre in Møre and Romsdal county (Fig. 1B). It has an average length of 11 km and is 2.5 km wide. The study area is in the middle of Halsafjorden between Jutvikneset and Skårneset (Fig. 1B). The seabed topography of Halsafjorden reaches up to 500m in depth, while the hills surrounding the area reach 400m in height. The bedrock of the area surrounding the Halsafjorden mainly consists of mica schist and granitic orthogneiss (Askvik and Rokoengen, 1985). Halsafjorden has already been studied by Bøe et al. (2004) for possible mass movements in the area. Rød (2022) has also investigated possible mass movements in the early-mid Holocene.

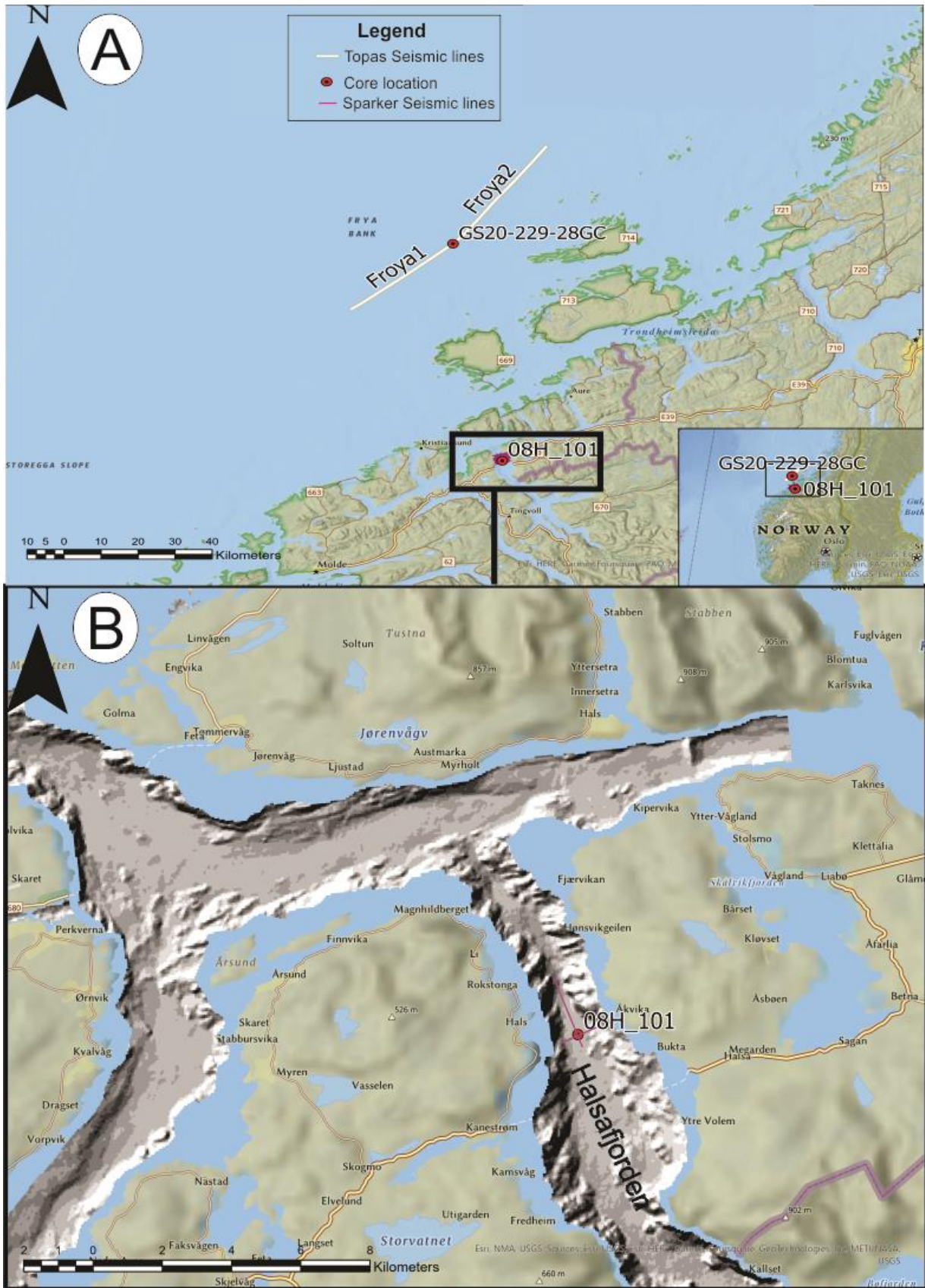


Fig. 1. (A) Study area in the mid-Norwegian continental margin. The locations of the cores are also mentioned. (B) the study area of Halsafjorden. The map was created using ArcGIS Pro.

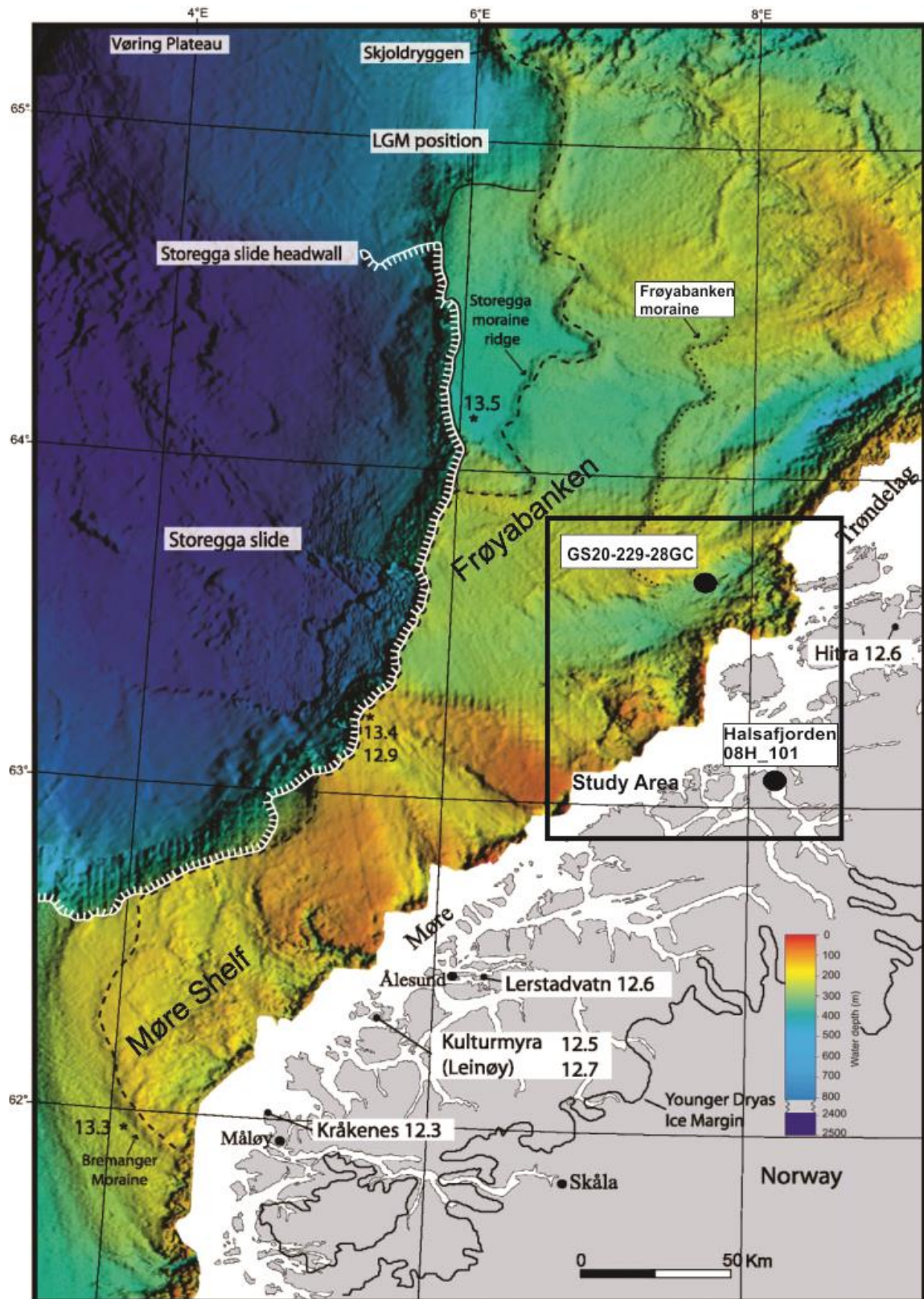


Fig. 2. Study area in the Norwegian outer self, along with the position of the LGM, Storegga Slide, and other localities along with their ¹⁴C ages. Modified after Nygård et al. (2004).

2.2 Glacial History

Late Weichselian glacial maximum (LGM)

Geologists have concluded that in the LGM, the ice sheet extended from the Norwegian Channel to Svalbard (Fig. 3A; Andersen et al., 1981; Mangerud, 2004; Olsen et al., 2013). The western part of the Scandinavian Ice sheet reached its maximum during the LGM between 25-28 ka (ka=thousand years) (Hughes et al., 2016; Mangerud, 1980, 2004; Olsen et al., 2013; Ottesen et al., 2022; Sejrup et al., 2022).

The LGM period was followed by a short interstadial period known as the Andøya-Trofors interstadial, reported from the data collected in most fjords, such as bulk sediments from the cave and lake sediments dating back to c. 14-20 ka through U/Th dating and ¹⁴C dating from Karmøy, Rondane, and Langsmoen (Alm, 1993; Bøe et al., 2007; Olsen et al., 2013; Vorren et al., 1988).

Following the LGM, the Bremanger ice sheet readvance occurred around 18.6 ka reaching the shelf margin of Northern Norway and southwest Norway (Figs. 3B and 4) (Nygård, 2003; Olsen and Bergstrøm, 2007). The ice sheet readvance happened at various places, such as Andøya and Risvik Moraines in Finnmark, which could be correlated with the Late Weichselian Karmøy readvance (Olsen et al., 2013; Vorren and Plassen, 2002). The correlation of all these locations could give a possible date to be 19.7 ka possibly (Olsen et al., 2013; Ottesen et al., 2022; Sejrup et al., 2022).

The late glacial period can be divided into 10-15 ka, in which two interstadial and stadial glaciers were observed: the Bølling, Older Dryas, Allerød, and Younger Dryas stadials (Fig. 3C) (Olsen et al., 2013). There are some uncertainties in the late glacial period owing to calibration to calendar years, problems in ¹⁴C dating, various microfossil contaminations, and dating of late glacial moraine ages (Olsen et al., 2013). The uncertainties include the conversion of ¹⁴C to calibrated years because it did not follow a simple linear function (Brendryen et al., 2020; Olsen et al., 2013). In addition, the uncertainties in the reservoir ages affect the dating of marine sediments (Brendryen et al., 2020; Mangerud, 2004).

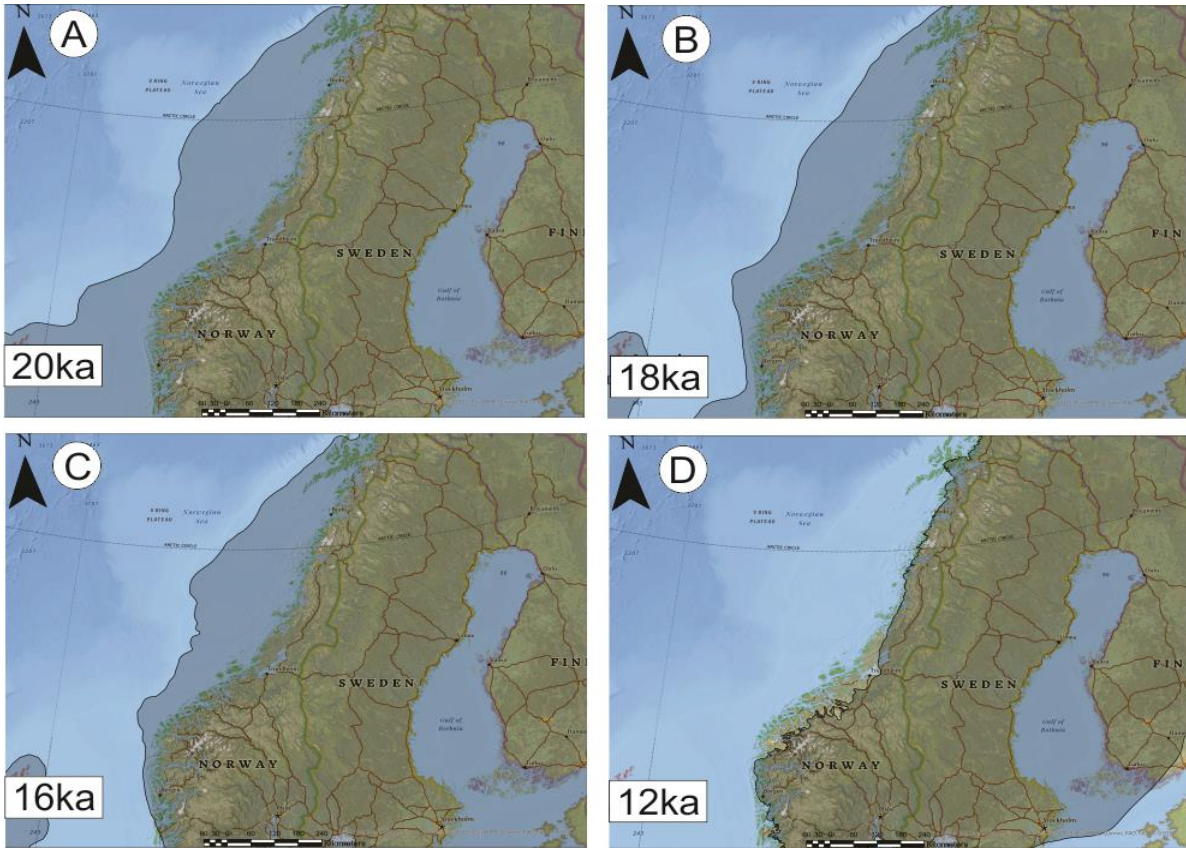


Fig. 3. (A) Full extent of FIS in LGM, i.e., 20 ka. (B) Retreat of FIS in 18 ka (C) Retreat of FIS in 16ka (D) The extent of FIS in Younger Dryas 12 ka, the extent of the FIS sheet. Modified after Hughes et al. (2016)

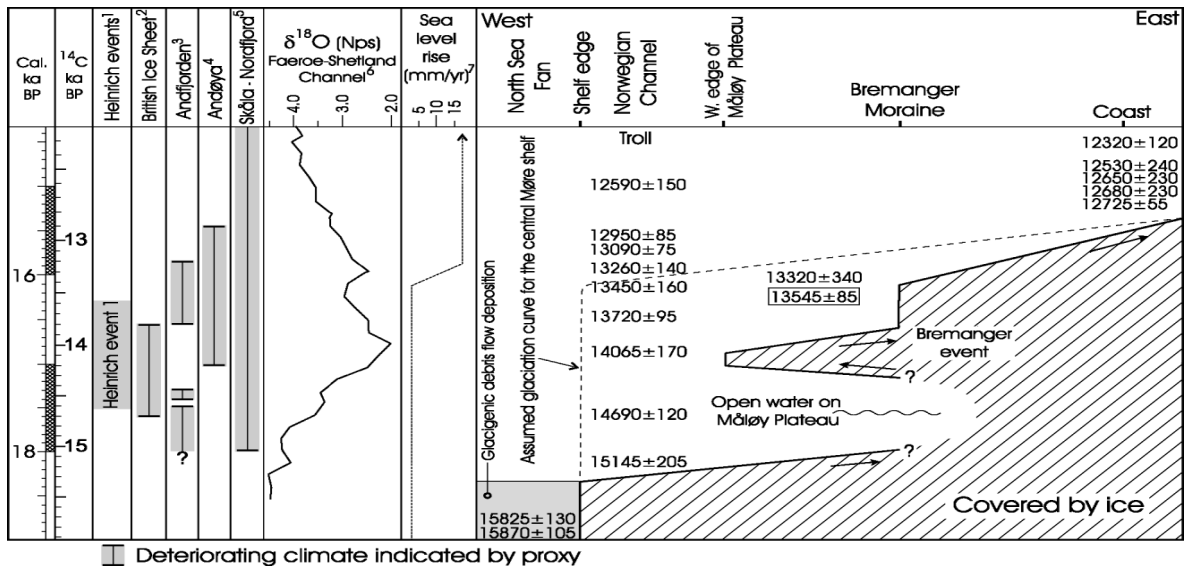


Fig. 4. The Time-distance diagram of the Måloy Platform represents the Breanger event readvance. Modified after Nygård et al. (2004)

In Norway, the Bølling interstadial period (15.3-14.1 ka cal. yrs BP) started a significant ice sheet retreat. Evidence from plant remains suggests that the ice sheet may have retreated to the inner fjord valleys of western Norway. In addition, evidence from shells suggests that the ice sheet retreat also occurred around the Arctic in Bølling period (Olsen, 2002).

Another ice sheet readvance in the Bølling-Allerød period was the Older Dryas ice sheet readvance that started around 14.2-13.7 ka cal. yrs BP (Olsen, 2002; Olsen et al., 2013). The extent of the ice sheet at the start of the Older Dryas readvance is unknown, but in Trøndelag (Olsen et al., 2013), it is estimated to have been readvanced by 5–10 km, whereas in Northern Norway, it is approximately 10–16 km (Olsen, 2002; Ottesen et al., 2022).

During the Allerød period, around 13.8-12.9 ka cal. yrs BP, it was observed that the ice retreat of this interstadial reached most of the fjords, indicating evidence from marine shells found in Troms, Holandsfjorden, and the extent of the Allerød period was probably observed in the western, central, and southern Norwegian fjords (Andersen et al., 1995; Bergstrøm et al., 2005; Klakegg et al., 1989; Mangerud, 1980; Olsen and Bergstrøm, 2007; Olsen et al., 2013; Svjeian, 1997; Vorren and Plassen, 2002).

Following the Bølling-Allerød, Younger Dryas ice sheet readvance began and significantly advanced in the Oslofjord region, Bergen, Trondheim, Northern Norway, and Southern Norway (Andersen et al., 1995; Bergstrøm et al., 2005; Olsen and Bergstrøm, 2007; Vorren and Plassen, 2002). However, in the northern part of Norway near the Svartisen glacier, the extent of the Younger Dryas ice sheet is less as it is reported to be a few meters off the margin (Fig. 3D) (Gjelle et al., 1995; Olsen et al., 2013). Halsafjorden was not influenced by the readvance during the Younger Dryas (Bellwald et al., 2019; Johansen et al., 1985)

In southwest Norway, the relative sea level rose to 10m during the Younger Dryas (Lohne et al., 2007). The reason for this rise in the relative sea level might be a combination of factors, such as isostatic rebound halting due to the readvance of the ice sheet (Anundsen and Fjeldskaar, 2020; Fjeldskaar and Kanestrøm, 1980; Lohne et al., 2007; Svendsen and Mangerud, 1987).

2.3 Postglacial mass movements

Following the Younger Dryas, the ice rapidly retreated, giving rise to glacioisostatic uplift, which led to the generation of seismic activity in Norway (Bellwald et al., 2019; Bøe et al., 2004). This seismic activity triggered slope stability, and many mass movements have been reported during the Holocene (Bellwald et al., 2019; Bøe et al., 2004).

After the Younger Dryas in the early Holocene, the ice sheets started to disintegrate, which triggered earthquakes in western Norway after a few hundred years (Bellwald et al., 2019). Data from paleoseismic studies show that the seismic activity was more than 6 in magnitude, which occurred in the 13000-9000 cal. yrs BP (Mörner, 2013; Muir-Wood, 1993). This seismic activity can be correlated with the glacioisostatic uplift that followed the Younger Dryas (Svendsen and Mangerud, 1987)). The mass movement peaked during 11.7-9.7 ka cal. yrs BP (Bellwald et al., 2019). Owing to the increased sedimentation rate and mass movement, many studies can see the first batch of sedimentation sequences with distinct patterns in most western Norwegian fjords (Bellwald et al., 2019).

Around 9.7 c ka and forward, mass movements became less frequent, and the only known mass movements were due to the Storegga Slide, with a possible magnitude of more than 7 (Bellwald et al., 2019; Bøe et al., 2004). Bøe et al. (2004) concluded that the area of Halsafjorden might have been affected by the Storegga Slide event. The Storegga slide generated a tsunami that affected most Norwegian continental shelf and coastal areas. Frøyabanken might have also been affected by the Storegga Tsunami (Fig. 2). Storegga Tsunami was so large that outside the Møre Shelf, the outermost part of the LGM deposits was eroded by it, dating back to 8.2 ka, as evidence suggested, such as end moraines and outermost till (Bugge, 1980; Haflidason et al., 2005; Hjelstuen et al., 2009; Olsen et al., 2013).

It has been observed that the period between 8 ka and 4 ka cal. yrs BP was less seismically active in western Norwegian fjords (Bellwald et al., 2019; Bøe et al., 2004). In comparison, the Late Holocene period is characterized by more frequent seismic activity related to mass movements in the Late Holocene. Halsafjorden is not affected by the Late Holocene mass movements (Bøe et al., 2004; Rød, 2022).

Sedimentary depositional systems in the fjords

Three typical seismic facies can be found in the western Norwegian fjords and offshore coastal areas (Hjelstuen et al., 2009). 1) Early deglaciation and subsequent deposition of glaciomarine sediments; 2) alternating frequent slide debrites; and 3) small-slide debrites. Figure 5 shows a conceptual model of sediments deposited during the deglaciation period.

1) Glaciomarine/hemipelagic sediments:

Bathymetric and seismic data from fjords revealed that the sediment distribution in western Norwegian fjords had a distinct pattern after the deglaciation period (Aarseth, 1997; Hjelstuen et al., 2009). Glaciomarine/hemipelagic sediments were deposited in the western Norwegian fjord system during the Bølling–Allerød period. These sediments were deposited before the Younger Dryas readvanced (Fig. 5) (Hjelstuen et al., 2009). The bedrock surface influences these sediment packages to mimic the bedrock in undulation and folds throughout the glaciomarine sediments (Hjelstuen et al., 2009).

2) Slide debrites and minor slide debrites

Elevated shorelines have been cited as evidence from previous studies suggesting that the glacio-isostatic rebound was very fast in the thousand years following the Younger Dryas retreat (Svendsen and Mangerud, 1987). Following the Younger Dryas readvance, the ice sheet rapidly retreats, leading to glacio-isostatic rebound (Fig. 5) (Andersen et al., 1981). Because of the glacio-isostatic rebound, many slide debrites or turbidites can be found in seismic surveys across fjords, termed slide debrites (Hjelstuen et al., 2009).

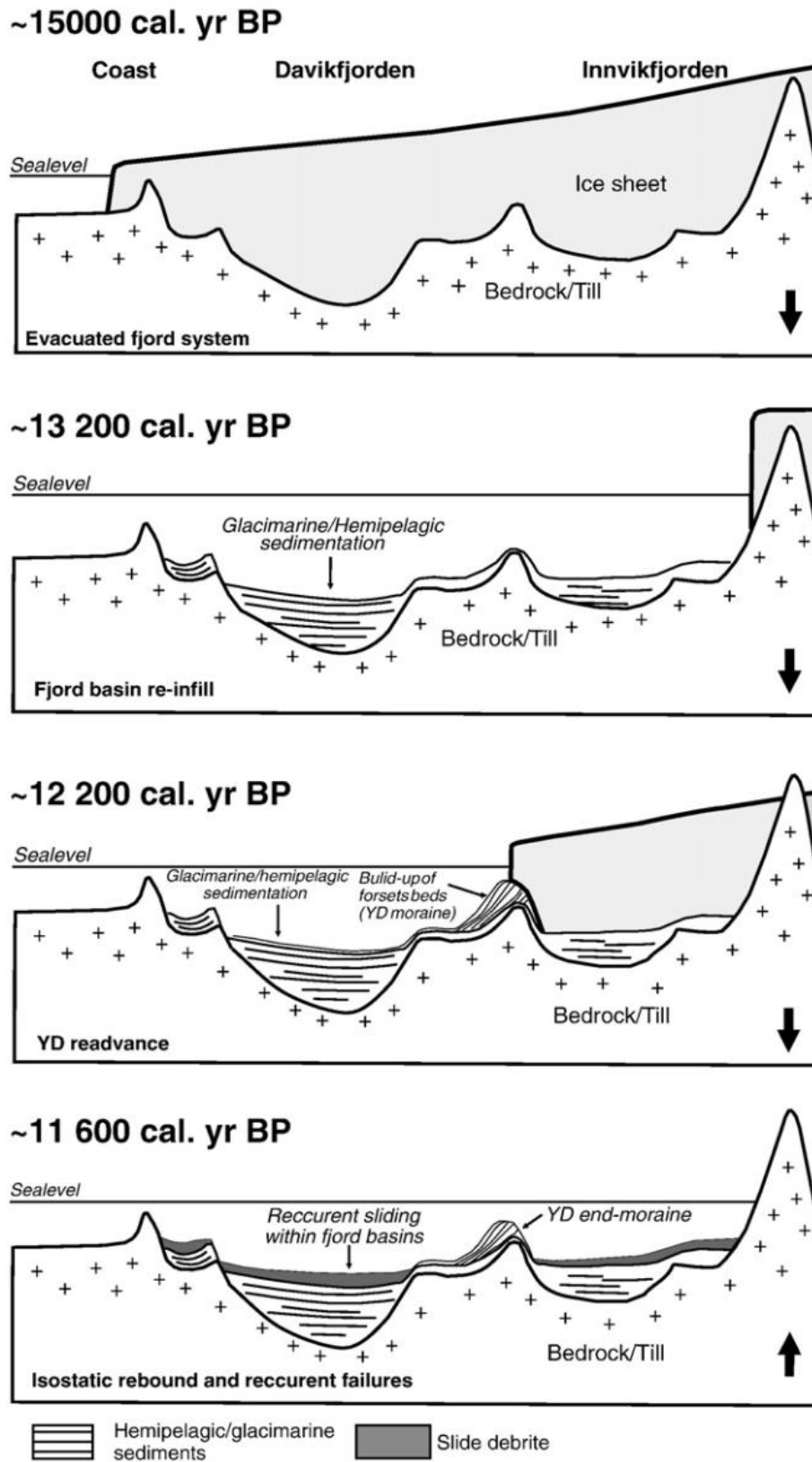


Fig. 5. Conceptual model for Nordfjord behind the sediment packages deposited after 15 ka cal. yrs BP YD: Younger Dryas modified after (Hjelstuen et al., 2009)

3 Materials and Methods

3.1 Core material

The cores applied in this study are the gravity core, GS20-229-28GC, retrieved in 2020 from Frøyabanken close to the island of Smøla. It was retrieved through a research vessel F/F GO SARS conducting a field in northern Norway to collect marine core sediments. The total length of the core was 4.27 m (Table 1). The data from Frøyabanken are correlated with the data from Halsafjorden provided by Fugro (Fugro, 2019). The 08H-101 borehole of 41.90m was used for the undrained shear strength analysis through a Cone Penetration test (Table 1) (Fugro, 2019).

The cores were retrieved using the Gravity Core System. The corer is a metal pipe typically measuring 1-5m in length and has a removable plastic tubing lining. Large weights were placed on top of the pipes. The core is lowered over the side of the ship using a winch and wire rope and allowed to fall freely into the sediments. The corer catcher uses the sediments in a tube to capture them. The core catcher is brought to the surface and placed on the ship. The core is then cut into sections and marked. One part of the core is stored in the archive, while the other is the working part used to study the properties of marine sediments in the lab.

Table 1. Sediment cores retrieved during a field excursion in 2020 and core data from Fugro, along with their water depth and coordinates.

Core	Length (m)	Water depth m	Latitude (N)	Longitude (E)
GS20-229-28GC	4.27	328	63° 43.0565'	07° 52.5464'
08H_101	41.90	481.2	63° 04.36482'	08° 09.8103'

3.2 Research Vessel

The research field was conducted using the research cruise R/V G.O. SARS research vessel jointly owned by the Institute of Marine Research and the University of Bergen. The ship is 4,067 tons in weight, 77.4 meters long, and 16.4 meters wide. The top speed of the R/V G.O. SARS is 17.5 knots (Havforskningsinstituttet, 2018).

The Fugro survey vessel used in the Halsafjorden is the MV DESPINA research vessel. The ship is 6072 tons in weight, 98.6 meters long, and 19 meters in width. Its top speed is 15.5 knots (Fugro, 2019).

3.3 Seismic data acquisition

R/V G.O. SARS has a TOPAS PS18, a sub-bottom profiler with a range of 100-130m depth in water. It is a single-beam sub-bottom profiler with electronic roll, pitch, and heavy stabilization. The data for Frøyabanken was retrieved through the TOPAS PS18 profiler. Six seismic lines were used in this study from Frøyabanken.

MS DESPINA used the Sparker system in the Fugro Survey to acquire seismic data from Halsafjorden. The total seismic lines were 107 lines that form a seismic grid to cover the entire area between Jutvikneset and Skårneset (Fugro, 2019).

3.4 Laboratory methods

3.4.1 ITRAX XRF core scanner

The ITRAX XRF Core scanner is an efficient scanner used to retrieve semi-quantitative chemical profiles of the bulk element composition of the cores and physical high-resolution images from the core surface. It uses optical sensors and micro-XRAY fluorescence to extract high-resolution images and elemental ratios for analysis. The working procedure behind the ITRAX XRF core scanner is based on the emission of X-ray radiation that splits the electron from the inner shell of the atom filled by the electron from the other shell, and the difference in energy between these shells is released as electromagnetic radiation (Croudace et al., 2006).

The ITRAX core scanner was operated on a computer using a Windows operating system. Q-Spec is software that is used to interact with the core scanner. The procedure includes placing a core into the cradle and plastic on it to prevent it from drying. There are some instructions to follow to scan the core.

The specific settings used for the marine core are as follows:

- 1) Surface image of the core
- 2) XRF parameters, 30 voltage, 50 mA
- 3) A resolution of 1 mm was used to scan every millimeter of the core.

This study uses XRF data and other sedimentary parameters to identify lithological units. In XRF data, various element proxies were used, such as Zirconium (Zr), Potassium (K), and Bromine (Br), have been used. Zr is a heavy mineral usually used to indicate the sandy siliciclastic material in a sedimentary environment (Dypvik and Harris, 2001; Rothwell, 2015).

Br indicates marine organic matter in sediment cores (Ziegler et al., 2008). K is a proxy for identifying clayey sediments (Rothwell, 2015). Calcium (Ca) and Iron (Fe) were used to identify the possibility of turbidite or sandy layer during the deglaciation period due to Ca and Fe properties being tracers of biogenic production and terrigenous material, respectively (Rothwell, 2015). The results of XRF analysis are then compared with grain size analysis to identify sediment grading and textural character (Rothwell, 2015).

3.4.2 Mastersizer

A Mastersizer is an instrument used for grain size analysis. The working principle behind the Mastersizer 3000 is laser diffraction, which passes through individual grains and refracts light from them at specific angles. Light is scattered according to the Mie theory of light scattering in which the light passes through particles; the more extensive the particles, the lesser the angle of light spread, while in the case of smaller particles, the greater the angle of the light spread (Fig. 6) (Hergert and Wriedt, 2012; Panalytical, 2021). The machine operates in a size range of 0.01-3500 μm .

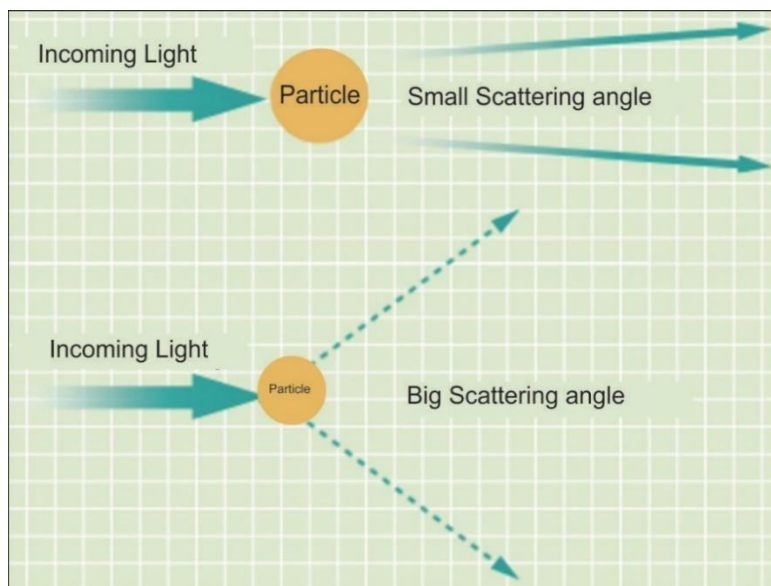


Fig. 6. Working principle behind Mavern Mastersizer 3000 modified after (Panalytical, 2021)

The Mastersizer is connected to the main computer along with Hydro LV. It is controlled using Mastersizer 3000E software. Before the sample is put in the Hydro LV. Settings were made in the software, and then, through each measurement, the machine was cleaned with water, and the preferred obscuration laser light was achieved.

For the grain size analysis, a total of sixty-nine samples were taken from the core at intervals of 10 cm and in one specific interval, i.e., 100-120 cm; the core was analyzed continuously in 1 cm intervals. Each sample was treated with a 0.05% Calogen mixture to prevent coagulation. New measurements were taken through the software, and the Hydro LV was cleaned each time before adding the sample by cleaning it three times. Subsequently, the software ensured degassing, and all instruments were working fine. The stirring speed was set to 3500 rpm because of the coarse material in the sediment core. The sample was then put in the Hydro LV, and an ultrasound was put on for 60 seconds to integrate the grains for further analysis. The sample is placed in the Hydro LV according to the obscuration laser light range of 5-15%. For finer grain sediments, the range is 5-8%, whereas, for coarser sediments, the range is 8-15%. Measurements were performed using a Mastersizer 3000 with an average of five readings.

3.4.3 Shear Strength Fall-cone test

The fall-cone test of Hansbo (1957) was used to measure the undrained shear strength of the sediments of Core GS20-229-28GC. A metal cone was placed on the sediment surface to carry out the test and then dropped onto the sediment surface. The cone penetrated the surface of the sediment, and measurements were taken. The readings are taken in millimeters (mm) and then are converted to (kilopascals) kPA by multiplying it by the gravitational constant (Hansbo, 1957). The weight of the cone is based on the visual description of the sediment core, i.e., if it is soft clay, a low-weight cone is chosen for a sandy textural sediment a high-weight cone would be selected.

For GS20-229-28GC, 100 g of the cone was used, and the cone was dropped freely close to the surface of the sediments. Three readings were taken on the core's left, center, and right sides at core depth of every 10 cm.

3.4.4 Fugro Cone Penetration Tests (CPT) from Halsafjorden

9 CPTs performed on borehole 08H_101 (Fugro, 2019). All tests were performed onsite to determine the geotechnical parameters. The Fugro Laboratory in the Netherlands calibrated the cones used in these tests (Table 2).

Table 2. Summary of CPT data used in this study, provided by Fugro (2019).

Borehole Core	CPT Number	Depth Range [m]	Cones Used
08H_101	CPT01 to CPT02	0.00 – 2.96	1706-2130
	CPT03 to CPT09	5.50 – 41.90	1706-1320

3.4.5 Radiocarbon samples

Five samples were taken from core GS20-229-28GC for radiocarbon sampling. The sample depths were chosen according to the main visible lithological differences in the sediment core (Table 3). The samples were placed on a shaker for six hours and sieved at 1000, 150, 125, and 63 μm . It was then dried for three days at 50 $^{\circ}\text{C}$.

Foraminiferal specimens were handpicked from the dried samples. The benthic foram species selected for analysis were *Uvigerina mediterranea* and *Nonionellina labradorica*. Table 3 gives the summary of the collected samples. The ^{14}C dates from borehole 08H_101 were provided by Fugro (2019). It should be noted here that the dating of 08H_101 at 3500-3580 cm interval might contain uncertainty as it was taken from a bulk sample.

Table 3. Samples at different intervals were picked up from the core along with their species, depth, and sample weights. The dates of core 08H_101 are from Fugro (2019).

Core ID	Species/materials	Depth (cm)	Sample weight (mg)
GS20-229-28GC	<i>Uvigerina mediterranea</i>	101-102	16
GS20-229-28GC	<i>Uvigerina mediterranea</i>	106-107	14
GS20-229-28GC	<i>Uvigerina mediterranea</i>	128-129	21
GS20-229-28GC	<i>Uvigerina mediterranea</i>	201-202	8
GS20-229-28GC	<i>Nonionellina labradorica</i>	418-419	8
08H_101	<i>N. commune</i> and bivalves	2340-2580	85
08H_101	Bulk	3500-3580	?

3.4.6 Radiocarbon Dating

Dating of the samples of GS20-229-28GC and 08H_101 was performed at BETA Analytical Inc. Laboratory in Florida, USA. An accelerated mass spectrometer (AMS) was used to analyze the samples. This method is widely used to date microfossils because of carbon isotopes, such as ^{14}C (unstable), ^{12}C , and ^{13}C . Microfossils such as foraminifera obtain ^{14}C in their shells, and once these organisms die, the radioactive decay of ^{14}C will start to act as a clock that tells when the organism has died. By identifying the element based on its unique atomic mass, AMS determines the number of ^{14}C atoms present in the sample (Olsson, 1968). For radiocarbon dates

to be exact and accurate, the stable isotopes ^{13}C and ^{12}C must be measured to account for isotopic fractionation.

3.4.7 Calibration

Calibration of the samples taken from GS20-229-28GC was performed using OxCal software (Ramsey, 2008, 2009). The calibration curve used for the Norwegian Sea was Marine29 for Holocene ^{14}C dates at intervals of 101-102, 106-107, 128-129, and 201-202 cm (Mangerud et al., 2006). For the Bølling-Allerød dates, the Normarine18 curve at 418-419 cm, in the OxCal Software (Brendryen et al., 2020). The reservoir age for the Norwegian Sea in earlier reconstructions of the Fennoscandian ice sheet was typically 400 years. The inability to comprehend how reservoir ages fluctuated over time has precluded a more thorough reconstruction of the deglaciation. Nevertheless, it is acknowledged that reservoir age significantly increases the uncertainty of calibrated data (Fig. 7) (Brendryen et al., 2020). To overcome this issue, enhanced ^{14}C dating and reservoir effects were considered to correctly date events, as presented by Brendryen et al. (2020).

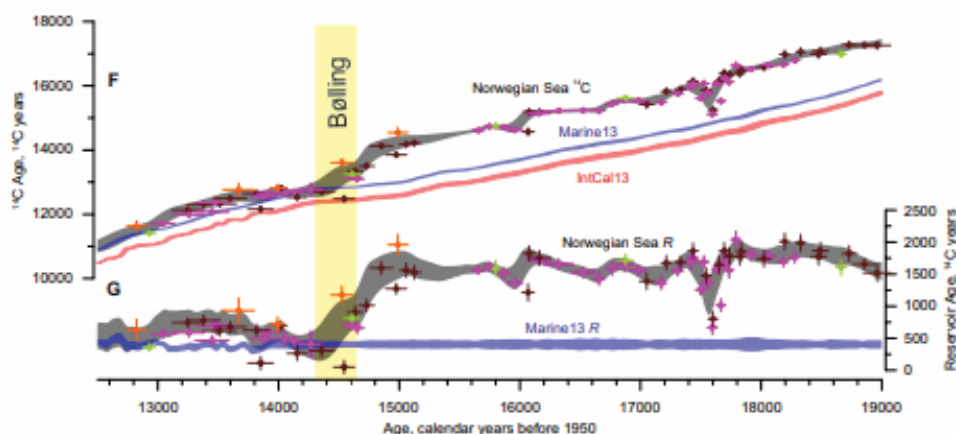


Fig. 7. Different calibration curves of IntCal13, Normarine18, and Marine13. The gray curve represents the Normarine18 curve, with blue representing Marine13 and red representing IntCal13. The lines below represent the differences when the reservoir age is added. The uncertainty intervals represented 68.2% of the depositional models. This figure has been modified from Brendryen et al. (2020).

The age model for GS20-229-28GC used the Bayesian depositional model with Oxcal software (Ramsey, 2008, 2009). The data were calibrated with the Normarine18 curve for the pre-Holocene date at 418-19 cm and Marine20 for the Holocene ^{14}C dates (Heaton et al., 2020). For the Holocene ^{14}C dates, ΔR value of 148 ± 33 ^{14}C years was applied (as calculated with the Calib

database based on western Norwegian reservoir ages) (Mangerud et al., 2006; Reimer and Reimer, 2001). The age model was then correlated with the sediment log of GS20-229-28GC to reveal information regarding the depositional history of the sediments. The age model was sequenced to correctly date the position of the sandy layer in the core using the Poisson process, that is, P_Sequence (Ramsey, 2008). P_Sequence uses a Markov chain Monte Carlo simulation that generates millions of realizations and then ages for specific depths. In addition, the top of the core age was determined through a function that defined the maximum age interval according to the dates specified by the user. The age model results are presented in the chronology subsection of the Results section.

Radiocarbon dating of the Halså Core, 08H_101, has already been provided by Fugro (2019). However, the basin depth and core dating were recalibrated using the Normarine18 curve for the pre-Bølling period.

3.5 Seismic Interpretation

2D Seismic interpretation of Halsåfjorden

A total of 107 seismic lines were interpreted from the dataset provided by Fugro (2019) for Halsåfjorden using PETREL software (Fig. 8B). Four reflectors were used: Seabed, RH1, RH2, and Glaciomarine (RH3). The seabed was interpreted both automatically and manually. RH1, RH2, and Glaciomarine (RH3) were also interpreted as a combination of automatic and manual interpretations. A borehole core 08H_101 from Fugro (2019) was placed on the seismic lines and part of the data from Halsåfjorden. A velocity model was created for the position of the borehole and its depth by using the created surface of the seabed with a velocity of 1480ms and 1530 as a constant.

2D Seismic Interpretation of Frøyabanken

Six lines were interpreted from a field cruise conducted in 2020 by the University of Bergen (Fig. 8A). There were five reflectors such as RF0 (Seabed), RF1, RF2, RF3, RF4, and RF5. All reflectors were interpreted both automatically and manually. A seabed surface was created using a velocity model to position the core.

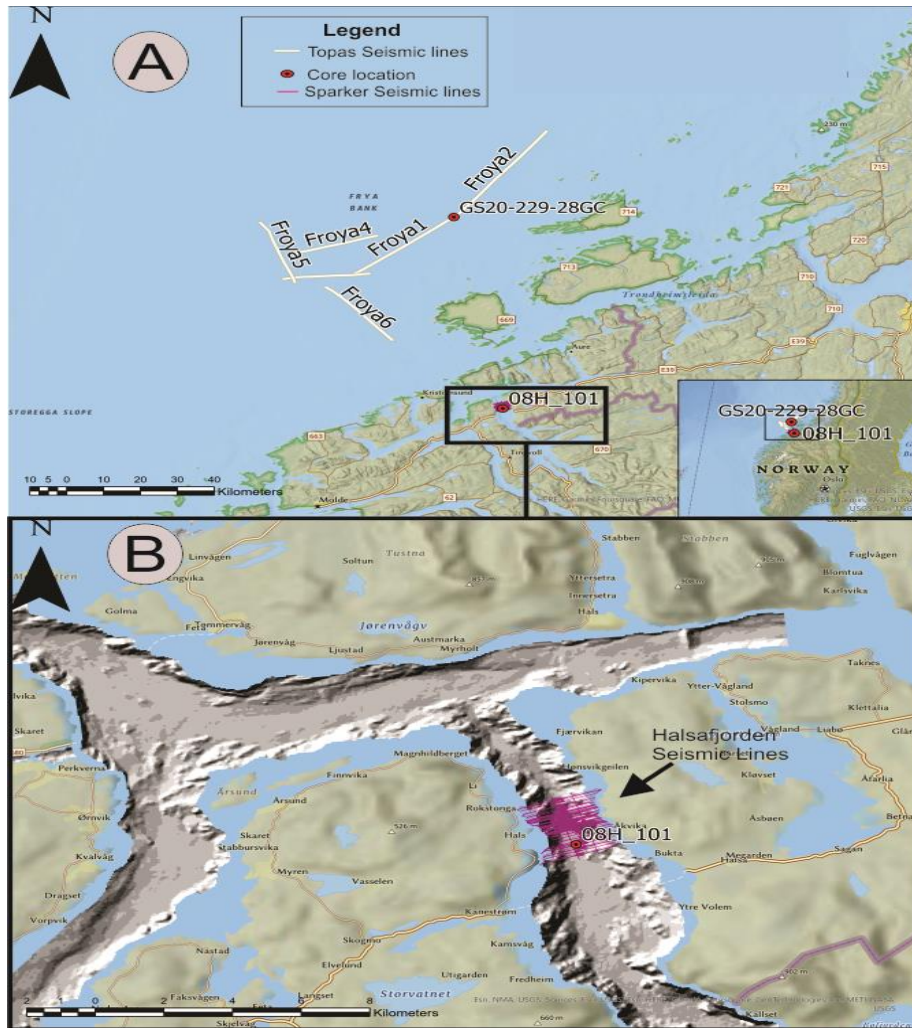


Fig. 8. (A) Seismic lines of Frøyabanken, i.e., Frøya1, 2, 3, 4, 5, and 6. (B) Halsafjorden seismic lines.

3.6 Software used

The figures and tables were created using CorelDraw and Microsoft Excel. The seismic interpretation of seismic line was interpreted using Petrel 2020. The bathymetric maps were provided by OLEX, which was processed in ArcGIS Pro to generate study maps. GRADISTAT was used for grain size distribution charts and grain size analysis (Blott and Pye, 2001). OxCal v4.4 software was used to recalibrate all dates to calibrate radiocarbon dates (Ramsey, 2008, 2009; Reimer et al., 2013).

3.7 Possible errors

3.7.1 Retrieving of core material

In retrieving the core, a possible error could be the measurement of the length of the core. An incorrect depth scale can lead to erroneous interpretations and affect the core study.

3.7.2 Laboratory methods

In XRF elemental analysis, the possibility of error can occur if the surface of the core has uneven bumps or if there are strange things on the surface that can decrease the accuracy of XRF analysis. In addition, the software Q-Spec should be set explicitly according to the instructions, as this could lead to a difference in the results and increase the possibility of an error.

In Mastersizer 3000, bubbles may appear in the Hydro LV if water is added rapidly, but they can also occur if the water is not supplied to the Hydro LV at room temperature. Water bubbles can be difficult to detect using a Mastersizer 3000, which treats them as particles larger than 100 m. If the sample is not entirely dissolved in Calogen water, errors may occur.

In the fall cone test, the cone might fall sideways because of the imbalance during free falling, which could give false readings; in that case, the test must be repeated.

In CPT tests, Cobbles and gravel were observed during the CPT investigation in Halsafjorden. This may result in errors in the CPT results. The results for 08H_101 were not affected by any reported problems (Fugro, 2019).

3.7.3 Radiocarbon dating

The samples could be contaminated by sieving and picking out microfossils. The addition of unusual factors during sampling can affect the sampling data.

There is uncertainty in the radiocarbon dating of ^{14}C because of changes in the Earth's magnetic field, human activities, atomic bomb influence, and solar activity variation in the atmosphere. This effect change is transferred to the water through precipitation. This change creates a reservoir effect in which ^{14}C is broken down, and a new ^{14}C is not supplied, leading to an apparent age difference. The age difference in the North Atlantic Ocean is approximately 400 years (Bard et al., 1991). To correct the indifference dating, calibration of radiocarbon dating is necessary, which is done using calibration curves (Reimer et al., 2013). The bulk sample for 08H_101 at the interval of 3500-3580cm might contain uncertainty, and the radiocarbon date might not be accurate.

4 Results





In this chapter, the results from the analytical work on core GS20-229-28GC and Borehole 08H_101 are described to understand the stratigraphy of the Frøyabanken and Halsafjorden. The results will be presented in the following manner:

- I) Seismic interpretation, lithostratigraphy, and chronology of Frøyabanken
- II) Seismic interpretation, lithostratigraphy, and chronology of Halsafjorden
- III) Recalibration of the previously published dates

4.1 Seismic interpretation of the Frøyabanken

Six lines were interpreted for Frøyabanken, Froya1, Froya2, Froya3, Froya4, Froya5, and Froya6. Core GS20-229-28GC is located on Froya1 (Fig. 9). Five horizons have been analyzed: Seabed (RF0), Sandy Layer (RF1), Top Glaciomarine (RF2), Base Glaciomarine (RF3), LGM (RF4), and RF5 (Fig. 10). All horizons were interpreted using a combination of manual and automatic interpretation. Based on the understanding of reflectors/horizons, the seismic characteristics of Frøyabanken (Table. 4) can be divided into F-I) transparent discontinuous facies with low-amplitude reflectors that are discontinuous and continuous in the NE and SW; F-II) semi-transparent discontinuous facies mostly discontinuous throughout the seismic lines; F-III) Laminated parallel facies discontinuous throughout the lines that probably might be glaciomarine or hemipelagic deposits, and F-IV) very low amplitude facies with parallel laminated reflectors that are hardly visible in the seismic lines that might be deposited after the LGM.

Table 4. Geophysical examples of seismic characteristics

	Seismic Facies	Example from Geophysical data
F-I	Transparent	
F-II	Semi-Transparent with very low reflection	
F-III	Parallel laminations with moderate-low reflections	
F-IV	Very low amplitude reflections, hardly visible	

4.1.1 Seismic stratigraphy

Based on the seismic characteristics of the reflectors, the seismic units can be divided into the following units:

Seismic unit SF1: SF1 is located between the RF0 and RF1 reflectors. The SF1 was transparent and discontinuous throughout the Froya1, Froya2, Froya3, Froya4, Froya5, and Froya6 lines (Figs. 10 and 11). There is a presence of low reflection amplitude in SF1. It is present in the NE and SW and is discontinuous in the middle of Froya1 and 2. It is very thin on Froya5 and Froya3. It disappears Northwest of Froya 5 (Fig. 12).

Seismic unit SF2: SF2 lies between the RF1 and the RF2 reflector. SF2 is more discontinuous relative to SF1. It was transparent and had a low reflection amplitude. The reflectors associated with this unit were present in the NE and SW. It is present in all lines except for Froya4. It is present in the Froya3 to Froya5 seismic lines and then disappears Northwest of Froya5 (Figs. 11 and 13).

Seismic unit SF3: This seismic unit lies between the RF2 and RF3 reflectors. The SF3 is characterized by moderate parallel reflections visible in the seismic lines. However, it is discontinuous throughout the lines. Because of the distinctive parallel characteristics of seismic reflectors, it may be interpreted as glaciomarine/hemipelagic sediments. In lines such as Froya3 and Froya5, the seismic unit at the base forms a drape deposited after a significant glaciation event, as shown in Figures 10, 11, 12, and 13. This drape pattern is visible with an upward trend from NW to SE. The top of the seismic unit is smooth in Froya1 and Froya2 lines, but in Froya3 and Froya5, it is disrupted in some places due to erosion or sliding events.

Seismic unit SF4: SF4 is only visible in some parts of the seismic lines and only occurs intermittently. The reflector RF3 separates the units SF3 and SF4, which is chaotic and discontinuous. (Figs. 10 and 11). SF4 can be observed in the Froya3 and Froya5 lines in the NW and SE parts of the lines. At the top of the seismic unit, the RF3 reflector is continuous throughout the seismic lines (Figs. 10 and 11). This SF4 is visible in Froya 5 and Froya 3, indicating that the units before RF3 eroded (Figs. 10 and 13). SF4 unit's base is indicated by RF4, which is hardly visible in seismic lines.

Seismic unit SF5: SF5 is hard to interpret due to the limitations of the seismic survey as it is only visible in Froya1 and Froya2 (Fig. 11). It has irregular patterns and might be subglacial till.

Ridges A, B, and C: Possible presence of a ridge can be interpreted in the seismic line Froya 1 (Fig. 10). The seabed surface and seismic interpretation show that Ridge A might be in a composite form, followed by a small ridge, that is, Ridge B. Some buried and erosive surfaces below Ridge A cannot be interpreted because of the limitations of the seismic survey (Fig. 10). Nygård et al. (2004) discussed the possibility of moraine in this offshore region, and Ridge A could be interpreted as Moraine because the reflectors are chaotic, followed by the SF3. It becomes less visible and hardly visible throughout the lines as it turns into small ridges. These ridges are parallel to the ice-flow direction, and based on evidence from previous studies, these could be interpreted as lateral moraines (Ottesen et al., 2022; Ottesen et al., 2005). Ridge C, visible on Froya2, is the most prominent ridge in Frøya, probably related to the event (Fig. 12). Another characteristic of Ridges A, B, and C is that they are up to 50m in height, as shown in Figures 12 and 13, which could be interpreted as being one of the characteristics of lateral moraines (Ottesen et al., 2022; Ottesen et al., 2005; Stokes and Clark, 2002).

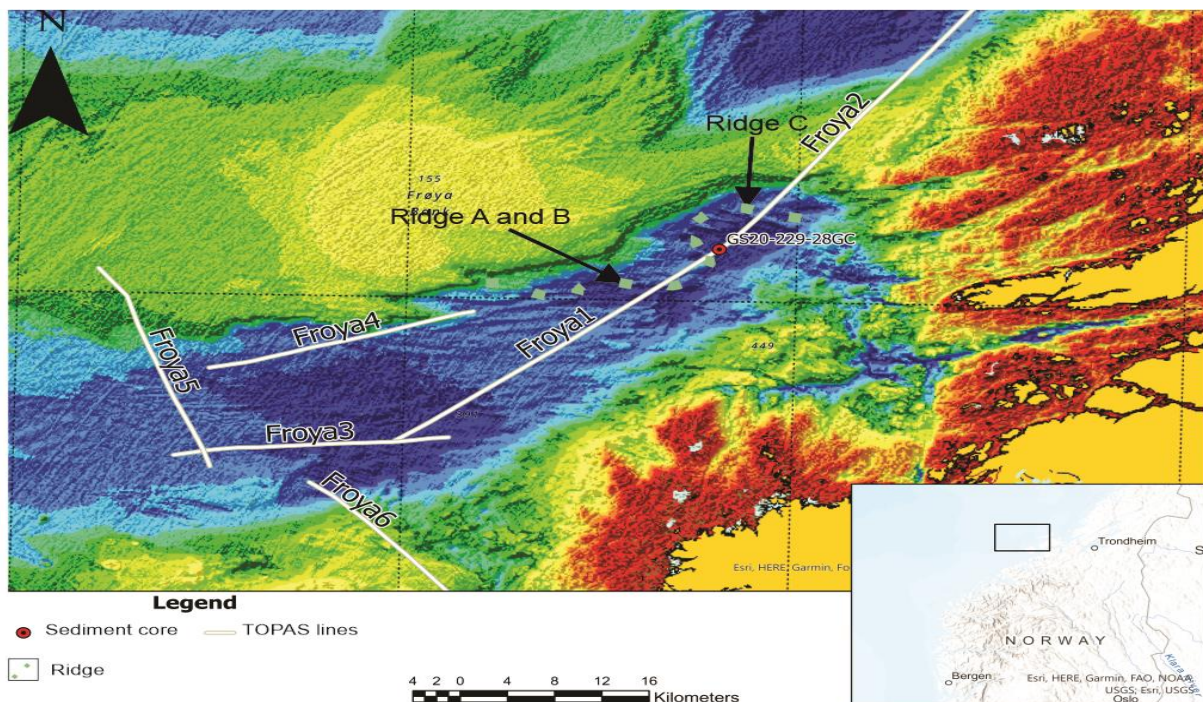


Fig. 9. Positions of seismic lines (white lines) of Frøyabanken along with core position and glacial landforms, i.e., Ridges A, B, and C.

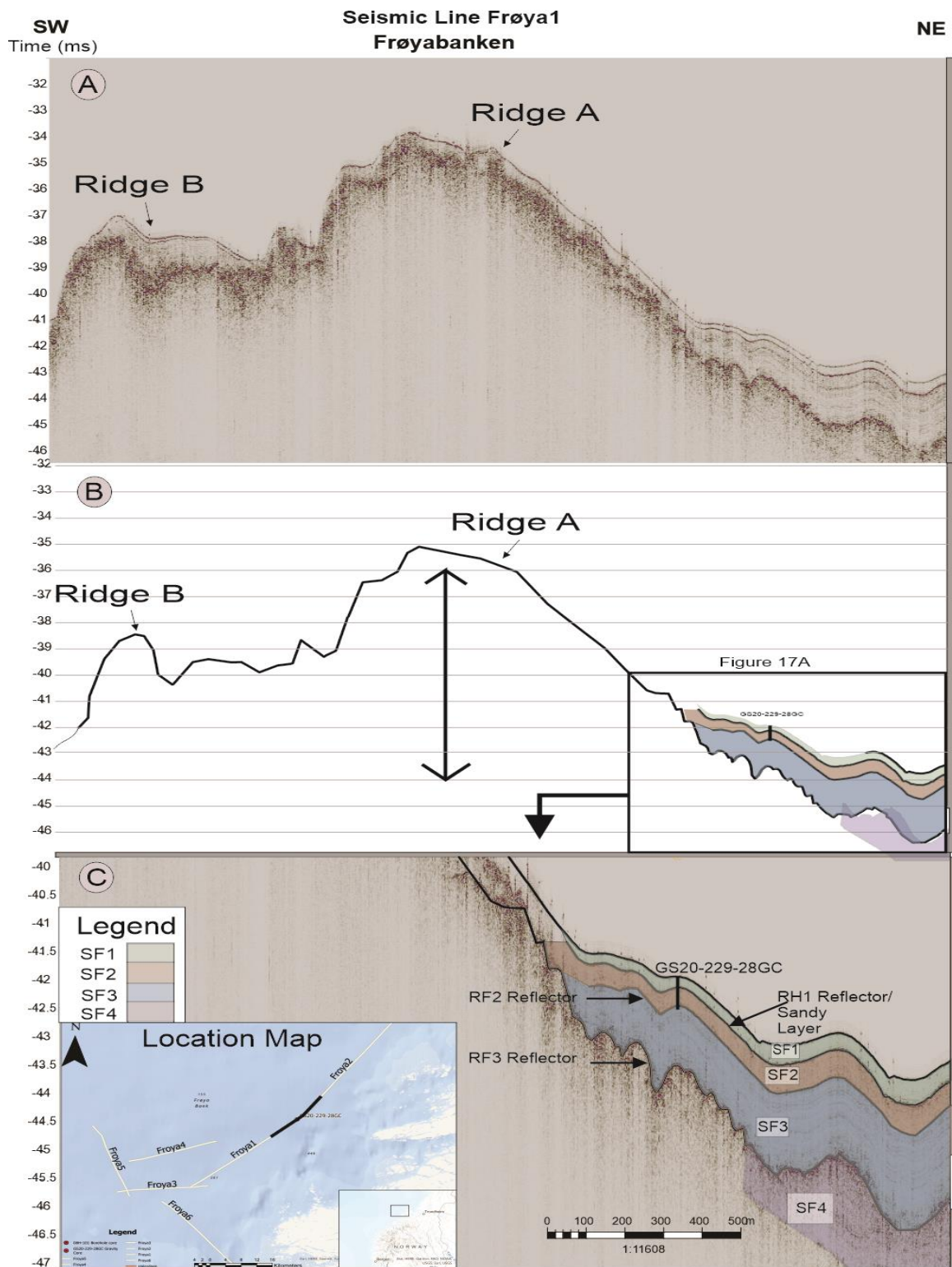


Fig. 10. (A) Seismic line of Frøya1 pre-interpretation (B) Ridges across the seismic lines of Frøya1. (C) Illustrates the seismic interpretation of Frøya1, the relative seismic units, and the core location: SF1, SF2, SF3, and SF4.

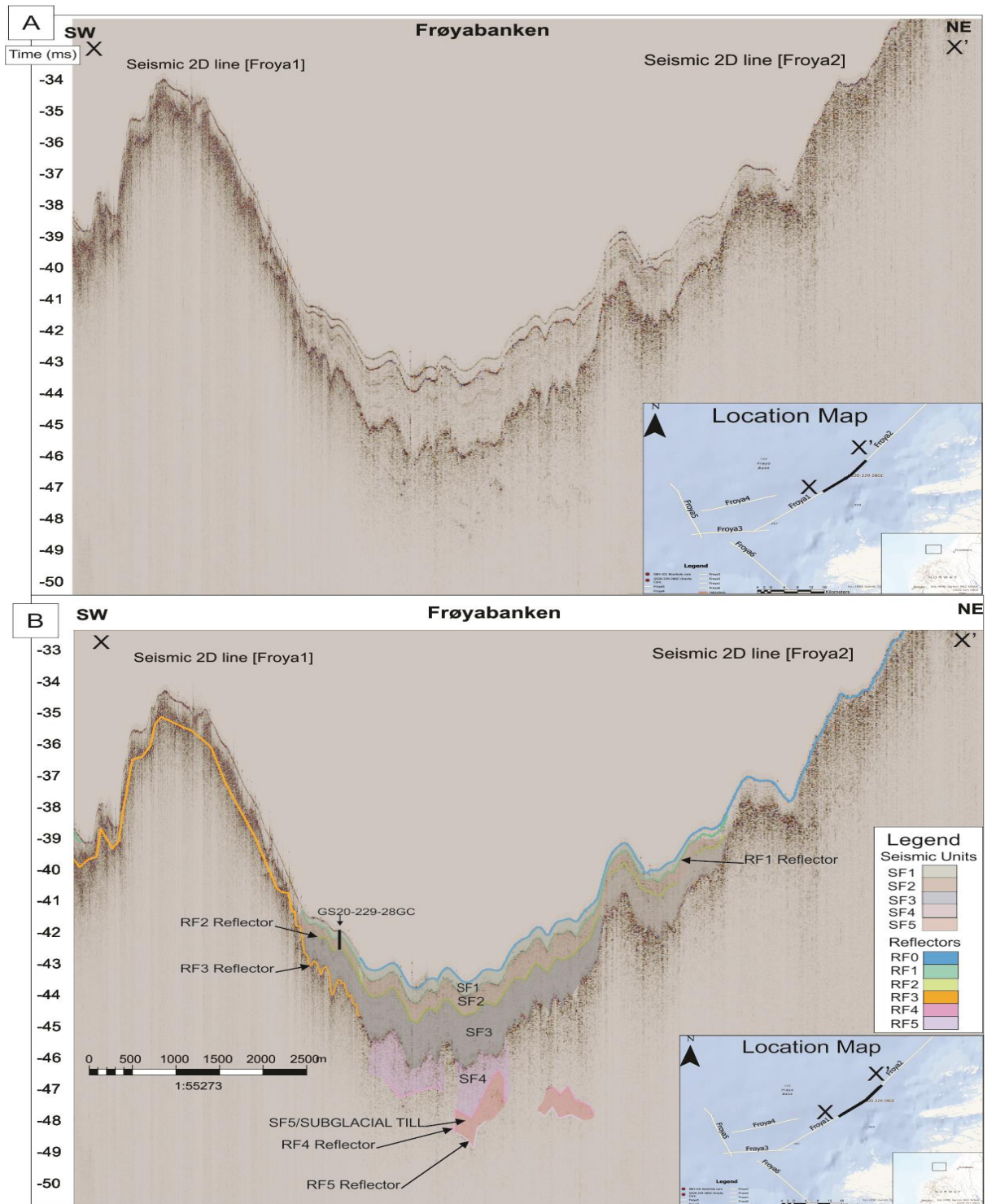


Fig. 11. A) Seismic line of Froya1 and Froya2 pre-interpretation (B) Illustrates the seismic interpretation of Froya1 and Froya2, the relative seismic units, and the core location: SF1, SF2, SF3, SF4, and SF5.

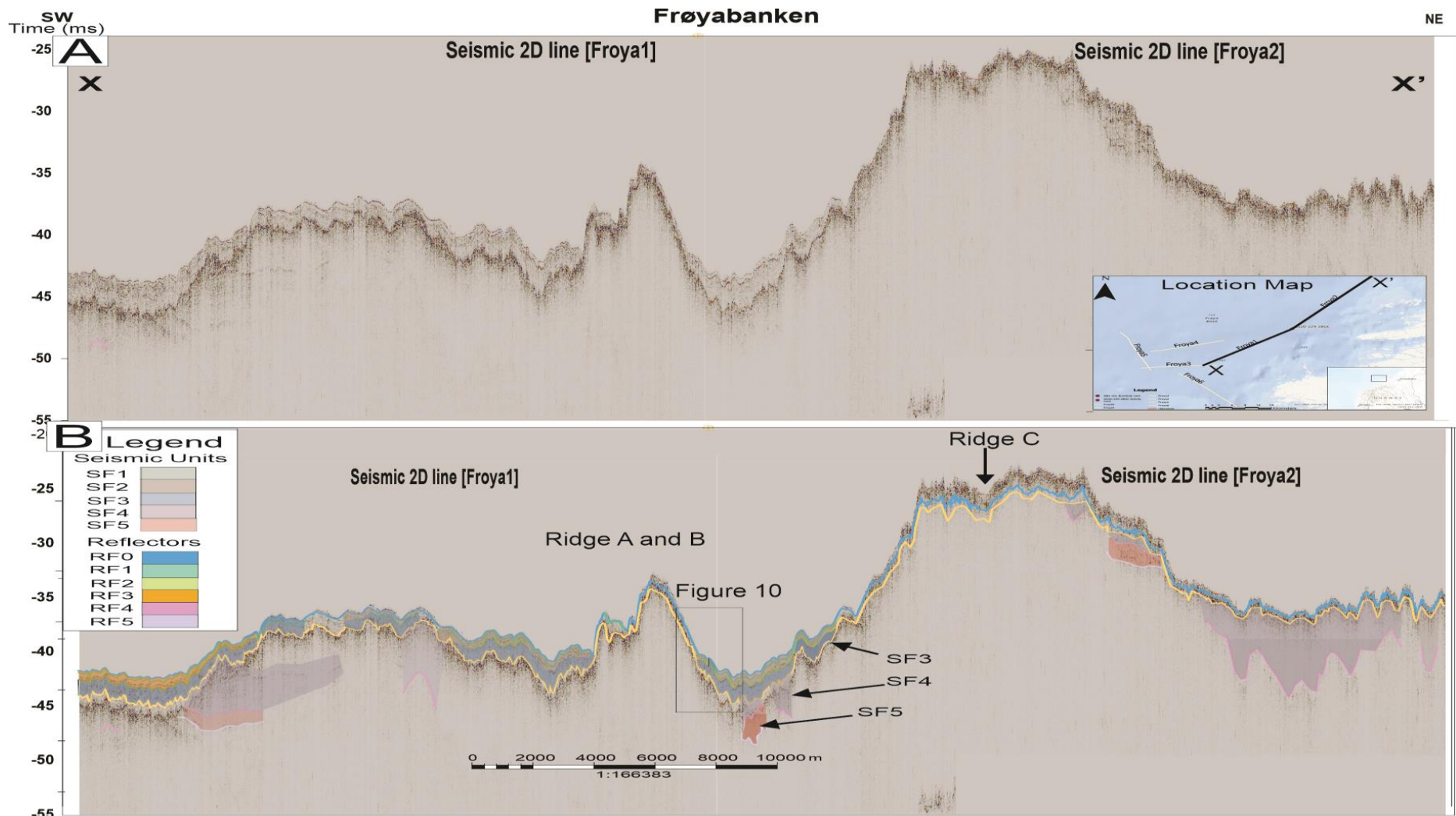


Fig. 12. (A) A raw seismic survey of the Froya1 and Froya2 lines. (B) Seismic interpretation of Ridges A, B, and C. It also shows the seismic units SF1, SF2, SF3, SF4, and SF5, and seismic reflectors: RF0, RF1, RF2, RF3, RF4 and RF5.

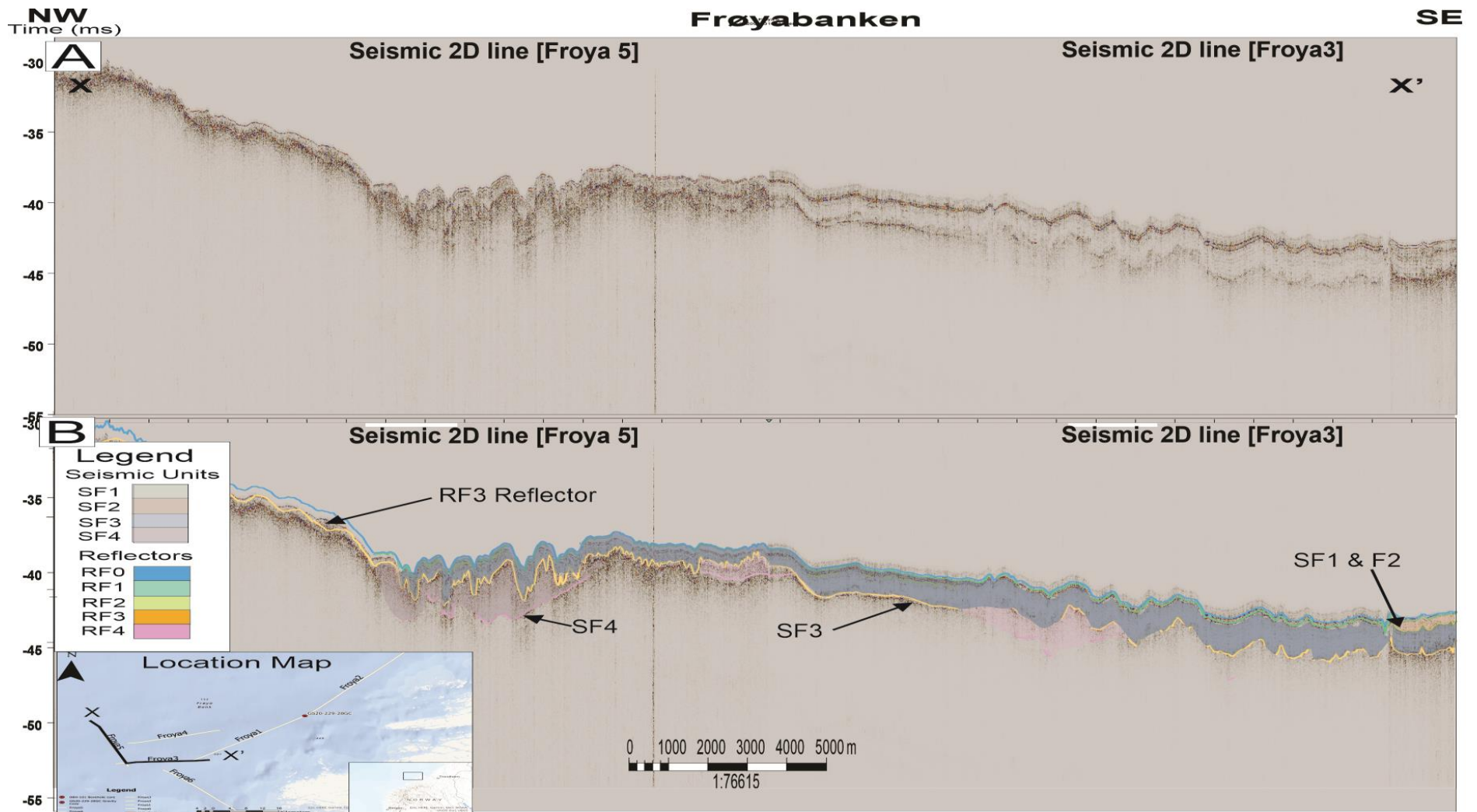


Fig. 13. (A) Raw seismic survey of the Froya5 and Froya3 lines. (B) Seismic interpretation of Froya5 and Froya 3 lines along with seismic reflectors: RF0, RF1, RF2, RF3, and RF4. It also shows the seismic units SF4, SF3, SF2, and SF1.

4.1.2 Core GS20-229-28GC (Frøyabanken)

Based on the visual description, grain size analysis, XRF elemental analysis, grain size analysis, and undrained shear strength, the gravity core GS20-229-28GC (4.27m) can be divided into four main lithostratigraphic units (Fig. 14).

LF4: LF4 is the lowermost part of GS20-229-28GC, extending from 140–427 cm in length. The lithology of the core is uniform in this part, as it is clayey silt and predominantly composed of shell fragments from 280-380 cm. There were also signs of minor bioturbation in this part of the core (Fig. 15). The grain-size distribution in this core unit was uniform. However, at the end of this unit, the grain size fluctuated slightly, especially that of $D_x(10)$, showing a much finer grain size at the end of the core, between 360 and 420 cm. The Ca/Fe elemental ratio decreased significantly in this unit (Fig. 14). It started with a slightly higher value and became uniformly low in the lower part of the unit. K (cps) is uniform. Zr (cps) and Br (cps) remained the same throughout LF4. The shear strength in this unit fluctuated but stayed at approximately 8-13 throughout the core (Fig. 14).

The grain size distribution is based on cumulative grain size, and the grain size has been divided into three-grain types, i.e., grain size particles greater than 63 μm , 125 μm , and 1000 μm according to the classification of Wentworth grain size distribution (Wentworth, 1922). Twenty-eight samples were collected from the core of this section for grain size analysis, each at an interval of 10 cm (Fig. 14). The presence of grain size particles $> 125 \mu\text{m}$ fluctuated while the $>63 \mu\text{m}$ and $>1000 \mu\text{m}$ remained uniform, with $>63 \mu\text{m}$ increasing in the amount at the end of LF4 between 140 and 200 cm; sand % increased close to 180 cm and 320 cm, while it decreased significantly at the bottom of the core (Fig. 15). According to the Sand Clay Silt diagram made through GRADISTAT software (Blott and Pye, 2001), the lithology of LF4 would be silt, as most of its grain size falls within that ratio (Fig. 15).

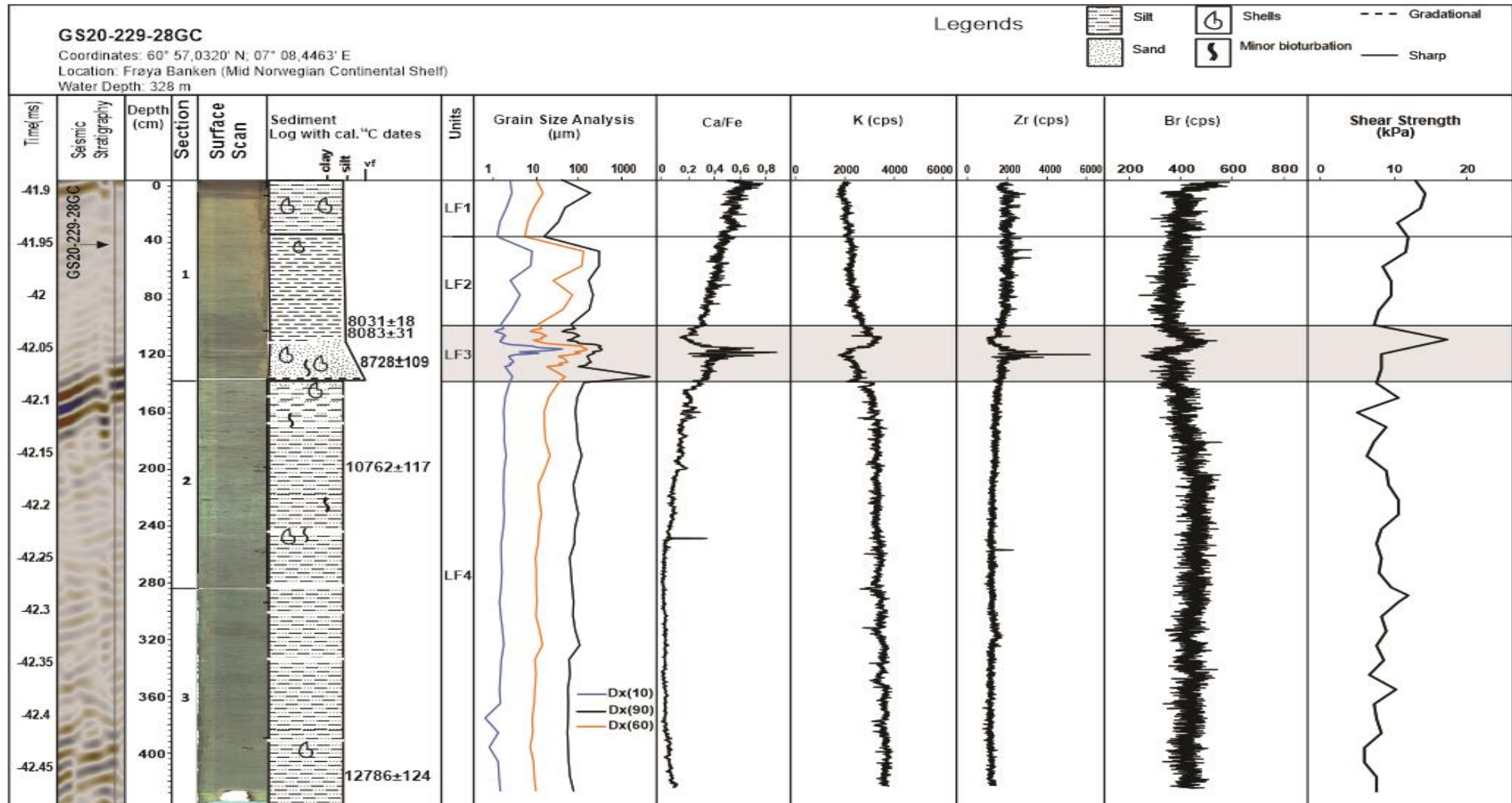


Fig. 14. Lithostratigraphy of GS20-229-28GC with seismic stratigraphy (time ms), core surface image, sediment log along with chronology, grain size distribution (μm), Ca/Fe ratio, K, Zr, and Br XRF elemental cps (counts per second), and shear strength kPa (kilopascal).

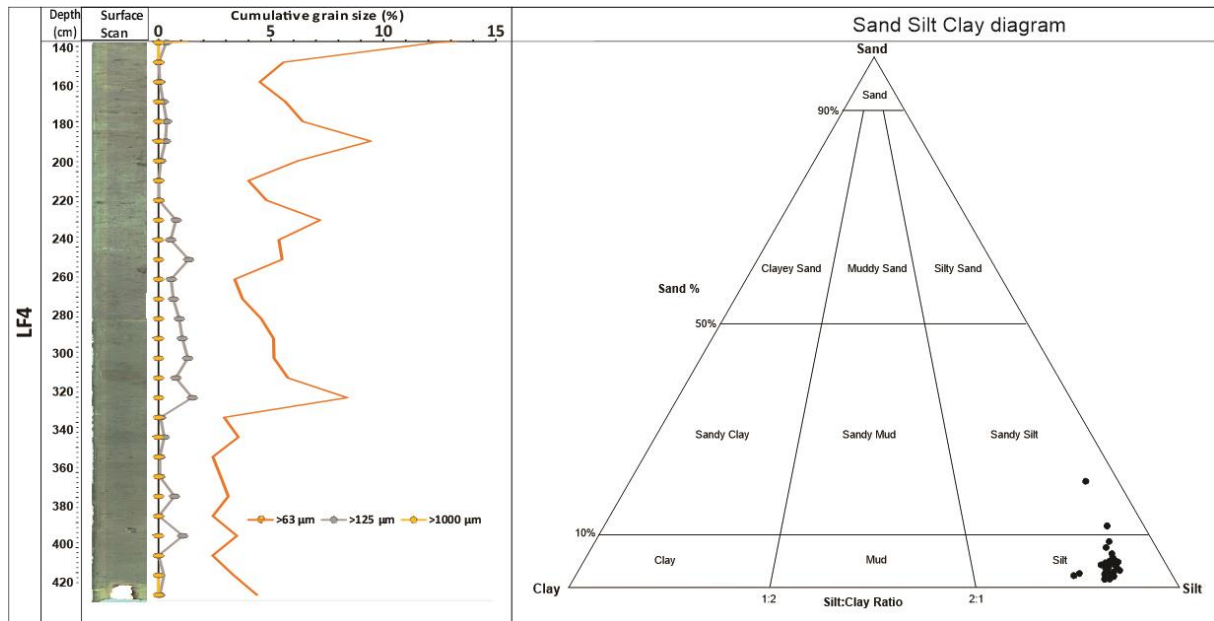


Fig. 15. Grain size distribution of LF4 with different grain sizes, i.e., > 63 μm , > 125 μm , and > 1000 μm . In addition, the sand silt clay diagram is also shown, which shows the scattering of grain sizes on the diagram.

LF3: LF3 starts at 100-145 cm and shows significant variations in grain size, XRF elemental analysis, and shear strength (Fig. 14). The lithology of this unit transitions from clay to silt to very fine silt. This transition is marked by the grain size analysis, showing an increase in the size of the particles to D_x (10), D_x (50), and D_x (90). The Ca/Fe ratio also increased at 100–145 cm intervals. Similarly, Zr and Br show spikes in the results between 110-120 cm, while K decreases after a spike (Fig. 14). The shear strength increased by up to 20 kPa in LF3. The sediment log shows the presence of a sandy layer, which can also be observed in the core surface scan of LF3.

The grain size analysis of LF3 was performed by collecting samples from 100 cm to 130 cm (Fig. 16). Thirty samples were collected from each unit. The detailed sampling for this unit was performed because of the lithological variation in the core, indicating the presence of a sandy layer (Fig. 16). The grain size started uniformly with less >125 μm grain size particles than >63 and >1000 μm at 100-105 cm. Then, the >63 μm particles increased abruptly from 1-70% between 112 and 17 cm (Fig. 16). The >63 μm grains maintained their presence at 117–130 cm (Fig. 16). However, at the end of the unit, from 130 to 140 cm, >63 μm grains fluctuate between 10-30%. The >63 and >125 μm grains decreased at intervals of 112–17 cm, close to 0 and 10% for clay and silt, respectively. Figure 15 shows spikes in the >1000 μm grains percentage at 130-140 cm within LF3.

Geologists have used the XRF analysis of various elements to understand paleoclimate proxies (Rothwell, 2015). As shown in Figure 14, the XRF analysis of different elements, Ca/Fe, Zr, K, and Rb, fluctuated in LF3. The Ca/Fe ratio spikes between 110 and 130 cm in LF3 and is uniform throughout the core. Similarly, K (cps), also used to identify the sandy layer in the core, showed variation in LF3. Zr and Rb also indicate the presence of a sandy layer (Croudace et al., 2006; Rothwell, 2015). Br (cps), as shown in Figure 14, indicated the presence of organic matter in LF4 (Thomson et al., 2006). Grain size grading and XRF elemental ratios can be correlated to identify the sandy layer and the presence of grain size variations, as shown in Figure 15 (Rothwell, 2015). LF3 represents the grain variation in the grain size and XRF elemental analysis. The grain size of sand increases significantly with Ca/Fe, K, Zr, and Rb, indicating the presence of a sandy layer at intervals of 100–140 cm, as shown in Figure 14 and Figure 16.

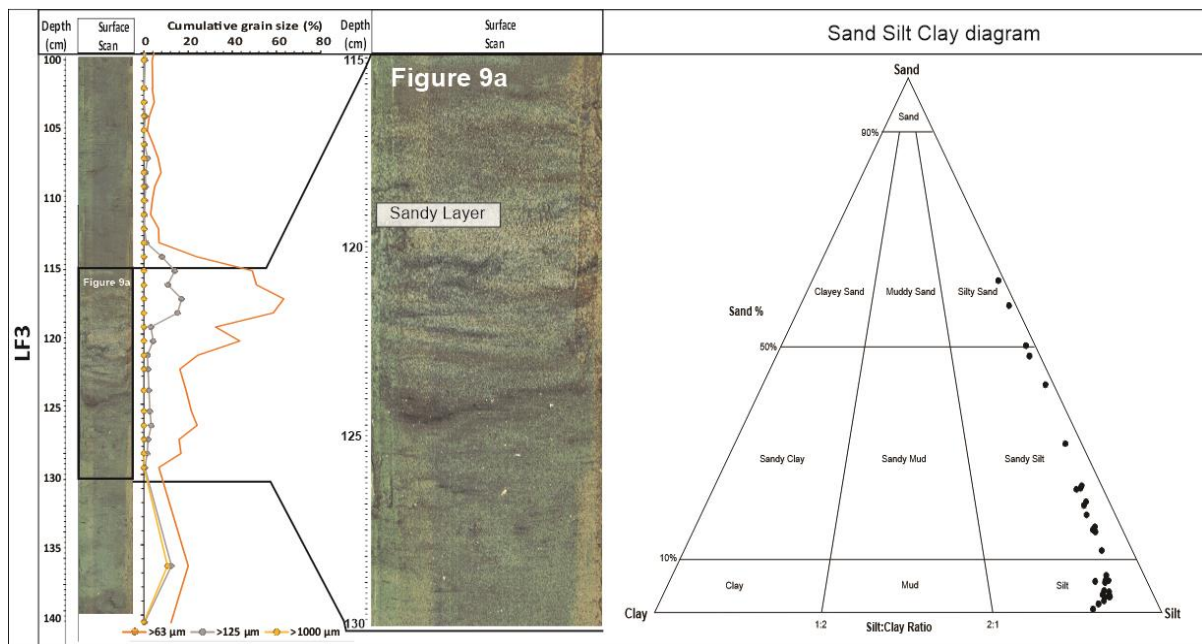


Fig. 16. Grain size distribution of LF3 with different grain sizes, i.e., > 63 μm, > 125 μm, and > 1000 μm. In addition, the Sand Silt Clay diagram is also shown, which shows the scattering of grain sizes on the diagram.

LF2: LF2 starts at 39-100 cm. LF2 is primarily clayey silt and shows a uniform lithology (Fig. 17). The grain size increased at the beginning of LF2 and gradually decreased within the unit. The XRF elemental ratio of Ca/Fe, along with K, Zr, and Br, remained uniform in this unit (Fig. 14). The shear strength fluctuated slightly but remained uniform throughout this unit.

Six samples were used for the grain size analysis. The grain sizes(%) of >125 and >63 μm grains started at 10 and 20% at intervals of 40 cm. The >63 and >125 μm grains remained steady throughout the unit (Fig. 17). In the Sand Silt Clay diagram, LF2's first two samples were plotted as silt. In contrast, the other samples are plotted as Sandy Silt and Silty Sand, respectively (Fig. 17).

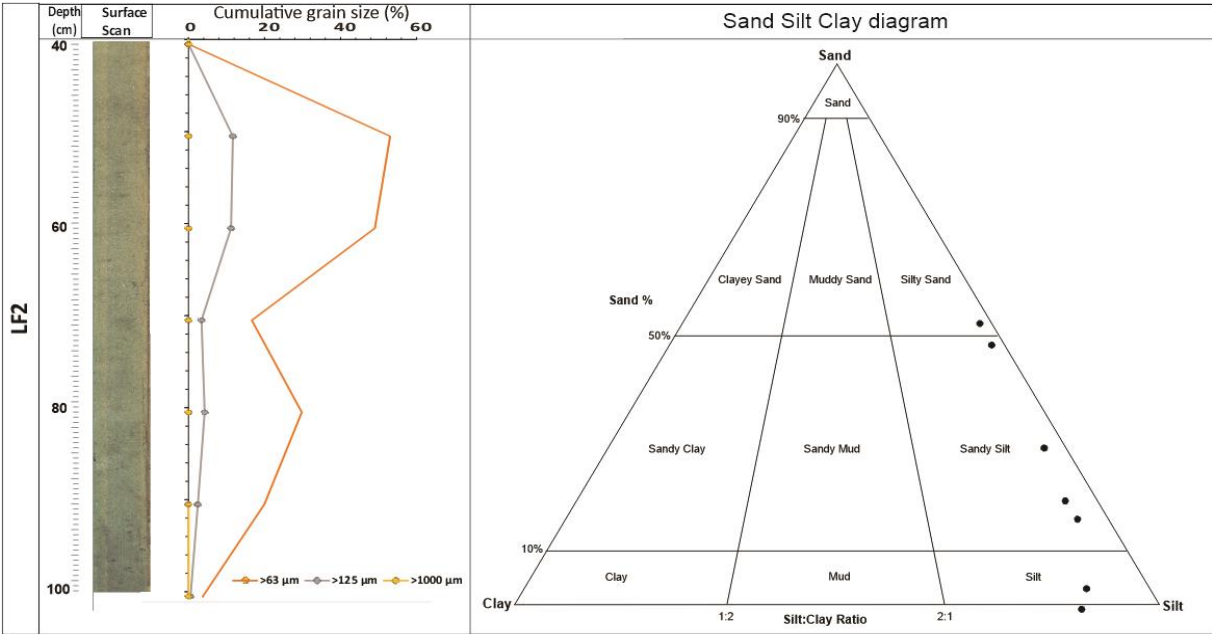


Fig.17. Grain size distribution of LF2 with different grain sizes, i.e., > 63 μm , > 125 μm , and > 1000 μm . In addition, the Sand Silt Clay diagram is also shown, which shows the scattering of grain sizes on the diagram.

LF1: LF1 is the uppermost core unit from 0-39 cm (Fig. 18). The lithology of LF1 is silt and comprises silt and clay. The sediment log showed the presence of shell fragments and minor bioturbation. The XRF elemental ratio of Ca/Fe remained uniform throughout LF1 with fewer spikes. Zr, Br, and K showed no significant changes throughout LF1 (Fig. 14). The shear strength increased slightly at the beginning of LF1 (0–20 cm) and decreased after 20 cm. Grain size showed no significant spikes, except for Dx (90) between 0 and 20 cm in LF1.

Five samples were taken at an interval of 10 cm for grain size distribution. The grain sizes of > 63 and >125 μm grains were 5% and 20%, respectively (Fig. 18). The number of >125 μm grains increased at intervals of 10 cm and then remained uniform throughout LF1. >63 μm grains remain uniform throughout the Unit (Fig. 18). In the Silt Clay Sand diagram, the four samples are plotted in silt, whereas the one with a high Sand % is plotted in Silty Sand (Fig. 18).

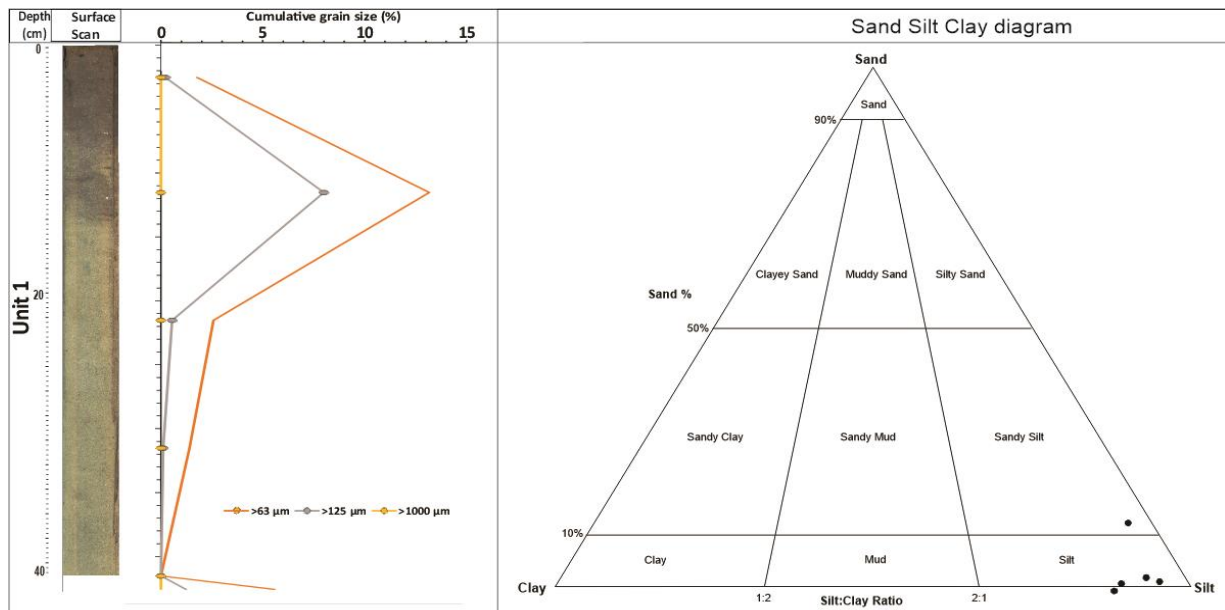


Fig. 18. Grain size distribution of LF1 with different grain sizes, i.e., $> 63 \mu\text{m}$, $> 125 \mu\text{m}$, and $> 1000 \mu\text{m}$. In addition, the Sand Silt Clay diagram is also shown, which shows the scattering of grain sizes on the diagram.

4.1.3 Correlation between the seismostratigraphy and core stratigraphy on Frøyabanken

Based on the seismic characteristics of the reflectors and the lithostratigraphy of the core, the seismic units can be divided into the following units:

SF1: Two units can be correlated to this SF1: LF1 and LF2. LF1 is very dark gray and goes from fine grain to medium grain size downward towards LF2. Because of its chronology and seismic characteristics, it can be regarded as a marine sediment. The geotechnical properties of this unit, that is, undrained shear strength, fluctuate between 9-15 kPa, and the sand content is 0-50%. The lithology of this seismic unit ranges from silty mud-muddy sand, and the grain size varies from fine to sand.

SF2: The unit associated with this seismic unit is LF3, which shows spikes in the grain size, XRF elemental analysis, and undrained shear strength. Due to the lithostratigraphy and seismic interpretation, this seismic unit could be interpreted as a sandy layer from a mega slide. In the sediment log (Fig. 13), there is the presence of a dark lamina in the sandy layer.

SF3: The unit associated with this seismic unit is LF4. Due to its low sand content and uniform grain size, its distinctive parallel reflectors might be interpreted as glaciomarine/hemipelagic sediments.

4.1.4 Chronology of Frøyabanken

The chronology was created based on lithological and grain size variations for the generation of the age model. Utilizing the OxCal calibration program, datings were generated in connection with the last seismic study reflector. Table 5 displays the dates derived from the 95.4% credible ranges using the Bayesian age model (Fig. 19). The dates for the Holocene period in Frøyabanken were calibrated using the Marine20 curve with ΔR of -148 ± 33 years as derived from the western Norwegian calibration database (Mangerud et al., 2006).

The age model for GS20-229-28GC revealed that the sedimentation of the SF3 unit of Frøyabanken might have started from 17.5 ka yrs cal. BP (Fig. 19A). The depositional history covers a period of 17.5 ka cal. yrs BP to recent times. Tau Boundary was used to reflect the homogenous sedimentation of SF3, as observed in the XRF and grain size analyses. The base of the last reflector age of the SF3 was modeled using the Normaine18 curve (Pre-Bølling) and Tau Boundary for a more exact age model. The sandy layer is separated by a P_Sequence to correctly date the depositional history of the sandy layer (Fig. 19B). For more uniform sedimentation in the SF3 above 128 cm depth.

Table 5. AMC ^{13}C data from GS20-229-28GC. The data are represented by conventional aging, calibrated ^{14}C (BP), and Modelled age at the percentile interval of 95.4%, along with its corresponding Units and Seismic Units. Note that the Holocene ^{14}C ages was calibrated using the Marine20 (Heaton et al., 2020) (with ΔR value of 148 ± 33) and the Normaine18 curve was used (Brendryen et al., 2020) for the pre-Holocene period.

Core no.	Lab id no	Depth core (cm)	Dated material	Conventional ^{14}C age $\pm 1\sigma$ (BP)	Calibrated ^{14}C Age (BP) median $\pm 1\sigma$	Litho Unit	Seismic unit
GS20-229-28GC	Beta-638586	101-	<i>Uvigerina</i>	7620 \pm 30	8031 \pm 18	LF3	SF2
		102	<i>mediterranea</i>		(Marine20)		
GS20-229-28GC	Beta-638587	106-	<i>Uvigerina</i>	7640 \pm 30	8083 \pm 31	LF3	SF2
		107	<i>mediterranea</i>		(Marine20)		
GS20-229-28GC	Beta-638588	128-	<i>Uvigerina</i>	8180 \pm 30	8728 \pm 109	LF3	SF2
		129	<i>mediterranea</i>		(Marine20)		
GS20-229-28GC	Beta-638589	201-	<i>Uvigerina</i>	9820 \pm 30	10762 \pm 117	LF4	SF2
		202	<i>mediterranea</i>		(Marine20)		
GS20-229-28GC	Beta-638590	418-	<i>Nonionellina</i>	11500 \pm 30	12876 \pm 124	LF4	SF3
		419	<i>labradorica</i>		(Normarine18)		

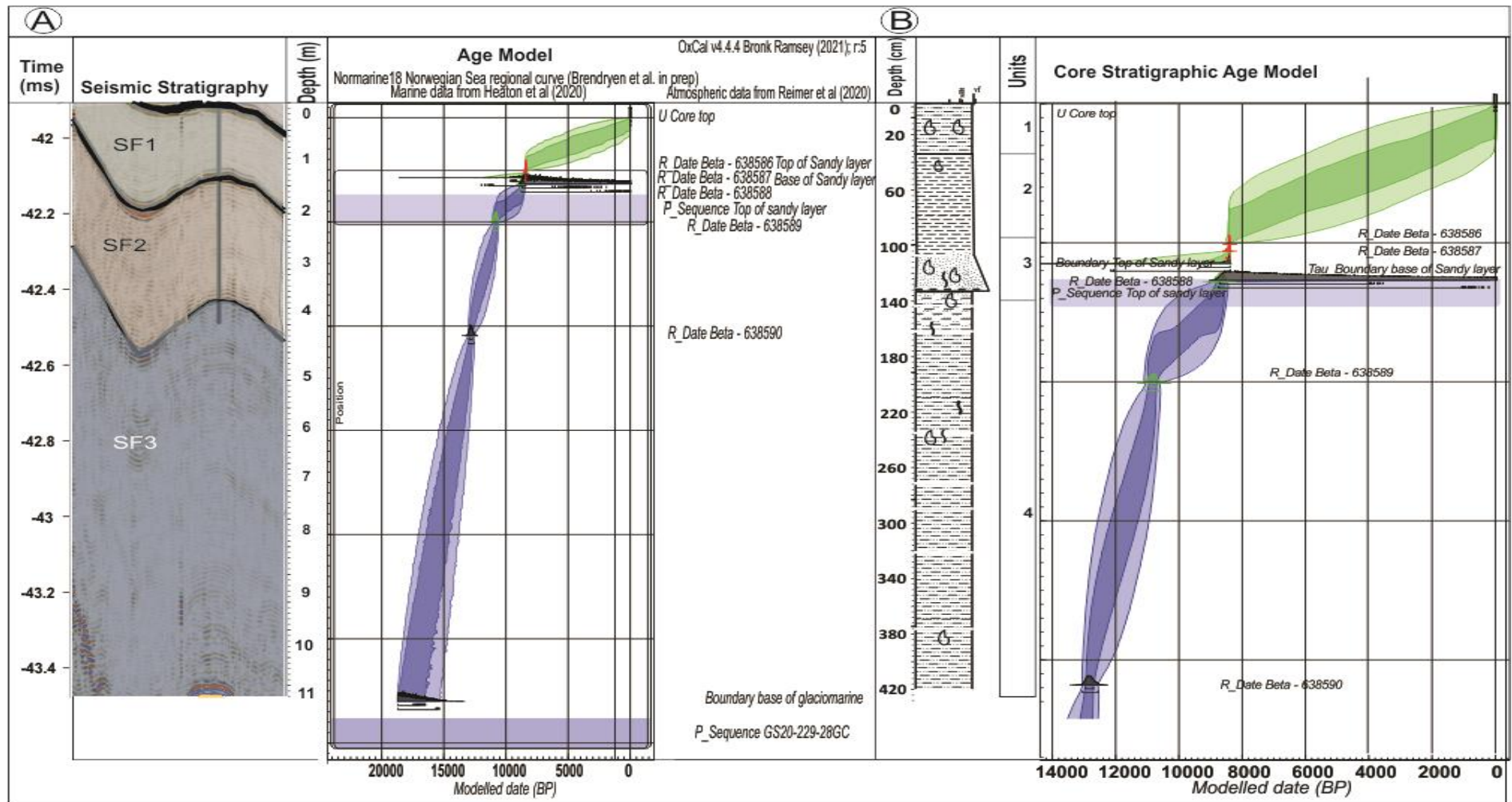


Fig. 19. (A) Age model Frøyabanken basin to the last reflector (RF3), along with the seismic stratigraphy and seismic units. (B) The core stratigraphy of the GS20-229-28GC age model is displayed along with the core log and its lithological unit.

Table 6. Characteristics of each seismic unit along with seismic facies, shear strength, and a possible interpretation.

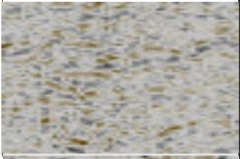

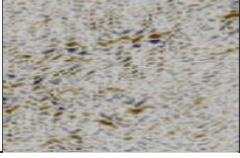
Seismic Units	Litho-Units	Seismic facies	Shear strength (kPa)	Sand content	Structures	Interpretation	Age (ka cal. BP)
SF1	LF1, LF2	F-I	9-15	0 %	Silty Mud, Muddy Sand, Grading into sand downwards from fine grain size	Marine	0-7
SF2	LF3	F-II	10-20	50-70%	Visible dark laminae of sandy layer for up to 10-20cm	Sandy Layer	7-8.5
SF3	LF4	F-III	10-15	5-10%	Downward uniform fine grading towards the bottom of the core	Hemipelagic/ Glaciomarine	10-17.5
SF4	None	F-IV	None	None	None	Glaciomarine	> 17.5 ka
SF5	None	None	None	None	None	Glacial Till	> 17.5 ka

4.2 Halsafjorden

4.2.1 Seismic Interpretation of Halsafjorden

For the seismic interpretation of Halsafjorden, 106 sparker lines were interpreted, and the stratigraphy was divided into five reflectors, including the seabed (RH0), RH1, RH2, RH3, and RH4 (Fig. 21). All reflectors were interpreted both automatically and manually. The seabed surface was also created for a more enhanced view of the bathymetry. Based on the location of Borehole 08H_101, Line H08H_01009, and Line H08H_01093 were used as examples of the seismic interpretation. Three seismic facies are found from these interpretations (Table. 7), i.e., H-I) Chaotic and discontinuous high amplitude reflectors, H-II) Continuous parallel reflectors with low-medium reflections, and H-III) Chaotic unparallel, and irregular reflections. Based on these seismic facies, the Halsafjorden will be divided into three seismostratigraphic units, i.e., SH1, SH2, and SH3, as shown in Figure 21.

Table 7. Examples of seismic facies from geophysical data.

	Seismic Facies	Example from Geophysical data
H-I	Chaotic and High amplitude discontinuous reflectors	
H-II	Parallel laminations with moderate-low reflections	
H-III	Chaotic and Irregular reflections, less continuous	

SH1: The SH1 lies between the reflectors of RH0, RH1, and RH2. It is separated into **SH1a** and **SH1b**. The seismic unit **SH1a** is transparent at the top and shows a quite chaotic reflection geometry at the base. **SH1b** seems to be dominated by transparent, high reflection amplitude (Fig. 20). This unit could be interpreted as Mass Transport Deposits (MTD) because of the chaotic and transparent reflectors (Fig. 21).

SH2: This unit lies between RH2 and RH3 (Fig. 21). This seismic unit shows distinctive parallel laminations with moderate reflection amplitude. The RH2 reflector is visible, and the reflections

are moderate throughout the seismic lines. RH3 is chaotic, and the reflections are low compared to other reflectors. Below the RH3, a chaotic and less visible reflector, i.e., RH4, can be seen throughout the lines that might indicate a presence of a glacial till (Figs. 21 and 23) that was deposited during the Last Glacial Maximum.

SH3: This seismic unit is not visible in the seismic interpretation (Figs. 21 and 23). It lies below the RH2 reflector and has some chaotic and less visible seismic characteristics. It might be a glacial till based on the chaotic and irregular pattern of reflections visible in the seismic lines.

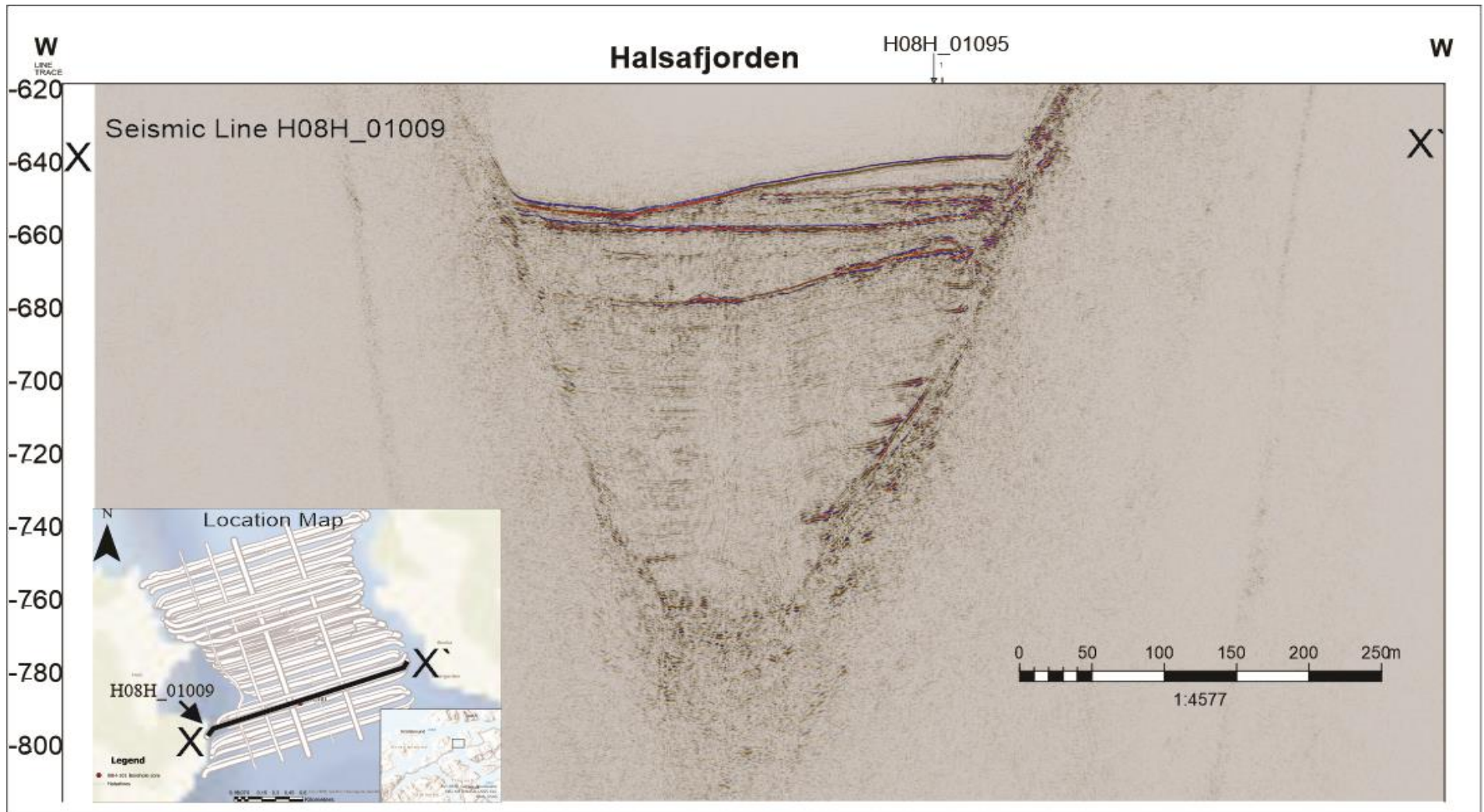


Fig. 20. Uninterpreted seismic profile of Line H08H_01009 showing the subsurface geology and possibly a glacial till.

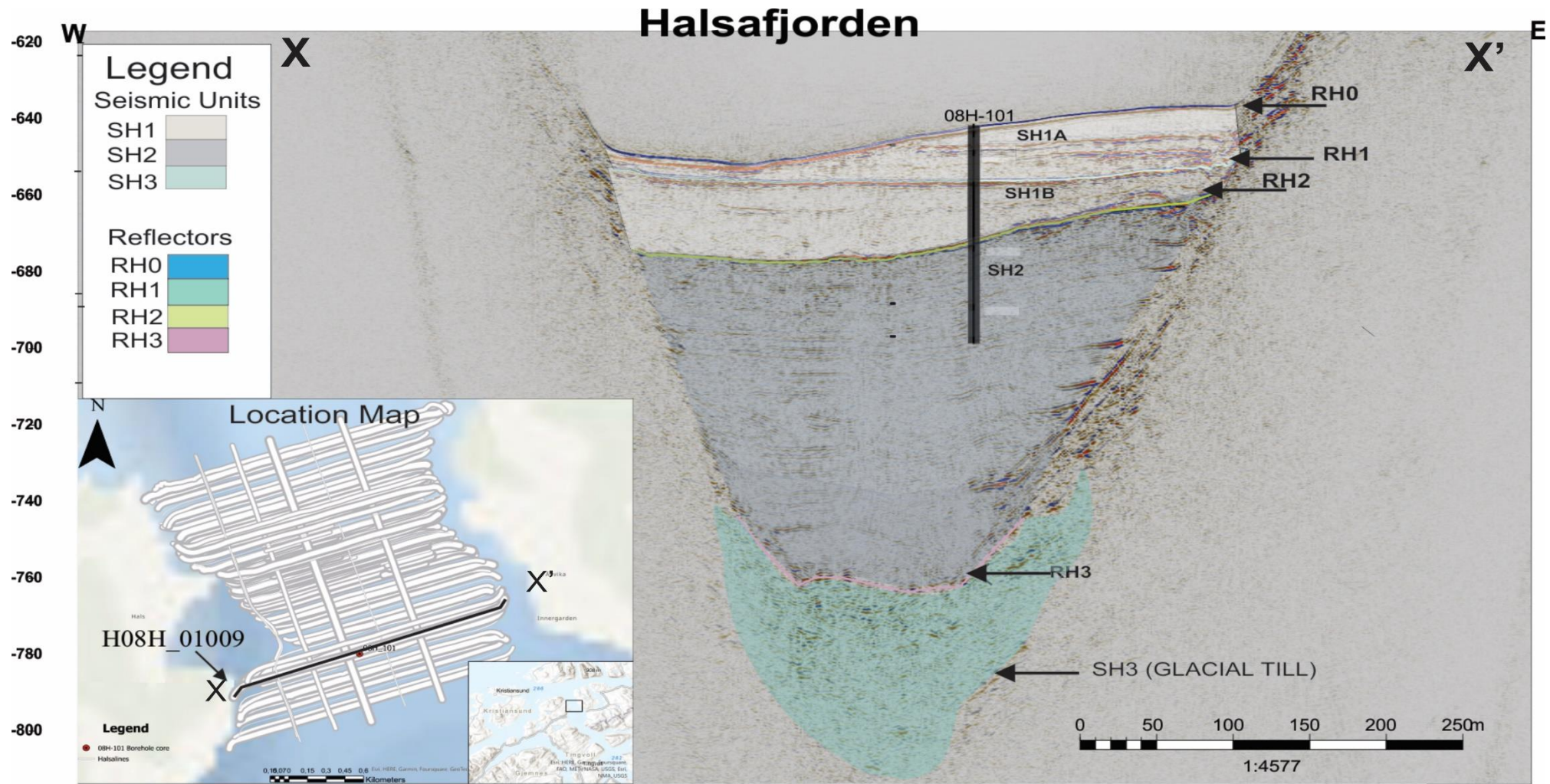


Fig. 21. Seismic interpretation of Halsafjorden Line H08H_01009. Along with seismic units, i.e., SH1A, SH1B, SH2, SH3 with reflectors RH0, RH1, RH2, RH3.



Fig. 22. Uninterpreted seismic profile of Line H08H_01095 showing the subsurface geology and possibly a glacial till. It also shows the line H08H_01005

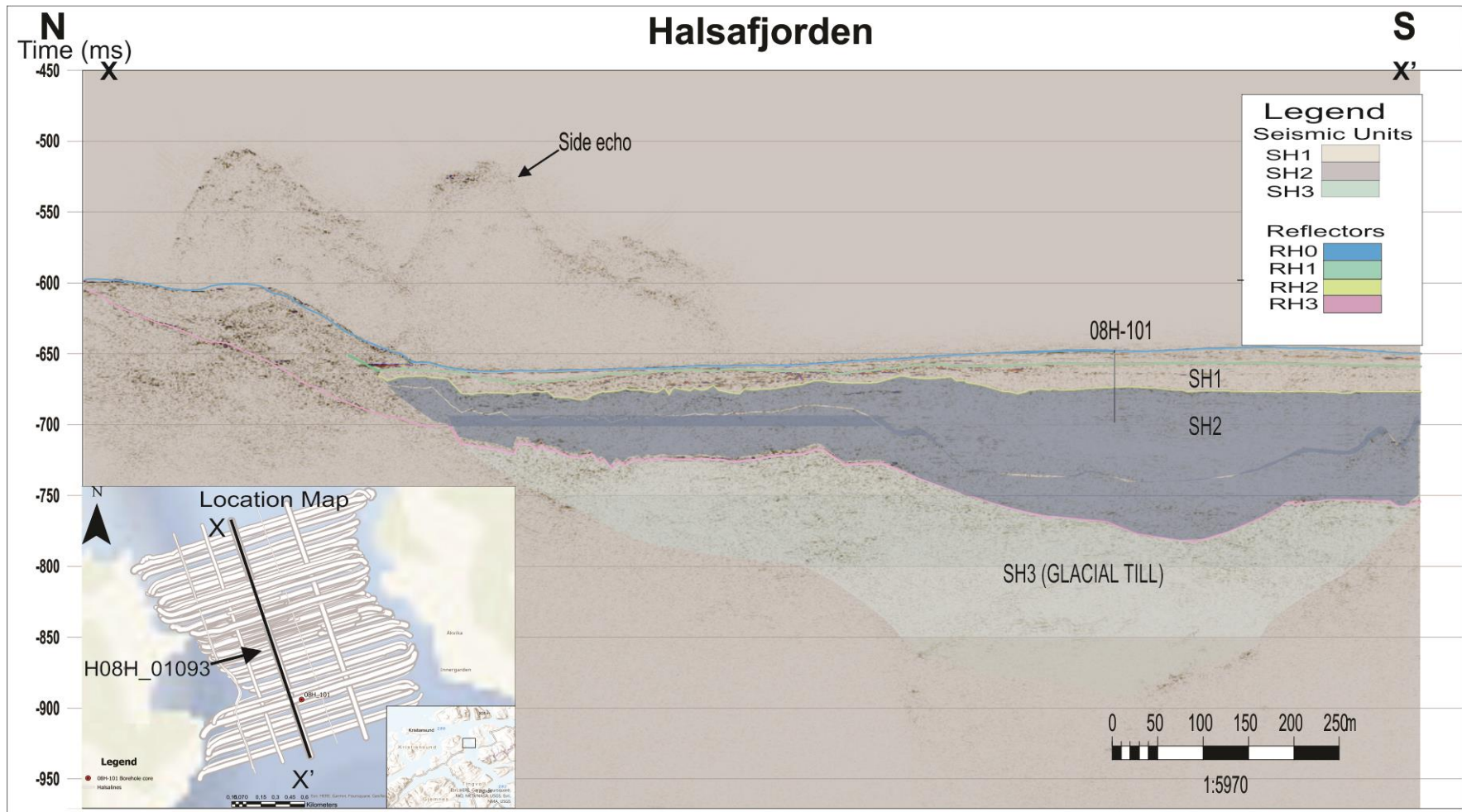


Fig. 23. Seismic line interpretation of H08H_01093. Seismic units of SH1, SH2, and SH3, along with reflectors RH0, RH1, RH2, and RH3.

4.2.2 Lithostratigraphy of Halsafjorden

For the lithostratigraphy of Halsafjorden, borehole core 08H-101 was used, which was 41.90m in length. The lithostratigraphy of the core was divided into two units: LH1 and LH2 (Fig. 24). The lithostratigraphy was divided based on grain sizes and seismic interpretation, along with the core chronology provided by Fugro (2019). The following sediment log (Fig. 24) was redrawn using the CorelDRAW Software from data provided by Fugro.

LH1: LH1 can be described as a combination of clay and sand lithologies with grain sizes ranging from silt to very coarse sand (Fig. 24). The sediment log from Fugro indicates that there are two sandy layers at the interval of 3-5m and 10-15m which might show an event in the area following the deglaciation period. The seismic stratigraphy of this unit is discussed in the seismic interpretation section.

LH2: LH2 from Halsafjorden is almost uniform in grain size and lithology (Fig. 24). It shows clay lithology with grain sizes ranging from silt to fine sand.

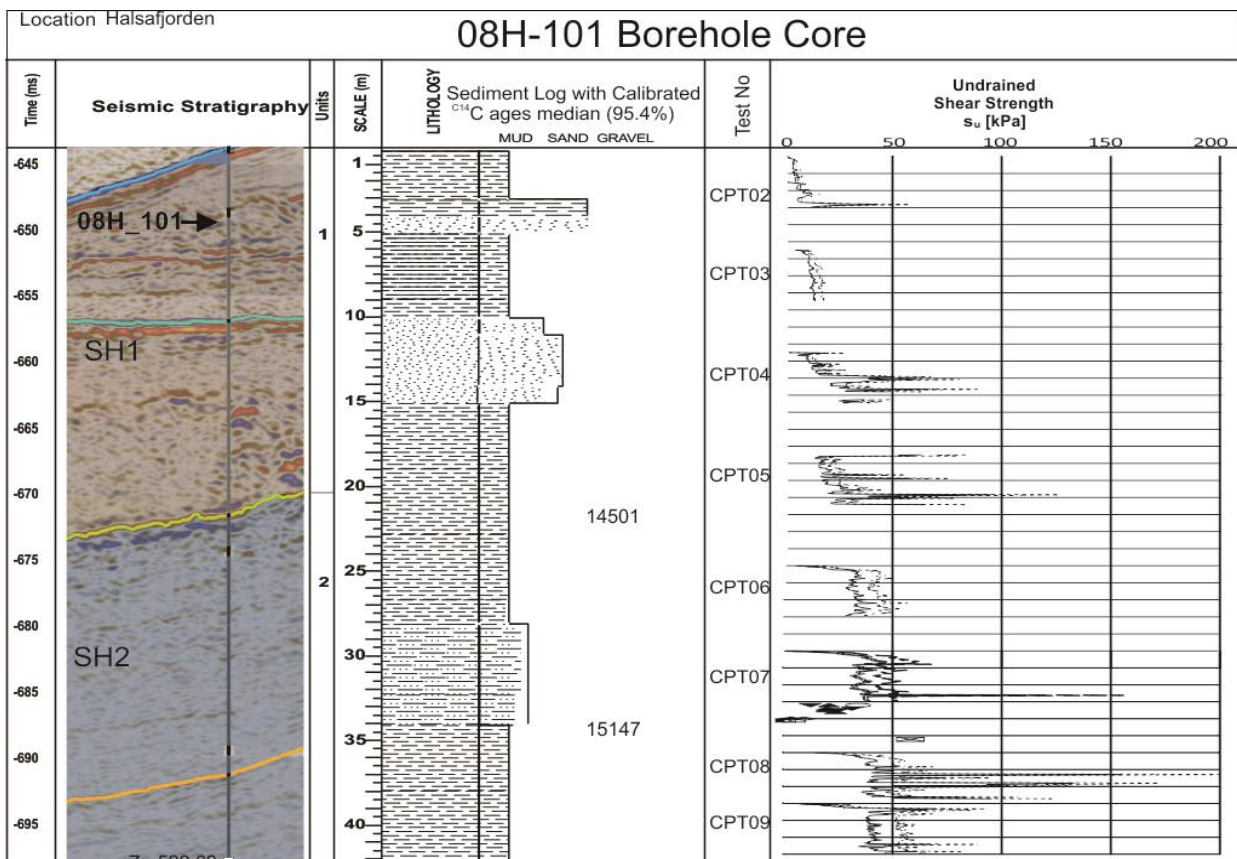


Fig. 24. Lithostratigraphy of the 08H_101 core along with its sediment log, undrained shear strength (kPa), and relative seismic stratigraphy. Data were obtained from Fugro (2019). The sediment log and CPT results were modified through Coreldraw, as described by Fugro (2019).

4.2.3 Shear strength analysis

Nine Cone Penetration Tests (CPT) were performed on this borehole to determine its shear strength (Fugro, 2019). The results show that CPT02-03 reveals that the undrained shear strength of the soil fluctuates between 0-50 kPa. CPT02 reaches up to 50 kPa, whereas CPT03 remains in the range of 20-30 (Fig. 24). CPT04 remained in the range of 0-90 kPa, while CPT05 fluctuated between 10-140 kPa. CPT06 remained in the range of 40-50 kPa. CPT07 and CPT08 increased to approximately 150 kPa and 200 kPa, respectively (Table.8). The last test, CPT09, was in the range of 10-90 kPa. Based on these results and the following parameters, the results can be interpreted as follows.

Table 8. Interpreted shear strength, along with the values obtained from the data of Fugro (2019).

Interpreted Shear Strength	Undrained Shear Strength [kPa]
Extremely low	< 10
Very low	10 - 20
Low	20 - 40
Medium	40 - 75
High	75 - 150
Very high	150 - 300
Extremely high	300 - 600
Ultra-high	> 600

Based on the above table, the CPT results can be interpreted as follows:

Table 9. Possible interpretations of CPT's shear strength are based on the table above.

CPT	Shear strength (kPa)	Interpretation
02	0-50	Medium Shear Strength
03	50	Low Shear Strength
04	0-90	Low-High Shear Strength
05	10-140	Low High Shear Strength
06	40-50	Low-Medium Shear Strength
07	150	Medium-High Shear Strength
08	200	High-Very High Shear Strength
09	10-90	Low-High Shear Strength

4.2.4 Chronology recalibration of Halsafjorden

The data for the radiocarbon dating of borehole 08H_101 were provided by Fugro (2019). It was calibrated using the Normarine18 curve for accurate dates, as Brendryen et al. (2020) described. This curve was used to provide a more detailed reconstruction of deglaciation due to

the uncertainty of reservoir ages of the Pre-Bølling Period (Brendryen et al., 2020). For correlation purposes, the dates of SH3 to the Base of the fjords have been recalibrated using the Normarine18 curve (Table 10).

Table 10. The difference in calibration of ages is based on curves used for calibration along with its conventional Age.

Core ID	Depth (m)	Lab ID	Conventional ¹⁴C(yrs) age BP	Calibrated ¹⁴C age cal yrs BP (Marine20 curve)	Calibrated ¹⁴C age cal yrs BP (Normarine18 curve 95.4%) median
08H_101					
08H_101	23.4-25.8	Beta-527806	13060±40	15100	14501 (14735-14223)
08H_101	35-35.8	Beta-527827	14360±40	16900	15147 (15460-15132)

The age model for 08H_101 reveals the stratigraphy of Halsafjorden from 14.5 k cal. yrs BP (Fig. 25). The depositional history covers the period of 14.5 k cal. yrs BP to 17.2 k cal. yrs BP. The last reflector age, the Base of the SH2, has been modeled using the Normaine18 curve (Pre-Bølling) and Tau Boundary for a more accurate modeled age. Tau Boundary has been used for more uniform sedimentation in the SH2 after 20m depth to reflect the homogenous sedimentation for the SH2 as observed in the sediment log and seismic stratigraphy (Fig. 25).

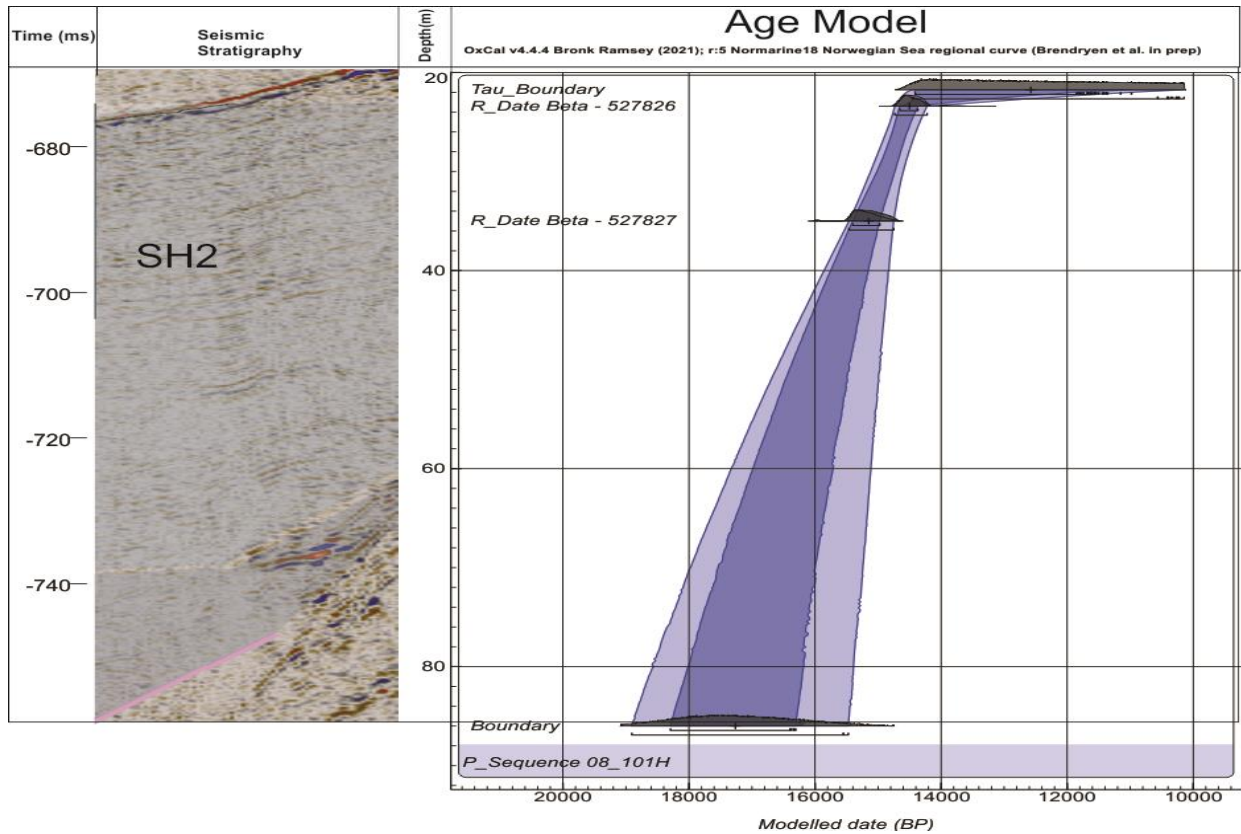


Fig. 25. Age model of 08H_101, explicitly covering the SH2/glaciomarine sediments.

Table 11. Overview of the results from Halsafjorden.

Seismic units	Litho -units	Seismic facies	Shear strength (kPa)	Structures	Interpretation	Age (cal. yrs BP)
SH1	LH1	H-I	10-80	Coarse sand, the possibility of gravel at 2.85 m, medium bed of sand at 13.8 m	Mass Transport Deposits (MTD)/Slope Sediments/MTD	12
SH2	LH2	H-II	10-220	Uniform grain size	Glaciomarine	14.5-15.1
SH3	None	H-III	None	None	None	>15.1

4.3 Recalibration of previously published ¹⁴C dates

The following dates have been recalibrated using the Normarine18 from other literature to ensure the accurate reconstruction of the Ice sheet following the last glacial maximum (Table 12). These calibration dates with Marine 20 were taken from Sejrup et al. (2022) data and were recalibrated using Normarine18. Radiocarbon dating is also used to reconstruct the time-distance diagram for the regional ice sheet movement. A map reference is also added to show the dating location in the Norwegian continental shelf (Fig. 26).

Table 12. Recalibrated dates used for the reconstruction of ice sheet movement following the LGM.

Map reference	Description	Core ID	¹⁴ C age, BP ± 1σ	Calibrated Marine20 median (95.4% Range)	Normarine18 median (95.4 % Range)	Lab ID	Geological Description	Glacial Context	Reference
1	North Sea Fan	79-08	16310±105	18816 (19139-18545)	17751 (18083-17372)	TUa-1251	The glacimarine unit above the glacigenic debris flow	Margin	King et al. 1998, Nygård et al. 2004
2	North Sea Fan	79-20	16690±120	19235 (19575-18875)	18063 (18475-17719)	TUa-1245	The glacimarine unit above glacigenic debris flow.	Margin	King et al. 1998, Nygård et al. 2004
3	North Sea Fan	83-06	16265±130	18771 (19124-18376)	17726 (18078-17334)	TUa-1246	The glacimarine unit above glacigenic debris flow.	Margin	King et al. 1998, Nygård et al. 2004
4	Måløy Plateau	74-A-07-14C	13760±340	15783 (16746-14887)	14855 (15660-14316)	T-2708	Pebbly mud above till (glacimarine).	Deglacial	Holtedahl & Bjerkli 1982
5	Trøndelag shelf	B77-118/4	15760±115	18240 (18600-17925)	17271 (17663-16806)	TUa-1042	Shell fragment, thin but well preserved	Advance	Rokoengen & Frengstad 1999; Nydal et al. 1985
6	Trøndelag shelf	B77-121/1	13985±85	16064 (16366-15749)	14890 (15263-14632)	TUa-898	Astarte sp. with both shell halves intact	Deglacial	Rokoengen & Frengstad 1999; Nydal et al. (1985)

7	Trænadjupet	JM96-47/1	13590±70	15545 (15829-15261)	14664 (14895-14395)	TUa-1767	The glacimarine unit above glacial debris flow.	Deglacial	Laberg et al. (2002)
8	Nordland	GS07-148-12GC	15680±70	18140 (18430-17855)	17173 (17652-16755)	Beta-295174	Glacimarine	Deglacial	Bøyum 2011
9	Nordland	GS07-148-12GC	15940±70	18425 (18665-18189)	17397 (17700-17189)	Beta-295175	Glacimarine	Deglacial	Bøyum 2011
10	Nordland 2.10 m close to Bremanger	GS08-155-48GC	14250±60	16406 (16686-16137)	15115 (15419-14742)	Beta-295180	Glacimarine	Advance	Bøyum 2011
11	Haltenbanken Advance	B78-4/2	12800±210	14408 (15072-13771)	14049 (14626-13407)	T-2928	Shell-bearing gravel and sand below till (Haltenbanken Moraine).	Advance	Bugge 1980
12	Haltenbanken Deglaciation	B78-4/2	12660±210	14198 (14900-13590)	13944 (14545-13286)	T-3411	Sand above till (Haltenbanken Moraine).	Deglacial	Bugge 1980
13	Trøndelag shelf	B77-121/1	13985±85	16064 (16366-15749)	14890 (15263-14632)	TUa-898	Astarte sp. with both shell halves intact	Deglacial	Rokoengen & Frengstad 1999; Nydal et al. 1985
14	Sør-Trøndelag ice free	Trondheim sleia	12630±100	14099 (14520-13755)	13953 (14475-13385)	AAR-5553	Glacimarine clay and silty clay.	Ice-free	Rise et al.,2006
15	Sør-Trøndelag ice free	Trondheim sleia	13180±80	15013 (15312-14679)	14522 (14752-14242)	AAR-5737	Glacimarine silty clay.	Ice-free	Rise et al.,2006
16	Sør-Trøndelag ice free	Trondheim sleia	13070±90	14846 (15178-14436)	14442 (14754-13706)	KIA-12441	Glacimarine silty clay.	Ice-free	Rise et al.,2006
17	Vartdalsfjorden	03VL_101	13600±80	15559 (15862-15258)	14669 (14906-14395)	Beta-530631	Advance	Advance	Aase (2022)

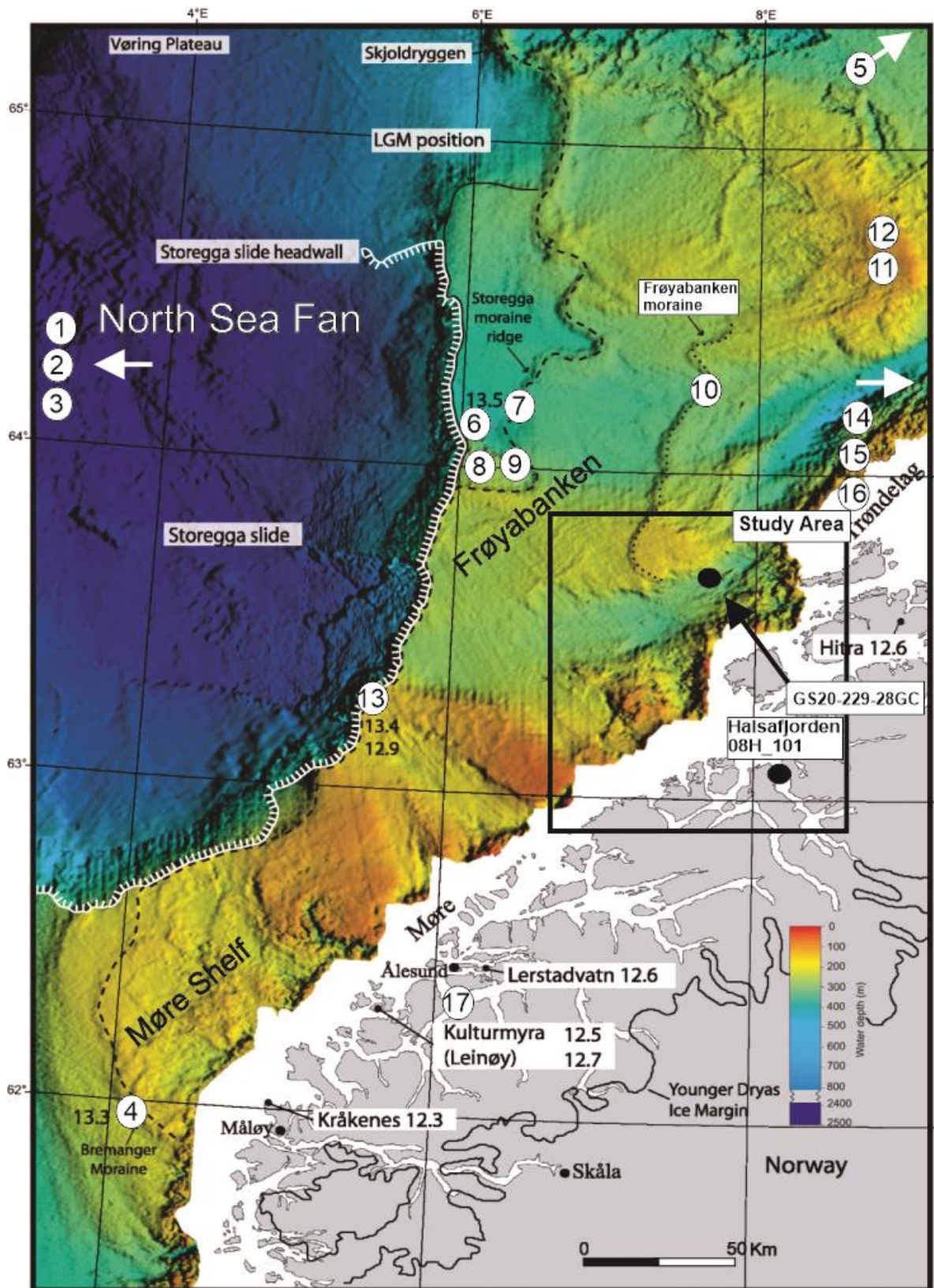


Fig. 26. Map of reference showing locations of dates described in Table 12. The numbers are ¹⁴C dates corrected for reservoir age by Nygård et al. (2004). Modified after Nygård et al. (2004).

5 Discussion

5.1 Glacial Dynamics and chronology of Frøyabanken and Halsafjorden

5.1.1 Frøyabanken

Here, the depositional history and ice sheet dynamics of Frøyabanken are reconstructed based on the stratigraphical and chronological analysis of sedimentary deposits in the Frøyabanken area (Figs. 10-13), as well as the recalibration of previously published marine ^{14}C dates using the Normarine18 curve of Brendryen et al. (2020) (Table 12). The reconstruction of the deglacial ice sheet movements in the Frøyabanken area is divided into four main phases (Fig. 27).

Phase 1, Glaciation: *Glaciation* represents the oldest phase, with deposits seen in the Topas data on the Frøyabanken recording sub-glacial conditions (Fig. 27A). In the Frøyabanken area, this phase is represented by seismic unit SF5, which is characterized by a chaotic seismic signature with high amplitude in the top, but where the seismic signal rapidly decreases downwards to the acoustic basement. SF5 is interpreted to be a subglacial till that formed during full glacial conditions. While there is no independent age control of SF5, the unit might be correlated with the Till Tongue 23 unit that extends to the edge of the outer Mid-Norwegian continental shelf (Fig. 11, Table 12) (King et al., 1998). Rokoengen and Frengstad (1999) dated this till tongue to have a maximum age of 17270 (17660-16810) cal. yr BP (Table 12).

The ice sheet is likely to have fully covered Frøyabanken during this phase as it is evident that the ice sheet extended to the shelf edge (Bøyum, 2011; Haflidason et al., 2013; Holtedahl and Bjerkli, 1982; Nygård et al., 2004; Olsen et al., 2013; Ottesen et al., 2022; Sejrup et al., 2022). Based on recalibrated date from King et al. (1998), Rokoengen and Frengstad (1999), and Nygård et al. (2004), shown in Table 12, the age of the full shelf edge glaciation might have been close to 20-17 ka cal. yrs BP and the SF5 are also inferred to have been formed with this stage.

Phase 2, Deglaciation 1: *Deglaciation 1* marks the initial ice sheet retreat from the shelf edge (Fig. 27B). An early retreat of the ice sheet from the shelf edge is reported from the Norwegian Channel, and the Møre-Trøndelag continental shelf (Bøyum, 2011; Nygård et al., 2004; Rokoengen and Frengstad, 1999; Sejrup et al., 2022). In the Frøyabanken area, this phase is believed to be represented by seismic unit SF4 that is characterized by parallelly laminated high

amplitude reflectors (Fig. 10, 11, and 12). The SF4 is interpreted as a meltwater plumite deposited in front of a retreating ice front, similar to the laminated seismic facies formed during the early deglaciation of fjords (Hjelstuen et al., 2009).

The upper boundary of SF4 is defined by reflector RF3, which is interpreted to represent an erosive event likely caused by an advancing ice sheet. This ice sheet advance eroded the SF4 so that it remains only in patches along the Frøyabanken Topas line (Fig. 27B). Ridge A, B, and C presence in Frøyabanken seismic lines might be interpreted as lateral moraines that formed during the ice sheet retreat before readvancing based on its characteristics (Ottesen et al., 2022). The seismic stratigraphy of Frøyabanken suggests that the SF4 (Fig. 27B) is correlated with the *Deglaciation 1* phase as the ice retreated to Frøyabanken area. as the ice retreated to the position of Frøyabanken area. However, the extent of the ice sheet retreat during Deglaciation 1 cannot be determined by the pre-existing data. The recalibrated dates from Bøyum (2011); Bugge (1980); Haflidason et al. (2013); Nygård et al. (2004) (Table 12) shows that *Deglaciation 1* might have occurred between 17.7-15 ka cal. yrs BP (Fig. 27B). Radiocarbon dating of deglacial sediments overlying till tongue 23 in GS07-148-12GC from the Trondelag shelf also shows the *Deglaciation 1* phase to be 17.1-17.7 ka cal. yrs BP (Bøyum, 2011) (Fig. 26, Table 12). In addition, the modeled age of reflector RF3 (Fig. 19B) suggests that SF4 is deposited before 17-18 cal. yrs BP in *Deglaciation 1* phase.

Phase 3, Readvance 1: *Readvance 1* is represented by the erosive surface of reflector RF3 that depicts the possible readvance of the ice sheet across the Frøyabanken following the *Deglaciation 1* event (Fig. 27C). Seismic profiles of Frøyabanken show a high amplitude reflector that is continuous throughout all the seismic lines (Figs. 11 and 12). Core GS08-155-48GC from near the Frøyabanken moraine penetrates a reflector similar to RF3 (Bøyum, 2011; Haflidason et al., 2013). Bøyum (2011) study near Frøyabanken moraine concluded that a readvance of the ice sheet occurred in the mid-Norwegian continental shelf around 15.1-15.3 ka cal. yrs BP based on his seismic survey and the analysis of sediment core, i.e., GS-08-155-48GC, and named it Haltenbanken readvance by comparing the results with Bugge (1980) study on Haltenbanken moraine, which is further up from the Frøyabanken. However, it should be argued that the dating difference between the two findings is significant as Bøyum (2011) investigations date the readvance event close to 15 ka cal yrs BP while the Bugge (1980) study dates the event to close 14 ka cal. yrs BP (Table 12). It should also be noted that the study area of Bugge (1980) is further up to the north and covers the area of Haltenbanken moraine, while

the Bøyum (2011) study area is close to the Frøyabanken. By analyzing the results from Bøyum (2011) study on the Frøyabanken moraine, it can be interpreted from the sediment log GS-08-155-48GC that the chaotic reflector is diamictite sediments (Fig. 29A). According to Boulton and Hindmarsh (1987), diamicton is a sediment that contains different rock fragments and might be associated with glacial ice sheet movement. The presence of diamicton can indicate the presence of an ice sheet readvance as it is often deposited as the ice sheet advances and retreats (Fig. 28A) (Bennett and Glasser, 2011; Bøyum, 2011; Bugge, 1980; Chandler and Evans, 2021; Evans, 2017; Haflidason et al., 2013). It is concluded that the RF3 reflector might be the same reflector that was observed in the Bøyum (2011) are more related to the findings of this study (Fig. 28A). Instead of naming it Haltenbanken readvance, it should be renamed Frøyabanken based on the locality and the evidence suggested above. Since Bøyum (2011) findings suggest that the readvance might have happened before 15 ka cal. yrs BP, it should be concluded that the Frøyabanken readvance happened around 15-16 ka cal. yrs BP based on the modeled age which can be correlated with the Bremanger ice sheet readvance that happened around 15-16 ka cal. yrs BP (Nygård et al., 2004). In addition, Ottesen et al. (2022) also separated Haltenbanken moraine from Frøyabanken moraine and suggested that Frøyabanken readvance might be part of Bremanger ice-sheet readvance. It should also be noted that the reflector seen in Bøyum (2011) study might also be related to the transition between the *Glaciation* and the *Deglaciation 1* phase as a correlative unit of SF5. The precise relationships between Storegga moraine ridge, Frøyabanken moraine ridge, and Haltenbanken ridges are uncertain, this should be further investigated by high seismic resolution and additional sediment cores that can precisely determine the ages of the different glacial events.

In addition, Ridges A, B, and C in Frøyabanken are present and could be regarded as lateral moraines, based on their features described in results (Figs. 9 and 10) (Nygård et al., 2004; Ottesen et al., 2022). It may be classified as a Frøyabanken moraine based on the lateral moraine ridges and the RF3 reflector, indicating that the readvance happened near Frøyabanken. The Frøyabanken readvance has also eroded the SF4, which may have accumulated prior to the readvance, observed along all seismic lines (Fig. 27C). The distinctive parallel laminations in the SF4 unit suggests that it was deposited before the readvance and was eroded after the readvance (Fig. 10). Also, the overlying SF3 sediments above RF3 forms a drape pattern. In marine geology, a draping pattern in seismic units can reveal the existence and movement of a glacial ice sheet. As the ice sheet grinds and pushes the material in front of it, a distinct layer

of highly disturbed sediments is left on the ocean floor, forming this pattern. The orientation and thickness of the drape pattern can be used to determine the direction and speed of ice sheet movement (Figs. 9-12) (Nielsen and Rasmussen, 2018). It can be suggested that *Readvance 1* is the Frøyabanken readvance based on the earlier evidence.

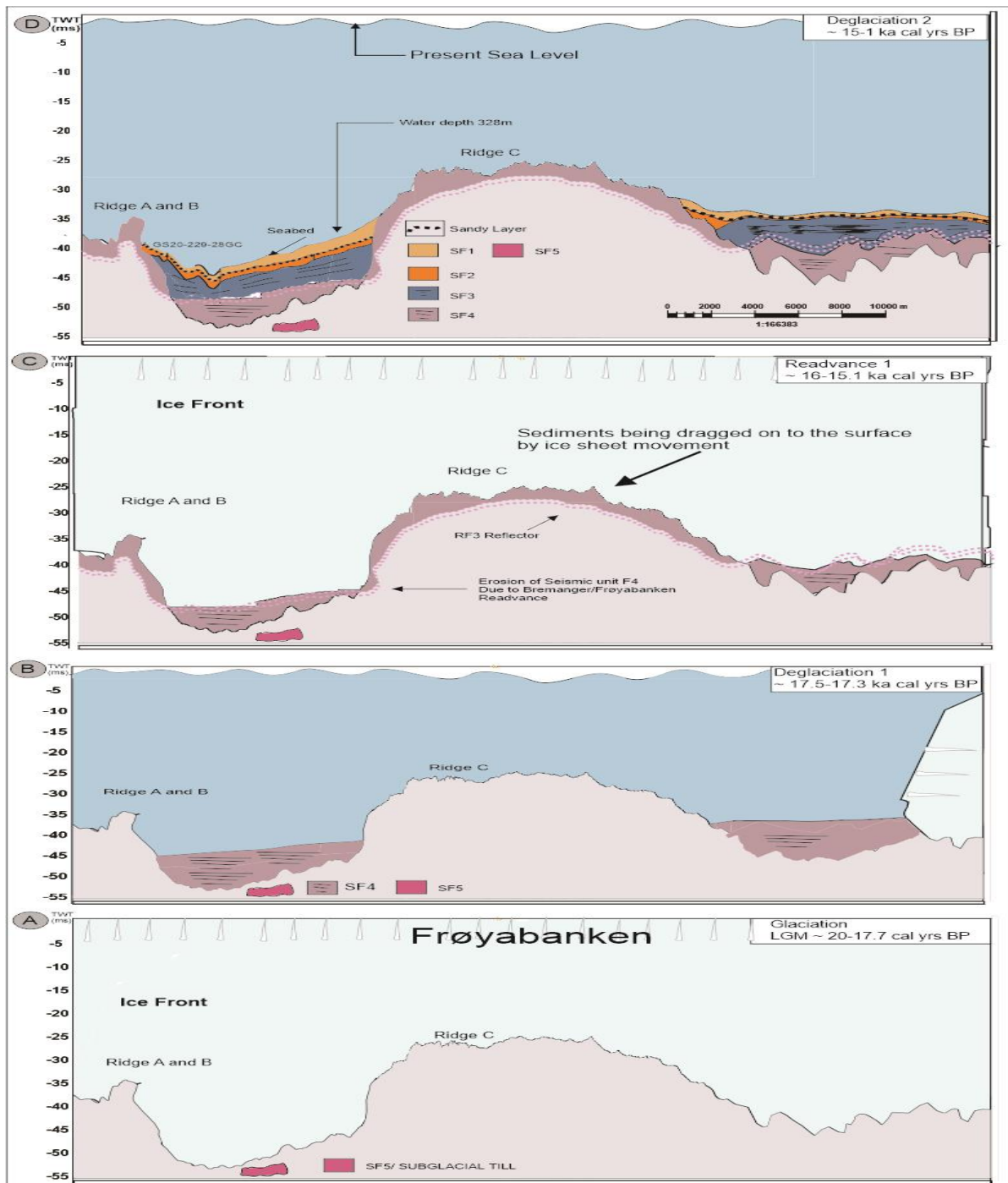


Fig. 27. A conceptual model based on the deglaciation of the ice sheet during distinct phases in Frøyabanken and sediment deposited during other times. Dates used are from recalibrated dates from Table 12 and the chronology of Frøyabanken.

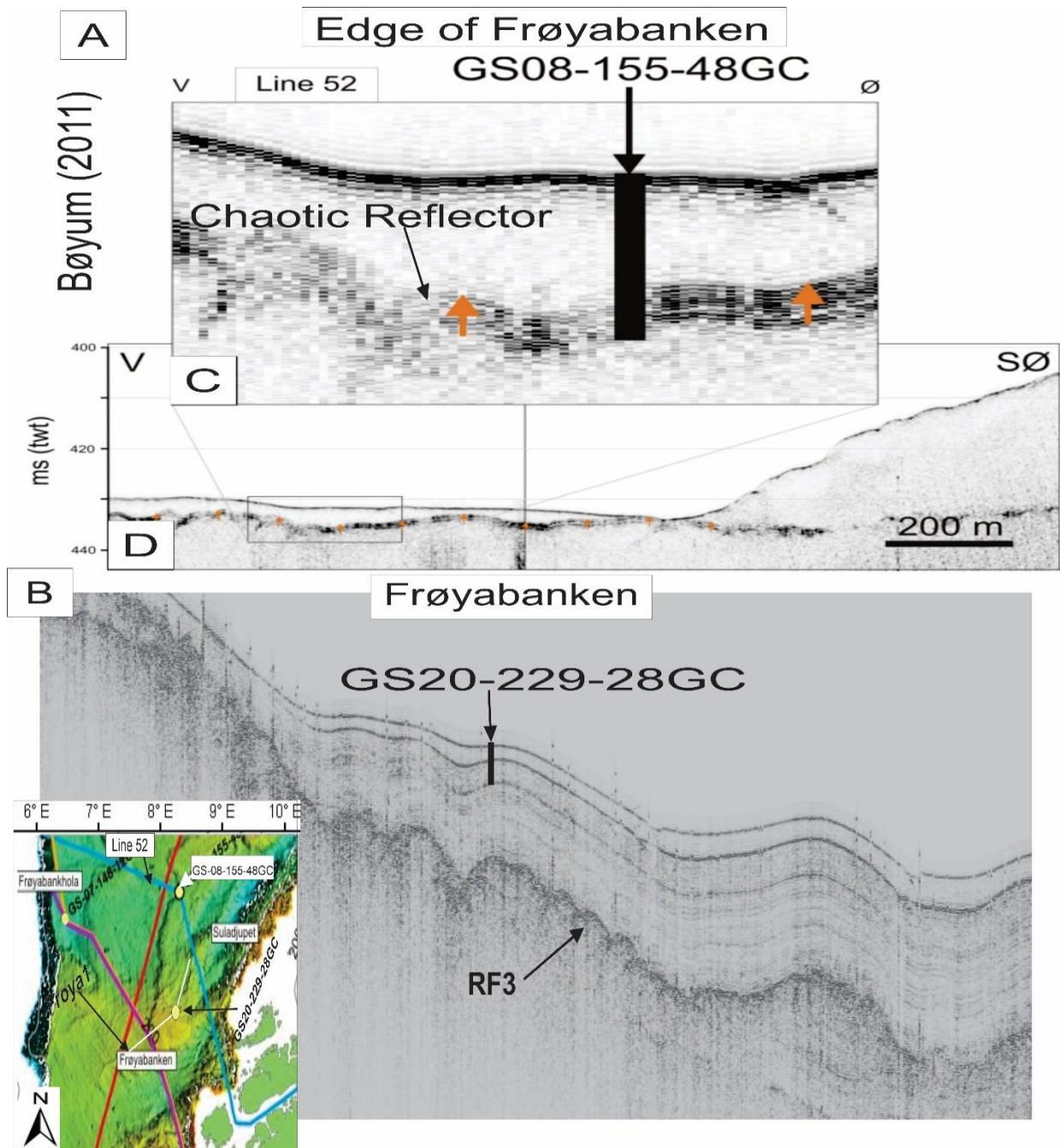


Fig. 28. (A) Bøyum (2011) seismic survey study of Line 52 on the Edge of Frøyabanken (B) Seismic study of Frøya1 (black line) in Frøyabanken, also showing the core location and RF3 reflector (C) GS08-155-48GC (yellow dot) location on Line 52 (blue line), it also shows the chaotic reflector (D) an overview of composite line 52 (blue line). The location map shows the seismic lines of both Frøyabanken and Edge of Frøyabanken, along with the core positions (yellow dot) with respect to each other. Modified after Bøyum (2011).

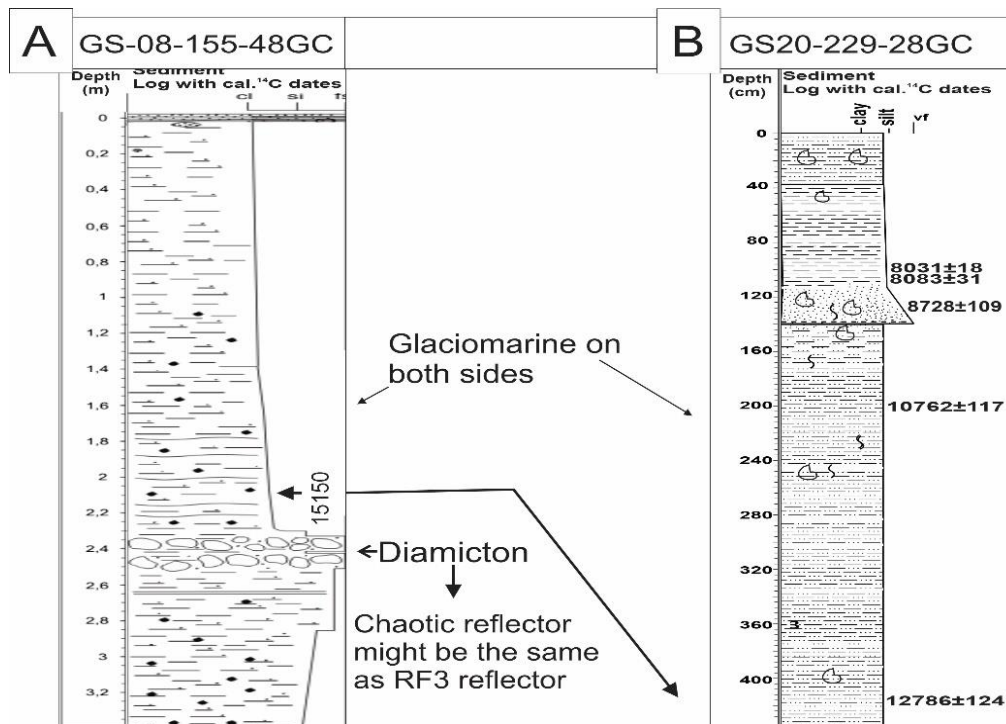


Fig. 29 (A) Sediment log of GS-08-155-48GC and the presence of diamicton and glaciomarine can also be observed. (B) sediment log of GS20-229-28GC showing its relation, that the lower lithological units might be connected to GS-08-155-48GC.

Phase 4, Deglaciation 2: *Deglaciation 2* depicts the deglaciation of the Frøyabanken and the ice sheet retreating following the *Readvance 1* (Fig. 27D). Based on the calibrated dates of GS20-229-28GC and Bøyum (2011)'s GS08-155-48GC, the ice sheet retreat would have occurred around 15-12.7 ka cal. yrs BP in Frøyabanken (Table. 12). The deposition of the SF3 occurred in this period (Fig. 27). The LF4 of GS20-229-28GC can be correlated with the seismic unit deposited in *Deglaciation 2* (Fig. 27D). *Deglaciation 2* was followed by the Holocene period in which SF2 and SF2 were deposited.

5.1.2 Halsafjorden

Based on the chronology, lithostratigraphy, and seismic analysis of Halsafjorden and Borehole 08H_101, the Halsafjorden deglaciation history can be divided into the following phases (Fig. 30):

Phase 1, Glaciation: The *Glaciation* phase, around 20-16 ka cal. yrs BP is in Halsafjorden represented by seismic unit SH3. SH3 is interpreted to be a subglacial till based on its irregular and chaotic seismic reflector. It is significantly less visible in the seismic survey, and based on the chronology of 08H_101, its age might be related to a period when the Halsafjorden was

fully glaciated in the LGM. However, further research is required to determine the glacial till age (Fig. 30A).

Phase 2, Postglacial stage: Following the *Glaciation*, the ice retreat from the Halsafjorden may have started around 16-14.5 ka cal. yrs BP during the *Postglacial phase* (Fig. 30B). Two post-glacial seismic has been defined in Halsafjorden SH2 and SH1 The SH2 lies directly above the glacial till in SH3 and may have been deposited between 16 ka and 14.9 ka cal. yrs BP, based on the recalibration of dates provided by Fugro (2019) (Tables 12 and 10). The SH2 seismic unit's parallel laminations indicates that it is glaciomarine and were likely deposited rapidly following the ice sheet's retreat (Hjelstuen et al., 2009). However, it should be noted that there is additional uncertainty regarding the dates of 08H_101 at 3500 cm. This data is taken on a bulk sample that might incorporate older redeposited carbon making the ^{14}C date appear older than the time of sediment deposition.

Johansen et al. (1985) and Bøe et al. (2004) have concluded that the Halsafjorden was ice freed around 15 ka cal yrs BP, and the extent of the Younger Dryas never reached till Halsafjorden. SH1 is interpreted to predominantly consist of post/glacial mass transport.

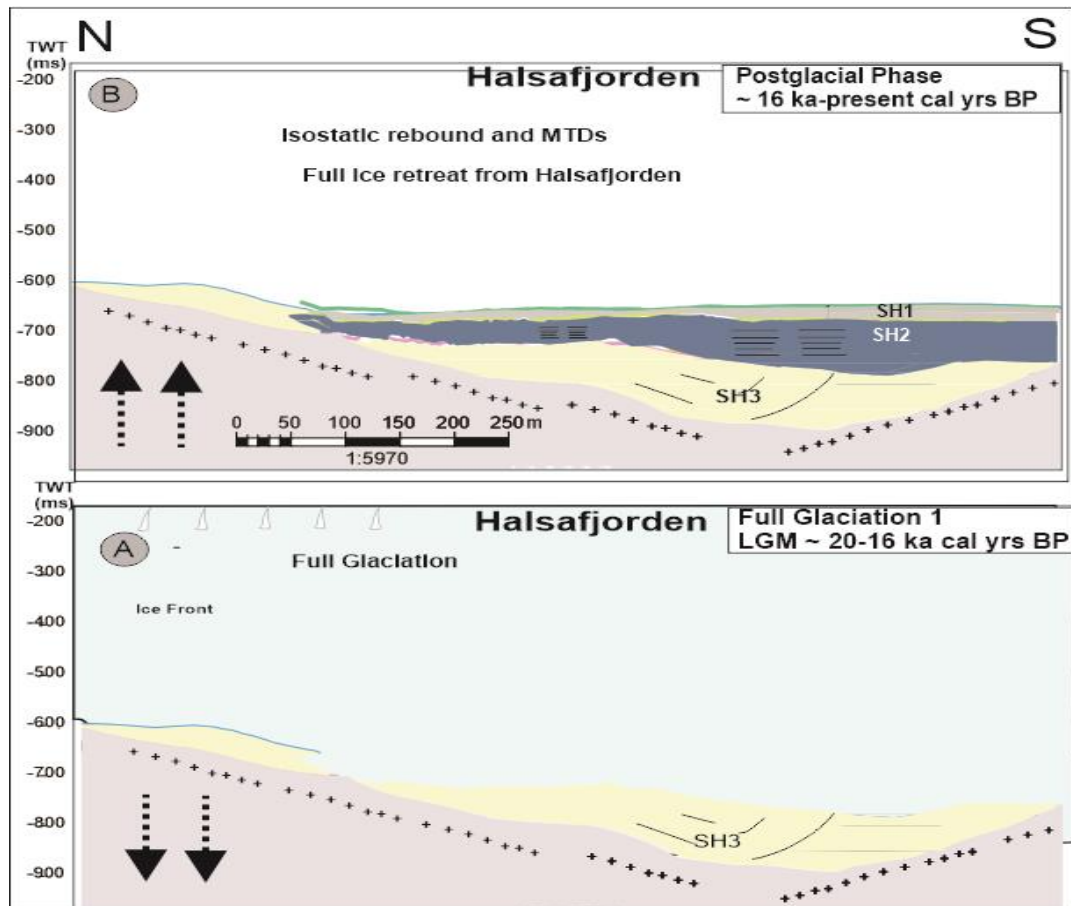


Fig. 30. The conceptual model of ice sheet retreat along a geological section of Halsafjorden and the deposition of seismic units. The arrows represent the glacial isostatic crustal movement after deglaciation. The chronology of the figure is based on the chronology of Halsafjorden and regional dates from Table 12.

5.1.3 Correlation between Halsafjorden and Frøyabanken:

The similarity of the seismic data from Frøyabanken and Halsafjorden suggests a possible relation between the two sites (Fig. 31). Halsafjorden and Frøyabanken's deglaciation and seismic stratigraphy suggest that they are likely to be connected because the ice may have retreated through Halsafjorden following the retreat from Frøyabanken. This is evidenced by the presence of glaciomarine sediments, as indicated by the distinctive parallel laminations found in both Halsafjorden and Frøyabanken seismic lines (Fig. 31C, D) (Hjelstuen et al., 2009; Johansen et al., 1985; Olsen, 2002). In addition, it should be noted that the parallel lamination is an indicator of ice-contact and ice-proximal marine depositional environments, which are commonly associated with the same glacial and interglacial cycles, and it is highly likely that the Glaciomarine sedimentation might have happened in the same ice retreat of the FIS around 15 ka cal. yrs BP (Bennett and Glasser, 2011).

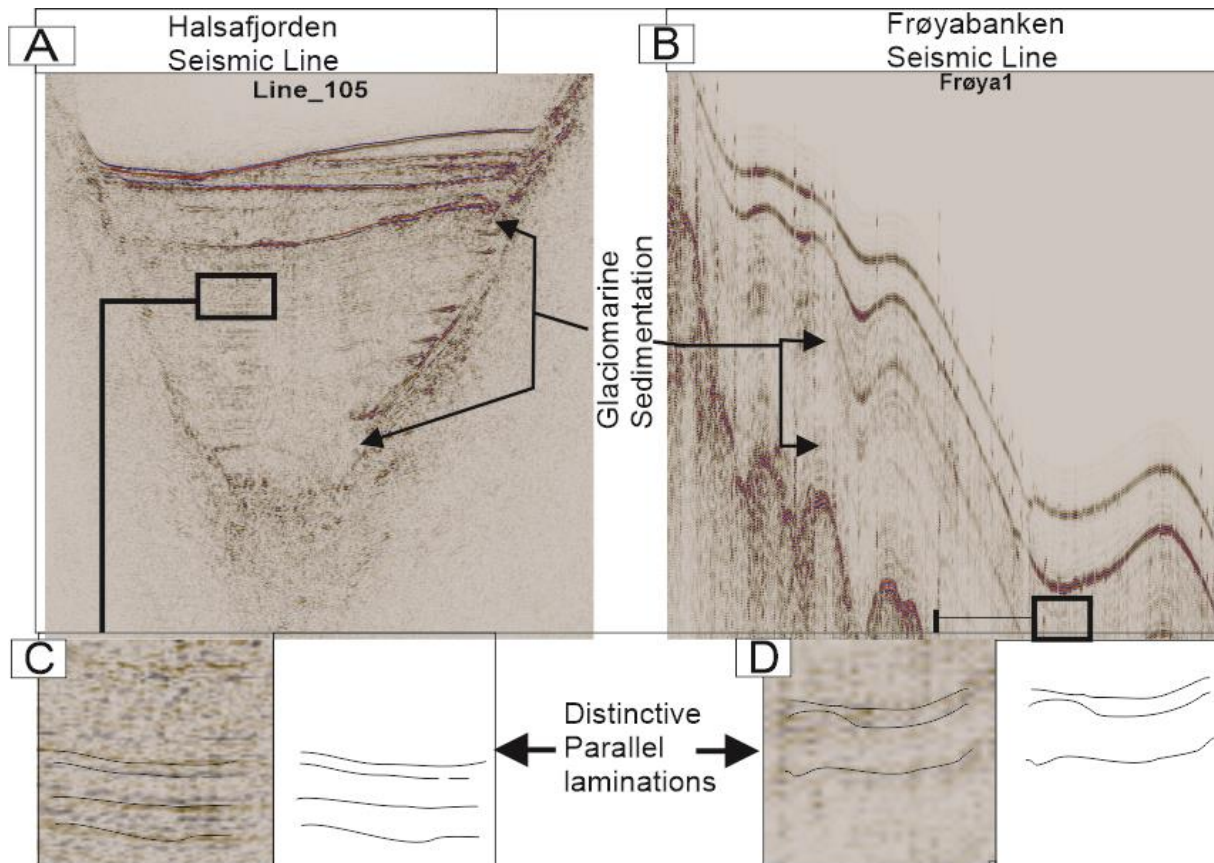


Fig. 31. (A) Halsafjorden Seismic line of H0080_105 shows distinctive parallel lamination in SH2(B) Frøyabanken seismic line of Frøya1, showing distinctive parallel lamination in SF3. (C) Close-up of the parallel lamination of SH2 representing the glaciomarine sedimentation in Halsafjorden (D) Close-up of the parallel laminations of SF3 representing the glaciomarine sedimentation in Frøyabanken

The correlation of both cores, i.e., GS20-229-28GC from Frøyabanken and 08H_101 from Halsafjorden, shows some lithological similarities as Frøyabanken shows more uniform grain sizes from 1.3 m to 4.27m (Fig. 32). Similarly, the 08H_101 sediment log shows uniform fine grain sizes in the lower lithological portion. Both could be interpreted as glaciomarine sediments probably deposited after the ice sheet retreat. However, both cores have chronological differences because GS20-229-28GC does not cover much of the SF3 unit (Fig. 32A). On the other hand, 08H_101 penetrates far away into the SH2 unit ranging up to 41.90 m and gives more chronological data as compared to GS20-229-28GC (Fig. 32B). In addition, the one dating for 08H_101 provided by Fugro (2019) was taken from a bulk sample at 35-35.9 m. Bulk sampling can cause chronological or dating problems because the sample may contain a mixture of different ages and layers of sediments deposited at different times due to bioturbation or other processes (Strunk et al., 2020). Due to this chronological problem, it is hard to interpret a correlation between Halsafjorden and Frøyabanken lithologies. However, based on the

evidence of seismic survey and grain size analysis, it could be interpreted that the ice sheet started retreating from Frøyabanken around 18-16 ka cal. yrs BP based on the modeled age, and reached Halsafjorden around 17-15 ka cal. yrs BP based on the bulk dating sample.

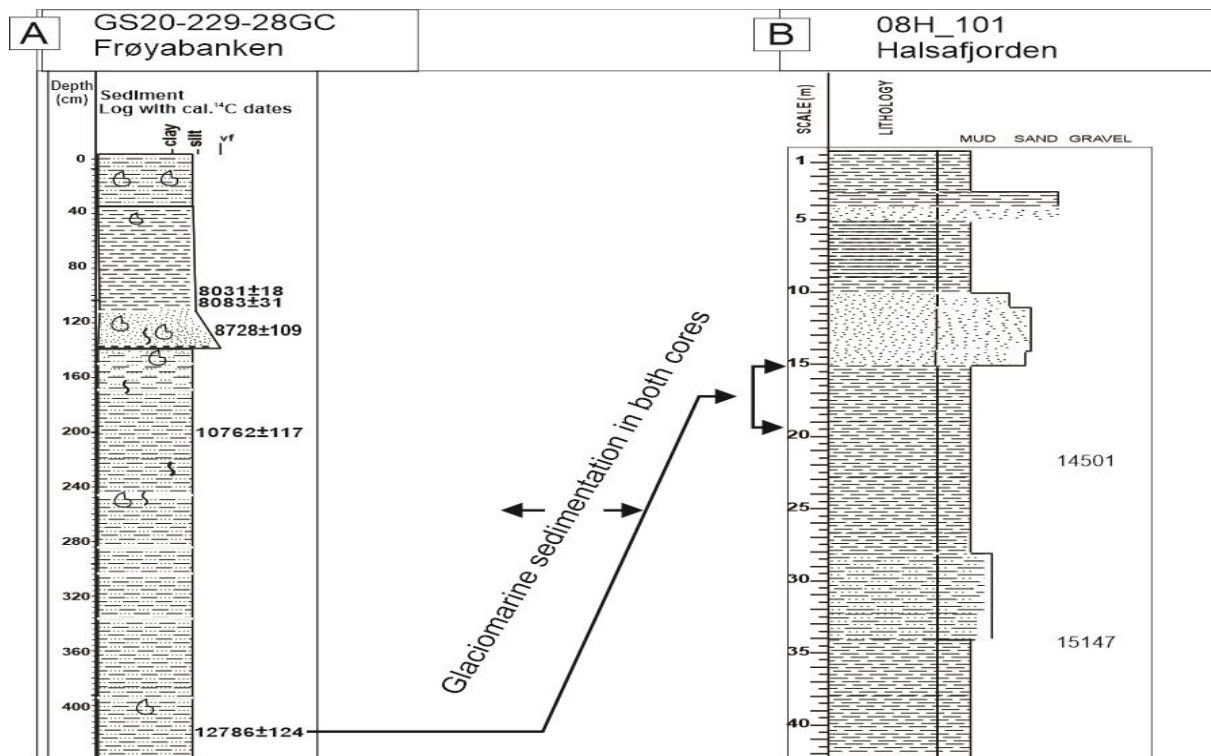


Fig. 32. (A) The sediment log of GS20-229-28GC, along with calibrated dates in correlation with (B) the Halsafjorden borehole core 08H_101 sediment log, represents its lithology and calibrated dates. The figure also shows glaciomarine sedimentation in both cores. The arrows represent a correlation between the lithologies of cores based on grain size and chronology.

In summary, the seismic survey and lithological data from Frøyabanken and Halsafjorden present a strong case for a relationship between the two sites. However, further research is needed to confirm this hypothesis as there is uncertainty in the chronology of both sites. Due to the lack of seismic lines linking Frøyabanken and Halsafjorden, it cannot be confirmed where the readvance of the ice sheet started after retreating. In the following Figure 33, the correlation between the two geological formations is shown in the simplified geological model.

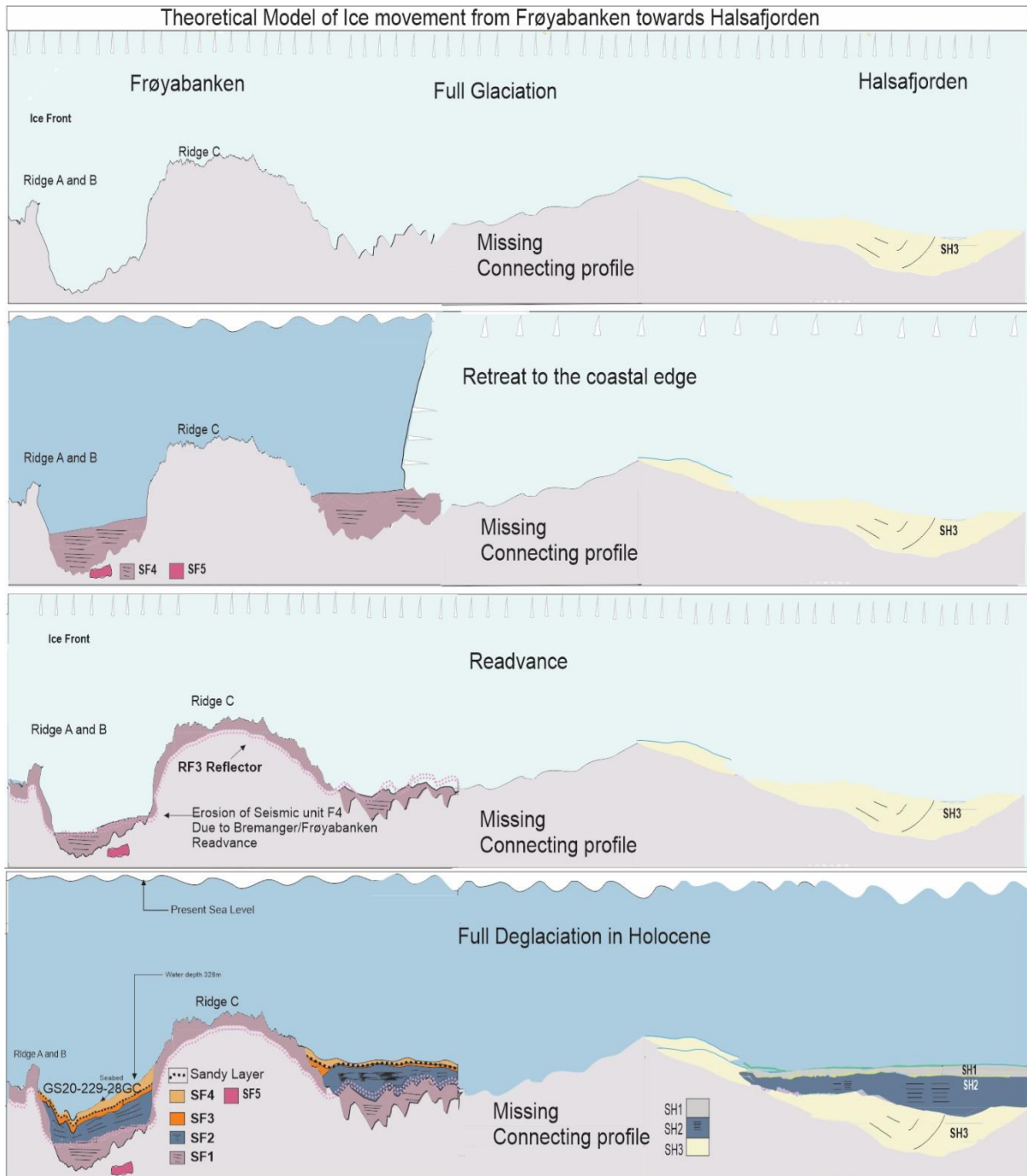


Fig. 33. Theoretical model that could explain the ice retreat during the deglaciation period between Halsafjorden and Frøyabanken.

The above model is based on the seismic profiles of Halsafjorden and Frøyabanken. The model shows that the ice retreat might have readvanced from the coastal edge between Halsafjorden and Frøyabanken. Further investigation in the theoretical connecting profile area might reveal more information about the movement of ice sheet extension and readvance.

5.2 Regional Ice Movement

Based on the lithostratigraphy, chronology, and seismic analysis of Frøyabanken and Halsafjorden, and the recalibration of marine and terrestrial dates relevant to the Scandinavia Ice sheet followed by the LGM. The reconstruction of the past glacial ice sheet has been mapped using the recalibrated dates and literature data. Uncertainty in the reservoir ages of the past geological reconstruction of the ages was corrected by the Normarine18 curve presented by Brendryen et al. (2020). The following reconstruction of the past glacial ice sheet is divided into six main phases (Fig. 34).

Phase 1, Full Glaciation: *Full Glaciation* represents the phase where the Scandinavian Ice sheet at its full extent close to the shelf edge during the LGM (Fig. 34A). The ages calibrated for the full extension of the ice sheet were from (Nygård et al., 2004) of the North Sea glacial debris flows, which shows the extent of the glacial ice sheet approximately close to 20 ka cal. yrs BP. This age corresponds to the Andya-Trofors interstadial dates (Olsen and Bergstrøm, 2007; Vorren et al., 1988). The Full Glaciation map is based on previous research that indicates the ice extent reached the shelf margin from Svalbard to the Norwegian Channel (Andersen et al., 1981; Mangerud, 2004; Nygård et al., 2004; Olsen et al., 2013; Ottesen et al., 2022; Ottesen et al., 2005; Rokoengen et al., 1977).

Phase 2, Deglaciation 1: *Deglaciation 1* represents the first ice sheet retreat that followed LGM, as shown in (Fig. 34B). The reconstruction of the ice sheet was based on by a previous study (Bøyum, 2011) where radiocarbon dating of core GS07-148-12GC on Trøndelag shelf indicated an age of around 17.1-17.7 ka cal yrs BP for this event. While the spatial extent of this deglaciation has not been fully recorded, the presence of glacially eroded acoustically laminated sediments in the Frøyabanken area cøpse tp the island of Frøya (Figs. 26 and 27) and in Vartdalsfjorden, Sunnmore (Aase, 2022), as well as evidence of open water at the Måløy Plateau (Nygård et al., 2004) suggest that the ice may have retreated to the coastal area in the Møre-Trøndelag area (Figs. 34 and 35).

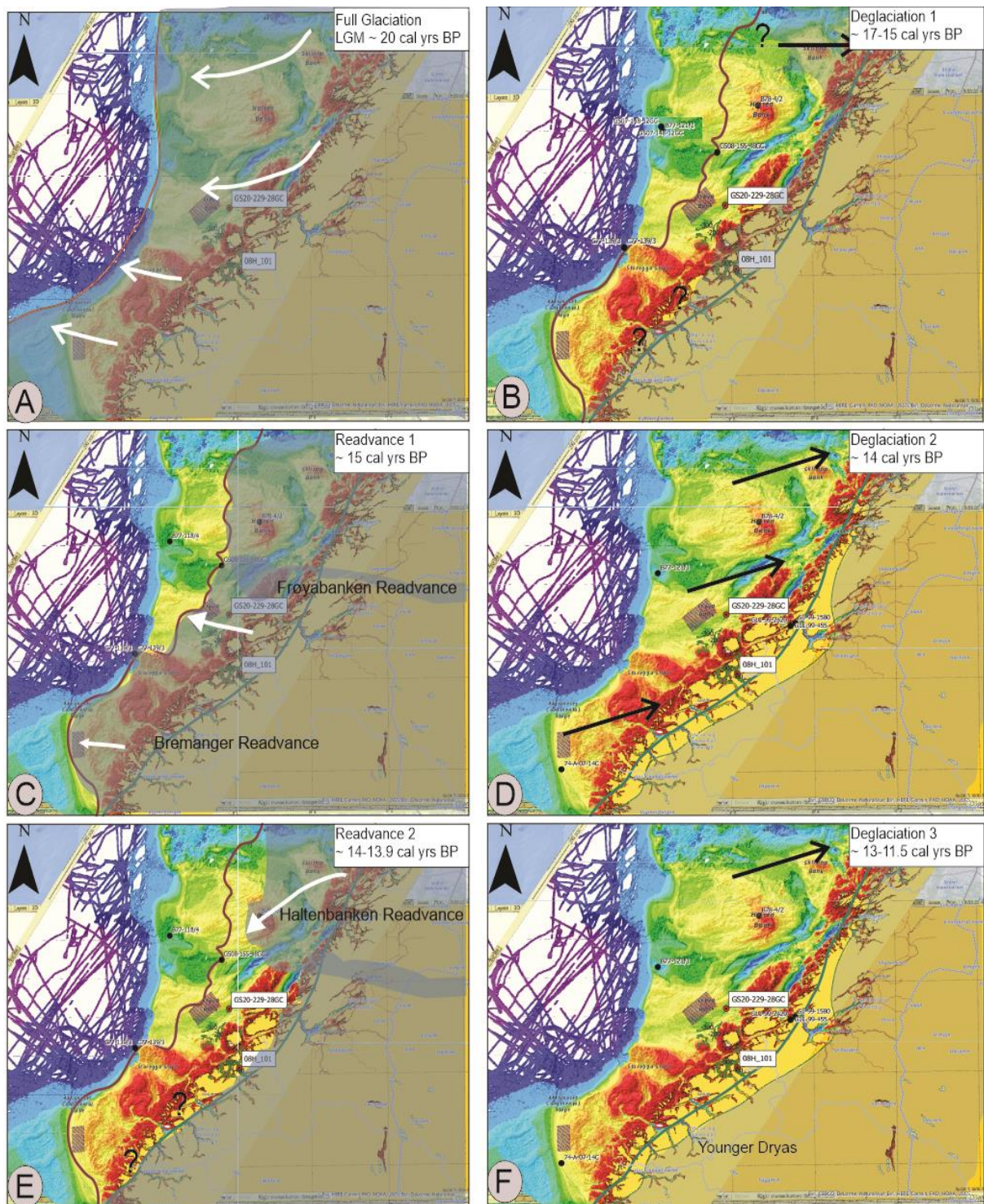


Fig. 34. Conceptual reconstruction of the Scandinavian ice sheet (white semi-transparent fill) at several phases of glaciation, based on the recalibrated dates from Table 12 (Bøyum, 2011; Bugge, 1980; Haflidason et al., 2013; King et al., 1998; Nygård et al., 2004; Olsen et al., 2013; Ottesen et al., 2022; Rise et al., 2006; Rokoengen and Frengstad, 1999; Sejrup et al., 2022). The White lines represent advance while the black lines represent retreat of the ice movements. Younger Dryas extent is based on dates from Olsen et al. (2013). White boxes and red circle dots represent the study area cores. CoreIDraw and ArcGIS Pro were used to produce the map. The Haltenbanken readvance extent is based on Ottesen et al. (2022) interpretation. The extent of the Bremanger-Frøyabanken readvance is based on Sejrup et al. (2022) interpretation. OLEX provided the base map.

Phase 3, Readvance 1: *Readvance 1* represent a readvance of the ice sheet in the Mid Norwegian Continental margin following the *Deglaciation 1*. Evidence for an ice sheet readvance is found both on Måløy plateau, where it is termed as the Bremanger event (Nygård et al., 2004), in Vartdalsfjorden (Aase, 2022), and in the Frøyabanken area (Bøyum, 2011; Haflidason et al., 2013) and also in this study (Figs. 27 and 28). The Bremanger readvance, located in the mid-Norwegian continental south shelf, and the Frøyabanken readvance, situated in the mid-Norwegian continental north shelf, are the two locations where the readvances have been found (Fig. 34C). The Frøyabanken advance could be correlated with the Late Weichselian Karmøy/Bremanger ice readvance (Nygård, 2003; Nygård et al., 2004; Olsen and Bergstrøm, 2007). The recalibration of the dates from GS20-229-28GC and dates from Table 12 puts the Frøyabanken readvance around 16-15 ka cal. yrs BP (Bøyum, 2011; Bugge, 1980; Haflidason et al., 2013). In addition, the seismic data from Frøyabanken shows a possible readvance in the form of a chaotic continuous reflector in all Frøyabanken seismic lines.

Phase 4, Deglaciation 2: *Deglaciation 2* depicts the deglaciation of the entire mid-Norwegian continental shelf and the ice sheet retreat to the inner fjords (Fig. 34D). The extent of this deglaciation goes to the western coast of Norway (Rise et al., 2006). This phase might be correlated to the Bolling-Allerød interstadial (Nygård et al., 2004; Olsen and Bergstrøm, 2007; Olsen et al., 2013; Ottesen et al., 2022). The recalibrated dates and seismic survey from the Halsafjorden and Frøyabanken also confirm the ice retreat in this phase. Based on the recalibrated dates, the ice sheet retreat would have occurred around 15-14 ka cal. yrs BP.

Phase 5, Readvance 2: *Readvance 2* is a local readvance in the norther part of the mid-Norwegian continental shelf reported by Bugge (1980) (Fig. 34E). Bugge (1980) based his evidence on the seismic analysis of Haltenbanken and the core collected from the Haltenbanken and argued that a possible readvance might have happened close to the Haltenbanken around 14 ka cal. yrs BP. The time-distance schematic diagram (Fig. 34) shows the difference between Haltenbanken and Frøyabanken readvance based on the recalibrated chronology of Table 12. The local Haltenbanken readvance that might have occurred following the Deglaciation 2 is also observed in the regional ice sheet based on the interpretation of Bugge's (1980) study (Fig. 34E). The Haltenbanken readvance is correlated with the Older Dryas cooling event. Olsen (2002) has dated it around 13.8-14.2 ka cal. yrs BP (Marine20 dates). The ice sheet readvance of the Older Dryas in the mid-Norwegian continental shelf is expected to be 5-10 km (Andersen et al., 1981; Mangerud, 1980; Olsen, 2002; Olsen et al., 2013).

Phase 6, Deglaciation 3: The last stage of complete ice retreat from the continental shelf is *Deglaciation 3*, which occurred during the Allerød period around 14-13 ka cal. yrs BP based on the dates from Table 12. This is the last ice sheet retreat from the Norwegian continental shelf to the inner fjords. During the Younger Dryas stadial, the ice sheet advanced again; however, this advance did not extend beyond the coast onto the shelf (Fig. 34F).

To summarize the glacial ice sheet movement, three different schematic time-distance diagrams show the regional ice sheet movement (Fig. 35). The correlation of the dates of regional ice movement is given in Table 12. These dates are discussed here to provide a regional overview of ice movement and the local readvancing of ice sheets.

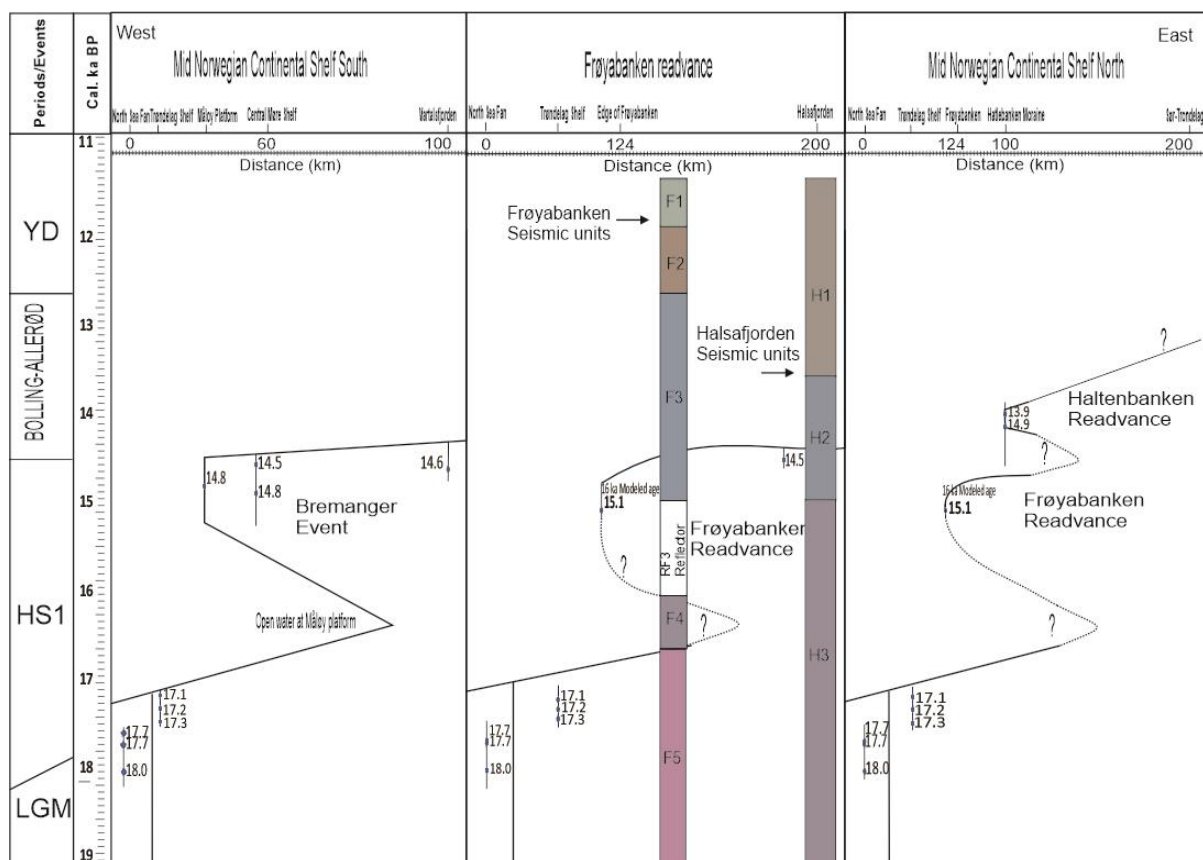


Fig. 35. Time-distance diagram for the mid-Norwegian Continental Shelf, North, from recalibrated dates from Table 12. The time-distance diagram for mid-Norwegian Continental Shelf South from recalibrated dates is based on Nygård et al. (2004) and Bøyum (2011) ^{14}C dates. Frøyabanken and Haltenbanken readvance. All the dates presented in ka are from Table 12. The extent of each ice extension is given in kilometers based on conceptual distance from the shelf edge. A possible correlation is also given with a more regional indicator, i.e., periodic events. The dotted lines present uncertainty in ice sheet movement.

5.3 Postglacial mass movements in mid-Norwegian continental shelf

5.3.1 Frøyabanken

The Storegga Slide/Tsunami was a large submarine slide that affected the Norwegian margin in some way, with more than 95000 km² area affected by it. It is supposed to be one of the most significant submarine slides in the world (Bellwald et al., 2019; Haflidason et al., 2005; Haflidason et al., 2002). This slide was caused by the collapse of a large portion of the continental slope, and it generated a huge tsunami that affected areas in Scotland, Norway, and Greenland (Bondevik et al., 1997; Haflidason et al., 2005; Haflidason et al., 2002; Haflidason et al., 2004). The tsunami generated from the slide might have the ability to erode the sediment into further places. When it moves into shallower water, a tsunami wave generates strong bottom currents, which can winnow the sediment and be sorted into a layer of sand through sediment transport (Bondevik et al., 1997; Canals et al., 2004; Ginsberg, 2011; Haflidason et al., 2004). The sandy layer observed in the Frøyabanken area, represented by the RF1 reflector in the Topas data and lithostratigraphical unit LF3 of core GS20-229-28GC (Fig. 36D) loosely correspond in time with the Storegga slide and was likely formed by sediment winnowing erosion by bottom currents generated by the Storegga tsunami (Bondevik et al., 1997). The sandy layer of LF3 is interpreted to be formed by bottom currents winnowing and not a classical turbidite formed in relation to a slide or slumping event because of that it can be traced over a large area on the shelf as it is observed along most of the seismic lines (Fig. 36). Mass flow turbidities are generally more local and not spread over a large area. Also due its thickness size; as compared to a sandy layer formed by mass flow, sandy layers formed by bottom currents are thinner as compared to mass flow deposits. Based on the grain size analysis, it is observed that the sandy layer was a few cm in length and might have been formed by bottom currents, while a sandy layer formed by mass flow would have been thicker in comparison (Nichols, 2009). In addition, the absence of graded bedding or scour marks in the sediment log of GS20-229-28GC provides more evidence that the sandy layer might be formed due to ocean currents (Bondevik et al., 1997; Nichols, 2009). Similar tsunami deposits are also reported in Scotland, Norway, and Greenland (Bondevik et al., 2012; Bondevik et al., 1997; Dawson et al., 1988; Haflidason et al., 2005; Haflidason et al., 2002; Wagner et al., 2007). The XRF analysis of LF3 units, shows that the Ca/Fe ratio shows strong spikes confirming that the sandy layer contains shells of microfossils which is usually found in large grain size layers (Rothwell, 2015).

Similarly, the K (cps) is a fine-grain mineral that indicates the presence of clay minerals, decreases a little bit in the LF3 unit, and confirms that the sediment contains large-grain particles (Rothwell, 2015). Zirconium (Zr) occurs in heavy minerals that also spikes in the LF3 unit, Zr is typically enriched in sand layer that is eroded and transported by bottom currents (Dypvik and Harris, 2001). To confirm the chronology of the event and relate it to the Storegga slide, three samples were taken at an interval of 106 and 128 cm. The dating results, i.e., 8083 ± 200 cal. yrs BP clearly can be correlated with Haflidason et al. (2005) dating 8100 ± 250 cal. yrs BP (Fig. 19B). The corresponding RF1 reflector (Fig. 16) to the LF3 unit has a seismic geometry of high amplitude reflector present in Froya1, Froya2, Froya3, and Froya5 seismic lines. However, it is not present in Froya4. RF1 might have been deposited by the bottom currents of the Storegga tsunami based on the evidence of lithostratigraphic analysis of GS20-229-28GC.

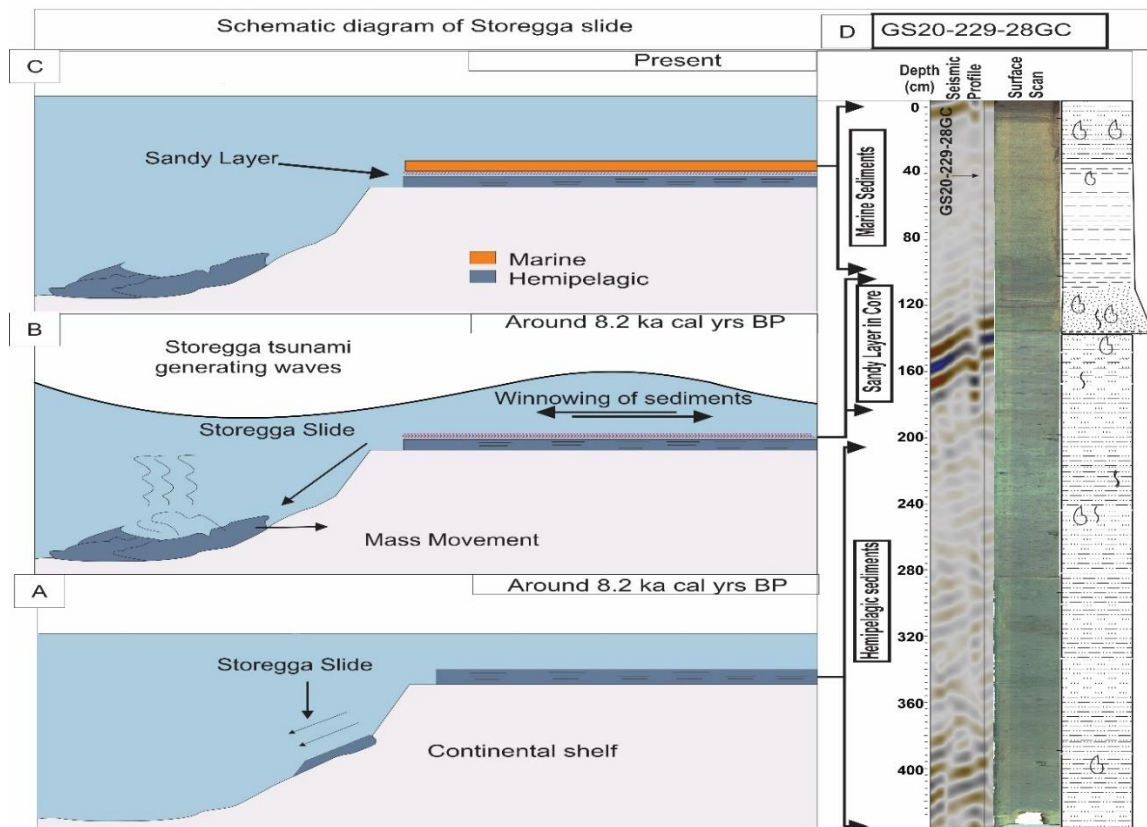


Fig. 36. The figure is based on a conceptual understanding of the sandy layer deposited by bottom currents through winnowing around the Norwegian continental shelf. A) Storegga slide being triggered from the continental shelf, B) Storegga slide generating tsunami waves and due to bottom waves, the hemipelagic sediments are being sorted as a sandy layer, C) Present scenario of the sandy layer formed due to bottom currents winnowing, D) The connection between GS20-229-28GC and different phases of the schematic diagram.

5.3.2 Halsafjorden

The seismic survey data is used to identify slide debrites or mass movements. Since mass movements or slide debrites usually have distinctive characteristics, such as high-frequency and low-amplitude waves (Bellwald et al., 2019; Hjelstuen et al., 2009; Lyså et al., 2010). These characteristics are different from the more gradual seismic signatures of sedimentary depositions. The seismostratigraphic SH1 unit is interpreted to be dominated by slide debrite usually formed in the late glacial period due to glacioisostatic crustal rebound. It has chaotic and high-frequency amplitudes, and also that coincides with the shape, size, and distribution of seismic units that are usually associated with slide debrites and mass movements in the western Norwegian fjords (Figs. 23 and 24) (Bellwald et al., 2019; Hjelstuen et al., 2009; Lyså et al., 2010; Rise et al., 2006). In addition, the lithostratigraphy of Halsafjorden shows that the lithological unit 1 that is associated with SH1 has a larger grain size that suggests that the sediments were transported over a short period and can be associated with the process of slide debrites or mass movements (Fig. 24). The combined analysis of seismic and lithostratigraphic data shows that these mass movements or slide debris indicate that submarine landslides occurred during the Holocene period in Halsafjorden. Rød (2022) has done detailed investigations on the mass movements in Halsafjorden in the Holocene period and suggested that a series of mass movements had happened between the deglaciation at 14 ka cal. yrs BP and the Mid Holocene. Rød (2022) dated the last landslide to happen at 5.5 ka cal. yrs BP. Bøe et al. (2004) have also suggested that mass movements in Halsafjorden might have been triggered in the Holocene period following the Younger Dryas. Bøe et al. (2004) also suggested that the Halsafjorden might have been affected by the Storegga tsunami.

5.4 Implications of results of Halsafjorden for E39 project

Based on the Halsafjorden seismic survey, chronology, and lithostratigraphy, these findings are crucial for the E39 project since they identify the seismic units that will be penetrated for potential bridge construction, regarding the implications of mass movements in Halsafjorden. Rød (2022) suggested that the last submarine landslide in Halsafjorden was around 5.5 ka cal. yrs BP and due to this low frequency of mass movements, it is improbable that the E39 project will be affected by it.

6. Conclusion

Based on the seismic stratigraphy, lithostratigraphy, the recalibration of ^{14}C dates from Frøyabanken and Halsafjorden, and its correlation with regional chronology from the North Sea fan to Haltenbanken. The results in this thesis conclude on the following points.

- Seismic stratigraphy of Frøyabanken shows that the deglaciation in Frøyabanken started around 17.7-17.1 ka cal yrs BP based on the recalibrated chronology and the deposition of seismic unit SF4. This retreat was followed by a readvance, i.e., the Frøyabanken readvance that seems to have happened around 16 ka cal yrs BP based on the evidence of the RF3 reflector geometry and the presence of moraine ridges. Recalibrated dates from the mid-Norwegian continental shelf also correlate with the Frøyabanken readvance.
- Following the Frøyabanken readvance, the ice sheet retreated to the inner fjord areas, and the ice sheet movement was studied from the seismic stratigraphy of Halsafjorden. It is suggested that the Halsafjorden was ice-free after 16 ka cal yrs BP based on the recalibrated chronology of the 08H_101 and the deposition of seismic units SH1 and SH2.
- The regional ice sheet retreat across the mid-Norwegian continental shelf started around 18 ka cal. yrs BP based on the recalibrated previously published chronology. It was followed by Late Karmøy/Bremanger readvance around 16-15 ka cal. yrs BP that could also be correlated with the cold spell phase of the Heinrich Event 1. The regional ice sheet mostly retreated from the shelf around 15 ka cal. yrs BP based on the recalibrated dates from previously published data. However, a small local readvance named the Haltenbanken readvance might have occurred around the Haltenbanken area (mid-Norwegian continental shelf North) around 13.9 ka cal. yrs BP.
- Based on the evidence of seismic survey of Frøyabanken, and lithostratigraphy, and chronology of the core GS201-229-28GC the widespread occurrence of a sandy sediment layer within in the Frøyabanken area is found to be related to the Storegga Slide.
- The presence of chaotic and transparent seismic facies overlying the deglacial sediments in the Halsafjorden sedimentary stratigraphy show that post-glacial mass movements have happened in the Halsafjorden as evident in most western Norwegian fjords.

7. Future work

The result of this study has highlighted several areas in which future research could expand based on the work presented here.

- 1) One potential area would be to conduct a more detailed analysis of the areas between Halsafjorden and Frøyabanken. This could be done by using a highly detailed seismic survey to identify the seismic sequences and retrace the Frøyabanken ice sheet readvance from Frøyabanken to Halsafjorden in much more detail.
- 2) Another potential area of research would be to conduct more detailed geochronological studies of Frøyabanken, Haltenbanken, and Storegga ridge moraines or tills to better understand the regional ice sheet movement following the Last Glacial Maximum in the mid-Norwegian continental shelf.
- 3) Finally, it would be interesting to investigate the potential of Storegga tsunami outreach in areas around Halsafjorden as the Storegga tsunami has been noted that it might have affected the Halsafjorden area.

References

- Aarseth, I., 1997, Western Norwegian fjord sediments: age, volume, stratigraphy, and role as temporary depository during glacial cycles: *Marine Geology*, v. 143, no. 1, p. 39-53.
- Aase, A. S., 2022, Depositional history and pockmarks in Vartdalsfjorden, Sunnmøre [Master: University of Bergen, 74 p.
- Alm, T., 1993, Øvre Æråsvatn-palynostratigraphy of a 22,000 to 10,000 BP lacustrine record on Andøya, northern Norway: *Boreas*, v. 22, no. 3, p. 171-188.
- Andersen, B. G., Bøen, F., Nydal, R., Rasmussen, A., and Vallevik, P. N., 1981, Radiocarbon dates of marginal moraines in Nordland, North Norway: *Geografiska Annaler: Series A, Physical Geography*, v. 63, no. 3-4, p. 155-160.
- Andersen, B. G., Mangerud, J., Sørensen, R., Reite, A., Sveian, H., Thoresen, M., and Bergström, B., 1995, Younger Dryas ice-marginal deposits in Norway: *Quaternary International*, v. 28, p. 147-169.
- Anundsen, K., and Fjeldskaar, W., 2020, Observed and theoretical late Weichselian shore-level changes related to glacier oscillations at Yrkje, south-west Norway, Late-and Postglacial Oscillations of Glaciers: Glacial and Periglacial Forms/Spät-und Postglaziale Gletscherschwankungen: Glazial-und Periglazialformen/Oscillations Fini-Et Postglaciaires des Glaciers: Formes Glaciaires et Periglaciaires, CRC Press, p. 133-170.
- Askvik, H., and Rokoengen, K., 1985, Geologisk kart over Norge, berggrunnskart Kristiansund. M 1: 250 000: Norges Geologiske Undersøkelse.
- Bard, E., Arnold, M., and Duplessy, J.-C., Reconciling the sea level record of the last deglaciation with the $\delta^{18}\text{O}$ spectra from deep sea cores, *in Proceedings Quaternary Proceedings 1991*, p. 67-73.
- Bellwald, B., Hjelstuen, B. O., Sejrup, H. P., Stokowy, T., and Kuvås, J., 2019, Holocene mass movements in west and mid-Norwegian fjords and lakes: *Marine Geology*, v. 407, p. 192-212.
- Bennett, M. M., and Glasser, N. F., 2011, *Glacial geology: ice sheets and landforms*, John Wiley & Sons.
- Bergström, B., Olsen, L., and Sveian, H., 2005, The Tromsø-Lyngen glacier readvance (early Younger Dryas) at Hinnoya-Ofotfjorden, northern Norway: a reassessment: *Norges Geologiske Undersøkelse*, v. 445, p. 73.
- Blott, S. J., and Pye, K., 2001, GRADISTAT: a grain size distribution and statistics package for the analysis of unconsolidated sediments: *Earth Surface Processes and Landforms*, v. 26, no. 11, p. 1237-1248.
- Bøe, A.-G., Murray, A., and Dahl, S. O., 2007, Resetting of sediments mobilised by the LGM ice-sheet in southern Norway: *Quaternary Geochronology*, v. 2, no. 1-4, p. 222-228.
- Bøe, R., Longva, O., Lepland, A., Blikra, L. H., Sønstegaard, E., Haflidason, H., Bryn, P., and Lien, R., 2004, Postglacial mass movements and their causes in fjords and lakes in western Norway: *Norwegian Journal of Geology*, v. 84, no. 1.
- Bondevik, S., Stormo, S. K., and Skjerdal, G., 2012, Green mosses date the Storegga tsunami to the chilliest decades of the 8.2 ka cold event: *Quaternary Science Reviews*, v. 45, p. 1-6.
- Bondevik, S., Svendsen, J. I., and Mangerud, J., 1997, Tsunami sedimentary facies deposited by the Storegga tsunami in shallow marine basins and coastal lakes, western Norway: *Sedimentology*, v. 44, no. 6, p. 1115-1131.

- Boulton, G., and Hindmarsh, R., 1987, Sediment deformation beneath glaciers: rheology and geological consequences: *Journal of Geophysical Research: Solid Earth*, v. 92, no. B9, p. 9059-9082.
- Bøyum, E., 2011, Siste deglasiasjon av midt-norsk kontinentalsokke [Master: University of Bergen, 55 p.
- Brendryen, J., Haflidason, H., Yokoyama, Y., Haaga, K. A., and Hannisdal, B., 2020, Eurasian Ice Sheet collapse was a major source of Meltwater Pulse 1A 14,600 years ago: *Nature Geoscience*, v. 13, no. 5, p. 363-368.
- Bugge, T., 1980, Øvre lags geologi på kontinentalsokkelen utenfor Møre og Trøndelag (Shallow geology on the continental shelf off Møre and Trøndelag, Norway) v. 104, p. 44.
- Bugge, T., Maisey, G., Rokoengen, K., Skaar, F., Thusu, B., and Løfaldli, M., 1975, Geological investigation of a lower tertiary/quaternary core, offshore Trøndelag, Norway, p. 254-269.
- Canals, M., Lastras, G., Urgeles, R., Casamor, J., Mienert, J., Cattaneo, A., De Batist, M., Haflidason, H., Imbo, Y., and Laberg, J., 2004, Slope failure dynamics and impacts from seafloor and shallow sub-seafloor geophysical data: case studies from the COSTA project: *Marine Geology*, v. 213, no. 1-4, p. 9-72.
- Chandler, B., and Evans, D., 2021, *Glacial Processes and Sediments*, p. 830-856.
- Croudace, I. W., Rindby, A., and Rothwell, R. G., 2006, ITRAX: description and evaluation of a new multi-function X-ray core scanner: *Geological Society, London, Special Publications*, v. 267, no. 1, p. 51-63.
- Dawson, A. G., Long, D., and Smith, D., 1988, The Storegga slides: evidence from eastern Scotland for a possible tsunami: *Marine Geology*, v. 82, no. 3-4, p. 271-276.
- Dypvik, H., and Harris, N. B., 2001, Geochemical facies analysis of fine-grained siliciclastics using Th/U, Zr/Rb and (Zr+Rb)/Sr ratios: *Chemical Geology*, v. 181, no. 1, p. 131-146.
- Evans, D. J., 2017, *Till: A glacial process sedimentology*, John Wiley & Sons.
- Fjeldskaar, W., and Kanestrøm, R., 1980, Younger Dryas geoid-deformation caused by deglaciation in Fennoscandia: *Earth rheology, isostasy and eustasy*, p. 569-574.
- Fugro, 2019, *Measured and Derived Geotechnical Parameters and Final Results Fjord Crossings E39 – Marine Ground Investigations, Halsafjorden*.
- Ginsberg, S. S., 2011, *Sediment Transport, BoD–Books on Demand*.
- Gjelle, S., Bergstrøm, B., Gustavson, M., Olsen, L., and Sveian, H., 1995, *Geology and landscape around the Arctic Circle in Norway: Weenebergs trykkeri AS, Trondheim*.
- Haflidason, H., Bøyum, E., and Oline Hjelstuen, B., The deglaciation history of the mid-Norwegian continental shelf, *in Proceedings EGU General Assembly Conference Abstracts2013*, p. EGU2013-3586.
- Haflidason, H., Lien, R., Sejrup, H. P., Forsberg, C. F., and Bryn, P., 2005, The dating and morphometry of the Storegga Slide: *Marine and Petroleum Geology*, v. 22, no. 1-2, p. 123-136.
- Haflidason, H., Sejrup, H., Bryn, P., Lien, R., Masson, D., Jacobs, C., Huehnerbach, V., and Berg, K., The architecture and slide mechanism of the Storegga Slide, Mid Norwegian margin, *in Proceedings NGF Abstracts and Proceedings, Annual Meeting in Trondheim, Norwegian Petroleum Society, Stavanger2002*, p. 80-81.
- Haflidason, H., Sejrup, H. P., Nygård, A., Mienert, J., Bryn, P., Lien, R., Forsberg, C. F., Berg, K., and Masson, D., 2004, The Storegga Slide: architecture, geometry and slide development: *Marine Geology*, v. 213, no. 1-4, p. 201-234.

- Hansbo, S., 1957, New approach to the determination of the shear strength of clay by the fall-cone test: Royal Swedish Geotechnical Institute, no. 14, p. 7-47.
- Havforskningsinstituttet, 2018, G.O. Sars.
- Heaton, T. J., Köhler, P., Butzin, M., Bard, E., Reimer, R. W., Austin, W. E. N., Bronk Ramsey, C., Grootes, P. M., Hughen, K. A., Kromer, B., Reimer, P. J., Adkins, J., Burke, A., Cook, M. S., Olsen, J., and Skinner, L. C., 2020, Marine20—The Marine Radiocarbon Age Calibration Curve (0–55,000 cal BP): *Radiocarbon*, v. 62, no. 4, p. 779-820.
- Hergert, W., and Wriedt, T., 2012, *The Mie theory: basics and applications*, Springer.
- Hjelstuen, B. O., Haflidason, H., Sejrup, H. P., and Lyså, A., 2009, Sedimentary processes and depositional environments in glaciated fjord systems—Evidence from Nordfjord, Norway: *Marine Geology*, v. 258, no. 1-4, p. 88-99.
- Holtedahl, H., and Bjerkli, K., 1982, Late Quaternary sediments and stratigraphy on the continental shelf off Møre-Trøndelag, W. Norway: *Marine Geology*, v. 45, no. 3-4, p. 179-226.
- Holtedahl, H., Nielsen, N., Hjulström, F., and Isachsen, F., 1956, On the Norwegian Continental Terrace, primarily outside Møre-Romsdal: its Geomorphology and Sediments: *Norsk Geografisk Tidsskrift - Norwegian Journal of Geography*, v. 15, no. 3-4, p. 172-181.
- Holtedahl, H., Sellevoll, M., and Delany, F., 1971, *Geology of the continental margin of the eastern Norwegian Sea and of the Skagerrak*: Institute of Geological Sciences Report, v. 70, p. 14.
- Horberg, L., 1947, *The Submarine Relief of the Norwegian Coast with Bathymetrical Map in Seven Sheets of the Norwegian Coastal Waters and Adjoining Areas*. Olaf Holtedahl: *The Journal of Geology*, v. 55, no. 1, p. 58-59.
- Hughes, A. L. C., Gyllencreutz, R., Lohne, Ø. S., Mangerud, J., and Svendsen, J. I., 2016, The last Eurasian ice sheets - a chronological database and time-slice reconstruction, DATED-1: *Boreas*, v. 45, no. 1, p. 1-45.
- Johansen, O.-I., Henningsmoen, K., and Sollid, J., 1985, Deglasiasjonsforlepet på Tingvollhalveya og tilgrensende områder, Nordvestlandet, i lys av vegetasjonsutviklingen.[Déglaciation of the Tingvoll peninsula and adjacent areas, Nordvestlandet, in light of the vegetation development]: *Norsk Geog Tidsskr*, v. 39, p. 155-174.
- King, E., Haflidason, H., Sejrup, H., and Løvlie, R., 1998, Glacigenic debris flows on the North Sea Trough Mouth Fan during ice stream maxima: *Marine Geology*, v. 152, no. 1-3, p. 217-246.
- Klakegg, O., AR, A., Sønstegaard, E., and Nordahl-Olsen, T., 1989, Sogn og Fjordane fylke. Kwartærgeologisk kart M 1: 250 000.
- Laberg, J., Vorren, T., Mienert, J., Evans, D., Lindberg, B., Ottesen, D., Kenyon, N., and Henriksen, S., 2002, Late Quaternary palaeoenvironment and chronology in the Trænadjupet Slide area offshore Norway: *Marine Geology*, v. 188, no. 1-2, p. 35-60.
- Lohne, Ø. S., Bondevik, S., Mangerud, J., and Svendsen, J. I., 2007, Sea-level fluctuations imply that the Younger Dryas ice-sheet expansion in western Norway commenced during the Allerød: *Quaternary Science Reviews*, v. 26, no. 17, p. 2128-2151.
- Lyså, A., Hjelstuen, B. O., and Larsen, E., 2010, Fjord infill in a high-relief area: Rapid deposition influenced by deglaciation dynamics, glacio-isostatic rebound and gravitational activity: *Boreas*, v. 39, no. 1, p. 39-55.
- Mangerud, J., 1980, Ice-front variations of different parts of the Scandinavian Ice Sheet, 13,000-10,000 years BP: *Studies in the lateglacial of North-West Europe*, p. 23-30.

- , 2004, Ice sheet limits on Norway and the Norwegian continental shelf: Quaternary glaciations—Extent and chronology, v. 1, p. 271-294.
- Mangerud, J., Bondevik, S., Gulliksen, S., Hufthammer, A. K., and Høisæter, T., 2006, Marine ¹⁴C reservoir ages for 19th century whales and molluscs from the North Atlantic: *Quaternary Science Reviews*, v. 25, no. 23-24, p. 3228-3245.
- Mörner, N., 2013, Patterns in seismology and palaeoseismology, and their application in long-term hazard assessments—the Swedish case in view of nuclear waste management: *Pattern Recognition in Physics*, v. 1, no. 1, p. 75-89.
- Muir-Wood, R., 1993, A review of the seismotectonics of Sweden.
- Nichols, G., 2009, *Sedimentology and stratigraphy*, John Wiley & Sons.
- Nielsen, T., and Rasmussen, T. L., 2018, Reconstruction of ice sheet retreat after the Last Glacial maximum in Storfjorden, southern Svalbard: *Marine Geology*, v. 402, p. 228-243.
- Nydal, R., Gulliksen, S., Loevseth, K., and Skogseth, F., 1985, Trondheim natural radiocarbon measurements IX: *Radiocarbon*, v. 27, no. 3, p. 525-609.
- Nygård, A., 2003, Pleistocene sedimentary processes and glacial history of the Southern Norwegian continental margin, Department of Earth Science, University of Bergen.
- Nygård, A., Sejrup, H. P., Haflidason, H., Cecchi, M., and Ottesen, D., 2004, Deglaciation history of the southwestern Fennoscandian Ice Sheet between 15 and 13 ¹⁴C ka BP: *Boreas*, v. 33, no. 1, p. 1-17.
- Olsen, L., 2002, Mid and Late Weichselian, ice-sheet fluctuations northwest of the Svartisen glacier, Nordland, northern Norway: *Geological Survey of Norway Bulletin*, v. 440.
- Olsen, L., and Bergstrøm, B., Glacier variations during the LGM interval in the Karmøy–Jæren district, SW Norway, *in Proceedings NGF Abstracts and Proceedings2007*, Volume 1, p. 73-74.
- Olsen, L., Sveian, H., Bergstrøm, B., Ottesen, D., and Rise, L., 2013, Quaternary glaciations and their variations in Norway and on the Norwegian continental shelf: *Quaternary geology of Norway*, v. 13, p. 27-78.
- Olsson, I. U., 1968, Modern aspects of radiocarbon datings: *Earth-Science Reviews*, v. 4, p. 203-218.
- Ottesen, D., Batchelor, C. L., Bjarnadóttir, L. R., Wiberg, D. H., and Dowdeswell, J. A., 2022, Glacial landforms reveal dynamic ice-sheet behaviour along the mid-Norwegian margin during the last glacial-deglacial cycle: *Quaternary Science Reviews*, v. 285, p. 107462.
- Ottesen, D., Dowdeswell, J., and Rise, L., 2005, Submarine landforms and the reconstruction of fast-flowing ice streams within a large Quaternary ice sheet: The 2500-km-long Norwegian-Svalbard margin (57–80 N): *Geological Society of America Bulletin*, v. 117, no. 7-8, p. 1033-1050.
- Panalytical, M., 2021, Mastersizer 3000.
- Ramsey, C. B., 2008, Deposition models for chronological records: *Quaternary Science Reviews*, v. 27, no. 1-2, p. 42-60.
- , 2009, Bayesian analysis of radiocarbon dates: *Radiocarbon*, v. 51, no. 1, p. 337-360.
- Reimer, P. J., Bard, E., Bayliss, A., Beck, J. W., Blackwell, P. G., Ramsey, C. B., Buck, C. E., Cheng, H., Edwards, R. L., and Friedrich, M., 2013, IntCal13 and Marine13 radiocarbon age calibration curves 0–50,000 years cal BP: *radiocarbon*, v. 55, no. 4, p. 1869-1887.
- Reimer, P. J., and Reimer, R. W., 2001, A marine reservoir correction database and on-line interface: *Radiocarbon*, v. 43, no. 2A, p. 461-463.

- Rise, L., Bøe, R., Sveian, H., Lyså, A., and Olsen, H. A., 2006, The deglaciation history of Trondheimsfjorden and Trondheimsleia, Central Norway: *Norwegian Journal of Geology/Norsk Geologisk Forening*, v. 86, no. 4.
- Rød, S. J., 2022, Holocene skredavsetninger i Halsafjorden, Nordmøre [Masters: Universitetet i Bergen], 106 p.
- Rokoengen, K., Bell, G., Bugge, T., Dekko, T., Gunleiksrud, T., Lien, R., Løfaldli, M., and Vigran, J., 1977, Prøvetaking av fjellgrunn og løsmasser utenfor deler av Nord-Norge i 1976: *Institutt for kontinentalsokkelundersøkelser, Norge*, p. 65.
- Rokoengen, K., and Frengstad, B., 1999, Radiocarbon and seismic evidence of ice-sheet extent and the last deglaciation on the mid-Norwegian continental shelf: *Norsk Geologisk Tidsskrift*, v. 79, no. 2, p. 129-132.
- Rothwell, R. G., 2015, Twenty years of XRF core scanning marine sediments: What do geochemical proxies tell us?, *Micro-XRF studies of sediment cores*, Springer, p. 25-102.
- Sejrup, H., Haflidason, H., Flatebø, T., Kristensen, D. K., Grøsfjeld, K., and Larsen, E., 2001, Late-glacial to Holocene environmental changes and climate variability: evidence from Voldafjorden, western Norway: *Journal of Quaternary Science: Published for the Quaternary Research Association*, v. 16, no. 2, p. 181-198.
- Sejrup, H. P., Haflidason, H., Aarseth, I., King, E., Forsberg, C. F., Long, D., and Rokoengen, K., 1994, Late Weichselian glaciation history of the northern North Sea: *Boreas*, v. 23, no. 1, p. 1-13.
- Sejrup, H. P., Hjelstuen, B. O., Patton, H., Esteves, M., Winsborrow, M., Rasmussen, T. L., Andreassen, K., and Hubbard, A., 2022, The role of ocean and atmospheric dynamics in the marine-based collapse of the last Eurasian Ice Sheet: *Communications Earth & Environment*, v. 3, no. 1, p. 1-10.
- Stokes, C. R., and Clark, C. D., 2002, Ice stream shear margin moraines: *Earth Surface Processes and Landforms*, v. 27, no. 5, p. 547-558.
- Strunk, A., Olsen, J., Sanei, H., Rudra, A., and Larsen, N. K., 2020, Improving the reliability of bulk sediment radiocarbon dating: *Quaternary Science Reviews*, v. 242, p. 106442.
- Svendsen, J. I., and Mangerud, J., 1987, Late Weichselian and Holocene sea-level history for a cross-section of western Norway: *Journal of Quaternary Science*, v. 2, no. 2, p. 113-132.
- Svjeian, H., 1997, Ice-marginal deposits and deglaciation chronology in Nord-Trøndelag and Fosen, Central Norway: *Norges Geologiske Undersøkelse*, v. 433, p. 52-53.
- Thomson, J., Croudace, I., and Rothwell, R., 2006, A geochemical application of the ITRAX scanner to a sediment core containing eastern Mediterranean sapropel units: *Geological Society, London, Special Publications*, v. 267, no. 1, p. 65-77.
- Vorren, T. O., and Plassen, L., 2002, Deglaciation and palaeoclimate of the Andfjord-Vågsfjord area, North Norway: *Boreas*, v. 31, no. 2, p. 97-125.
- Vorren, T. O., Vorren, K. D., Alm, T., Gulliksen, S., and Løvlie, R., 1988, The last deglaciation (20,000 to 11,000 BP) on Andoya, Northern Norway: *Boreas*, v. 17, no. 1, p. 41-77.
- Wagner, B., Bennike, O., Klug, M., and Cremer, H., 2007, First indication of Storegga tsunami deposits from East Greenland: *Journal of Quaternary Science: Published for the Quaternary Research Association*, v. 22, no. 4, p. 321-325.
- Wentworth, C. K., 1922, A scale of grade and class terms for clastic sediments: *The journal of geology*, v. 30, no. 5, p. 377-392.
- Ziegler, M., Jilbert, T., de Lange, G. J., Lourens, L. J., and Reichert, G. J., 2008, Bromine counts from XRF scanning as an estimate of the marine organic carbon content of sediment cores: *Geochemistry, Geophysics, Geosystems*, v. 9, no. 5.

